May 2017

Volatile Technetium Oxides: Implications for Nuclear Waste Vitrification

Bradley Covington Childs
University of Nevada, Las Vegas

Follow this and additional works at: https://digitalscholarship.unlv.edu/thesesdissertations

Part of the Chemistry Commons

VOLATILE TECHNETIUM OXIDES: IMPLICATIONS FOR

NUCLEAR WASTE VITRIFICATION

By

Bradley Covington Childs

Bachelor of Science - Chemistry

South Carolina State University

2010

A dissertation submitted in partial fulfillment

of the requirements for the

Doctor of Philosophy – Radiochemistry

Department of Chemistry and Biochemistry

College of Sciences

The Graduate College

University of Nevada, Las Vegas

May 2017

UNLV | GRADUATE COLLEGE

Dissertation Approval

The Graduate College
The University of Nevada, Las Vegas

December 12, 2016

This dissertation prepared by

Bradley Covington Childs

entitled

Volatile Technetium Oxides: Implications for Nuclear Waste Vitrification

is approved in partial fulfillment of the requirements for the degree of

Doctor of Philosophy – Radiochemistry
Department of Chemistry and Biochemistry

Frederic Poineau, Ph.D.
Examination Committee Chair

Kenneth Czerwinski, Ph.D.
Examination Committee Member

Alfred Sattelberger, Ph.D.
Examination Committee Member

Gary Cerefice, Ph.D.
Examination Committee Member

Michael Pravica, Ph.D.
Graduate College Faculty Representative

Kathryn Hausbeck Korgan, Ph.D.
Graduate College Interim Dean

Abstract

Volatile Technetium Oxides: Implications for Nuclear Waste Vitrification

By: Bradley C. Childs

Dr. Frederic Poineau, Advisory Committee Chair

Professor of Chemistry

University of Nevada, Las Vegas

From 1943 to 1987, the Hanford site was the primary location for the production of Pu for military applications in the United States. Decades of Pu production have been accompanied by generation of large amounts of liquid and solid radioactive waste. One of radioelements present in the Hanford wastes is Tc, principally the isotope ^{99}Tc (~1500 kg). In the waste, it is primarily present in the heptavalent state as TcO_4^-. One option for the management of Tc at the Hanford site is its vitrification into a borosilicate glass. The behavior of Tc during vitrification is problematic, as it volatilizes and only a fraction is retained in the glass. Minimization of Tc volatility is a challenge for the development of safe vitrification processes. The nature of the volatile Tc species has been discussed and $HTcO_4$, Tc_2O_7 and alkali pertechnetate salts have been proposed. Until now, no characterization of the volatile Tc species has been performed.

In this context, the vitrification of Tc in simulated borosilicate glass was performed and the volatile Tc species were characterized by X-ray absorption spectroscopy. The EXAFS results indicated the presence of $TcO_3(OH)(H_2O)_2$ in the volatile species. The mechanisms of formation of volatile species were proposed and involved the oxidation of TcO_2 to Tc_2O_7 followed by the hydrolysis of Tc_2O_7 to $HTcO_4$.

In order to better understand the mechanism of formation of volatile Tc species, the gas-phase and solid-state chemistry of Tc_2O_7 was revisited. Here, Tc_2O_7 was synthesized from the oxidation of TcO_2 with O_2 and its crystallographic structure was determined at 100 K and the data compared with the previous structure elucidated in 1969. The electron impact-mass spectrum of Tc_2O_7 consisted of both mononuclear and dinuclear species. The main dinuclear species in the gas-phase were Tc_2O_7 and Tc_2O_5, while the main mononuclear species were TcO_3 and TcO_2. The optimized structure of the Tc_2O_7 molecule was in good agreement with the experimental one. Energetic calculations confirmed the linear structure to be the most favorable in the solid-state, while the bent geometry is the most stable in the gas-phase. Stability with respect to compression and high cohesive energy per molecule are possibly the reason why the linear structure is observed in the solid-state. Finally, because water can be present during the vitrification process, studying the effect of water on the nature of the volatile species is of importance. The effect of water on the nature of the volatile species formed during oxidation of TcO_2 was studied. The oxidation of TcO_2 with water and O_2 was performed at 250 °C; after the reaction a red product was observed and characterized by mass spectrometry.

iv

Acknowledgements

What has been accomplished in this document has been aided by the help, support, encouragement, motivation and teachings of the most influential people in my life. I must first thank my dissertation committee. Not only have they been excellent in teaching me valuable lessons in chemistry, but they have also provided teachings that I will carry with me every day in life. Thank you again to Gary Cerefice, Alfred Sattelberger, and Michael Pravica for the time and advice that you all have given me. This along with strong encouragement and a bit of comedic relief will never be forgotten. I must extend a thank you to Ken Czerwinski for presenting me with the opportunity to join this program and the ability to explore many avenues that this field has to offer. My gratitude also goes to my graduate chair Frederic Poineau. His enthusiastic approach to research provided an environment that bred production, enhanced skills, and also fostered many laughs to ease the hard times. Professors that I currently interact with as well as those that have help to nurture, mold, and guide me through coursework and research, I offer my sincerest gratitude.

A big thank you must go out to all of my friends and family who have supported me since the day that I was born. To my mother and father, Derrick and Yolanda Childs, my brother, Kyle Childs, thank you for everything that you have done and the sacrifices that you have made to see me reach my goals. To my Purple, thank you for always being at my side and supporting me unconditionally. To all my friends who been there from day one, I appreciate each and every one of you. Thank you.

Table of Contents

List of Tables

List of Figures

List of Equations

Chapter 1: Introduction

1.1   The Hanford site

The Hanford site was the primary location for the production of Pu for military applications in the United States; it is located in Washington State on the Columbia Plateau (Figure 1.1). The site consists of 586 square miles, the Columbia River runs through the site's northern region as well as forming the eastern boundary.[3] This site was chosen for Pu production based on the following criteria: area of at least 12 x 15 miles, population no greater of 1,000 within 20 miles, 25,000 gallons of water per minute to cool reactors, 100,000 kilowatts of electricity, access to railroads and highways, flat landscape, and available fuel and concrete aggregate.[4]
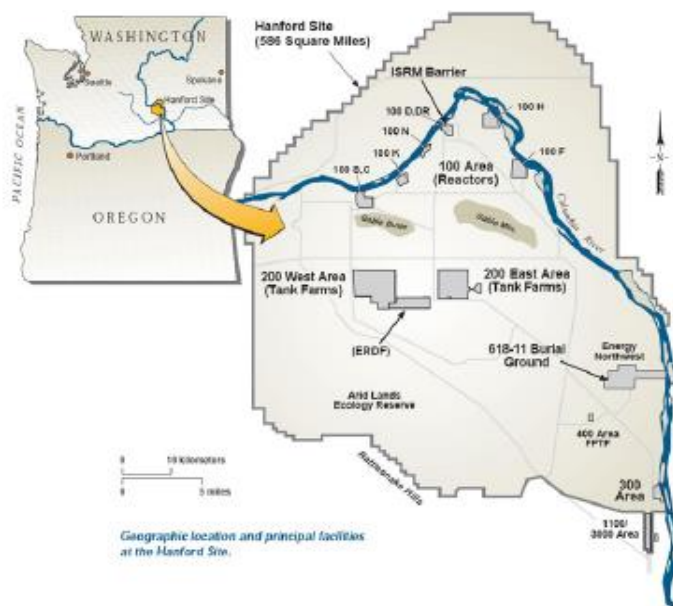
Figure 1.1. Geographic location of the Hanford site.

Plutonium produced at the Hanford site was used in nuclear devices in the Trinity test, as well as Fat Man, the nuclear device that was detonated over Nagasaki, Japan. Between 1945 and 1953, the Hanford site was responsible for the entire United States nuclear Pu arsenal, and over 65% in the history of Pu production in United States.[4] Due to the large amount of industrial, chemical, and radiological processes that were required, decades of Pu production have been accompanied by generation of large amounts of liquid and solid radioactive waste. High level and low level radioactive waste were directed and stored in underground tanks. The Hanford site produced Pu until the late 1980s, the production was suspended after the Chernobyl accident in 1986.[4]

There are 177 total underground tanks that were created for storing nuclear waste, 149 are single-shell tanks and 28 are double-shell tanks (Figure 2).[4] The tanks contain 57 million gallons of waste and 200 megacuries of radioactivity. Due to the heat generation from the waste as well as the causticity, as many as 67 of the 149 single-shell tanks have leaked more than one million gallons of waste.[5] The composition of the waste varies from tank to tank. High activity fission products, such as ^{90}Sr and ^{137}Cs, are planned to be separated from low-level activity isotopes such as ^{99}Tc and ^{129}I. Low activity waste primarily consists of Na^+, K^+, $Al(OH)_4^-$, Cl^-, F^-, NO_2^-, NO_3^-, OH^-, CO_3^{2-}.[6] These tanks contain organic complexants such as nitrilotriacetate, ethylenediaminetetracetate, citrate, and gluconate.[7] The aging tanks represent a challenge for the management of the 57 million gallons of radioactive waste.

The Hanford Tank Waste Treatment and Immobilization Plant (WTP) proposes that two waste streams would be created and vitrified.[8] The first waste vitrification stream would be a low-

volume and high-level waste (HLW) glass, and the second would be a high-volume and low-level

waste (LLW) glass.
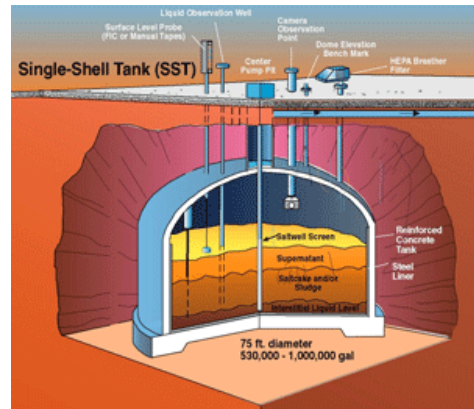
Figure 1.2. Left: construction of 12 waste tanks at the Hanford site. Right: diagram of a single-

shell tank.
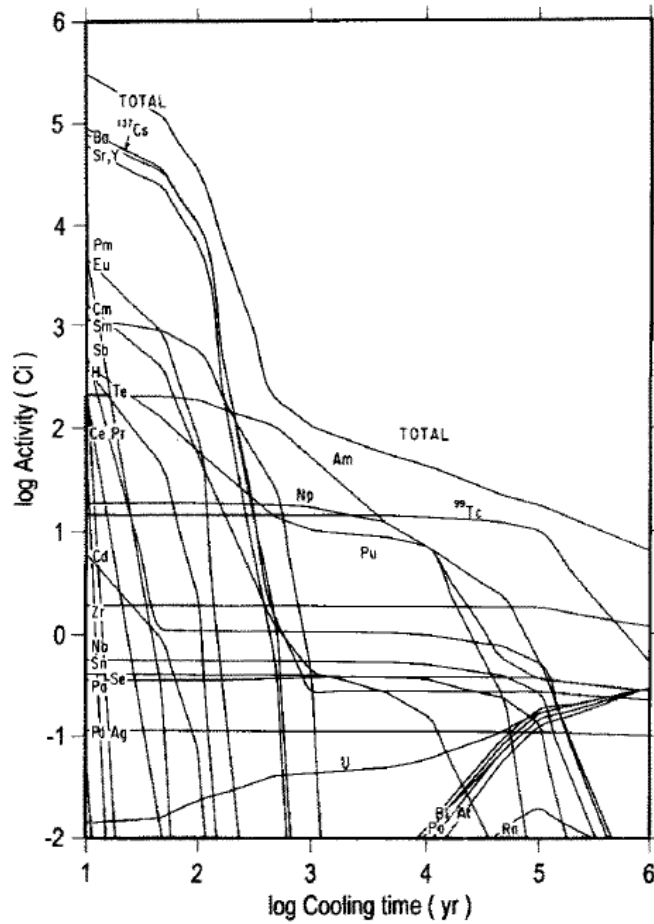
Figure 1.3. Plot of the specific activity (Ci) and major radionuclides in high level nuclear waste as a function of cooling time (years).[9]

1.2   Technetium at the Hanford site

One of isotopes present in the Hanford site tanks is ^{99}Tc (~1500 kg). In the waste, Tc is primarily present in the heptavalent state as TcO_4^-. Due to its mobility [10] and long half-life ($t_{1/2}$ = 213,000 y), ^{99}Tc presents a significant concern and is a major contributor to long-term storage of LLW.[6]

4

One option for the management of Tc at the Hanford site is its vitrification into a borosilicate glass. The behavior of Tc during vitrification is problematic, as it volatizes (30% - 70%) and only a fraction is retained in the glass.[11] Minimization of Tc volatility is a challenge for the development of safe vitrification processes. The nature of the volatile Tc species has been discussed and $HTcO_4$, Tc_2O_7, and alkali pertechnetate salts have been proposed.[6] Previous studies have focused on the speciation of Tc in the glass[12,13,14] and until now, no characterization of the volatile technetium species has been performed. In this context, the vitrification of $NaTcO_4$ in simulated borosilicate glass was performed and the volatile Tc species characterized by X-ray absorption fine structure spectroscopy.

1.3 Technetium generality
1.3.1 Technetium isotopes and applications

Technetium, element 43, is the lightest radioelement. The name technetium comes from the Greek word "technetos", which means artificial. It was produced by Perrier and Segrè from the irradiation of a Mo foil at the Berkeley cyclotron.[15] There are 34 known isotopes of Tc, and the isotopes that are the longest lived and highest in abundance are ^{97}Tc, ^{98}Tc, and ^{99}Tc (Table 1.1). The heaviest of the three most common isotopes, ^{99}Tc, is a fission product (fission yield ~ 6.1% from ^{235}U) of the nuclear industry.[16]

Technetium isotopes with masses above 100 amu have half-lives that do not exceed 20 minutes; with the amount time spent fuel is stored in storage pools, the presence of ^{97}Tc and ^{98}Tc

in the spent fuel are negligible and therefore not considered fission products.[17] Both ^{97}Tc and ^{98}Tc can be produced in a cyclotron.[15]

Table 1.1. Technetium isotopes and properties.[2]

Isotope	Atomic Mass (amu)	Spin and Parity [h/2π]	Half-life (t$_{1/2}$)	Mode and Energy of Decay (keV)
^{97}Tc	96.906364	9/2+	4.2 x 10^6 yr	E
^{98}Tc	97.907215	(6)+	4.2 x10^6 yr	β$^-$ 397; γ 745, 652
^{99}Tc	99.907657	9/2+	2.1 x 10^5 yr	β$^-$ 292, 203
^{99m}Tc	-	1/2-	6.006 hr	IT 140, 143;β$^-$; e$^-$;γ 322, 233

Another important isotope is ^{99m}Tc, a low-energy gamma emitter. Due to its optimal nuclear properties and versatile chemistry, it is widely used as an imaging agent for radiopharmaceuticals application (80% of the radio diagnostic).[2] This isotope is produced from the beta decay of ^{99}Mo (Figure 1.5). The isotope ^{99}Mo can be obtained from the fission of highly enriched uranium (HEU) target or from the irradiation of ^{98}Mo with slow neutrons in a reactor (Figure 1.3).[18] In medical facilities, ^{99m}TcO$_4^-$ is eluted off an alumina column of a ^{99}Mo generator with a saline solution.[19] One ^{99m}Tc complex used for heart diagnostics is Cardiolite (Figure 1.4).
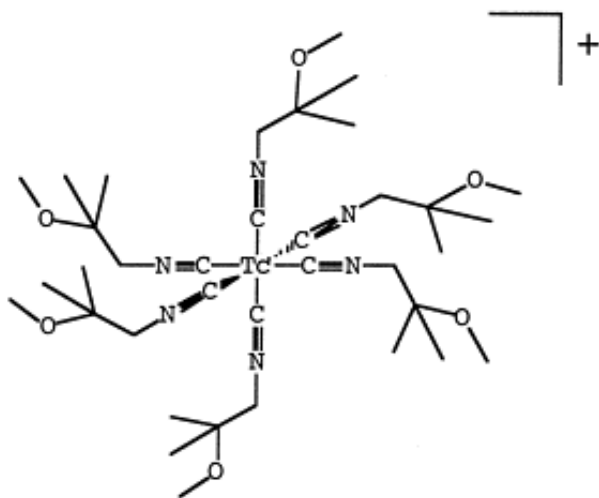
Figure 1.4. Cardiolite - $[Tc(CNCH_2C(Me)_2OMe)_6]^+$; Heart imaging agent.
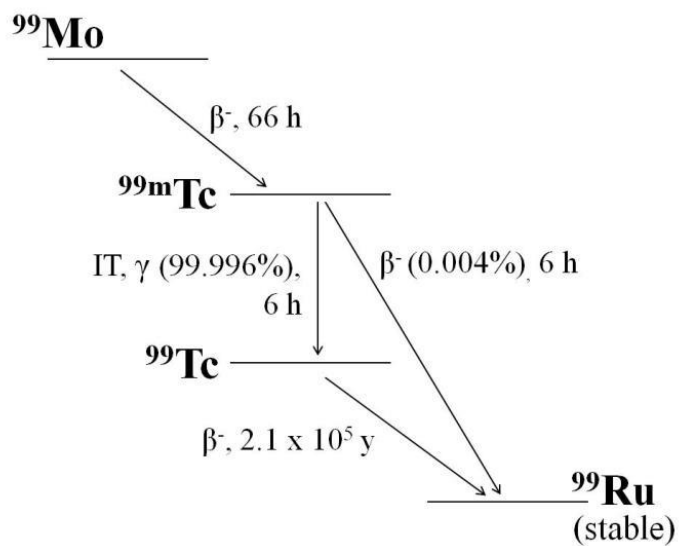
Figure 1.5. Decay scheme of ^{99}Mo.

1.3.2 Technetium in the nuclear fuel cycle

One metric ton (MT) of spent nuclear fuel contains 0.8 kg of ^{99}Tc (33 MWd/kg U), its current inventory in the U.S. is ~56 MT. In the spent nuclear fuel, ^{99}Tc is present in metallic inclusion, along with Mo, Ru, Rh, and Pd, called the epsilon phase (Figure 1.6). The composition (at. %) of the epsilon phase is: Mo (40), Ru (30), Tc (10), Pd (15), Rh (5).[20]
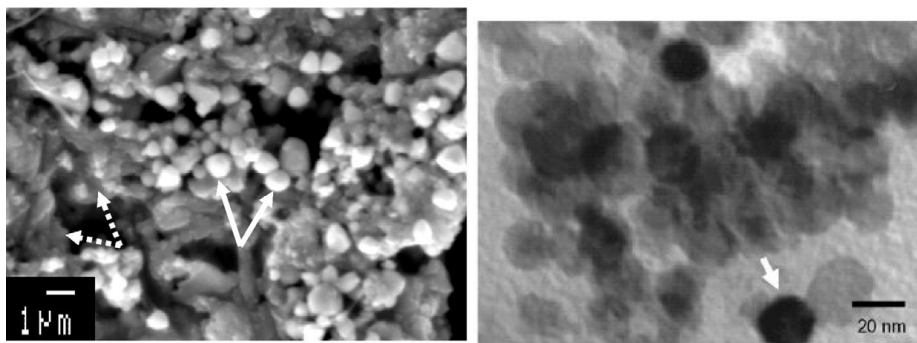
Figure 1.6. SEM (left) and TEM (right) images of epsilon phase.

Technetium can be recovered after treatment of spent nuclear fuel. Different separation processes have been proposed: uranium extraction (UREX) and plutonium and uranium extraction (PUREX).[21] The PUREX process has been used at the industrial level in France, Russia, Japan and United Kingdom to reprocess nuclear fuel. The UREX process has been proposed in the US and successfully tested on spent fuel at the laboratory scale.[22]

In the PUREX process, the zircaloy cladding is first removed and the spent fuel rods are dissolved in hot nitric acid. In the dissolution process, a part of Tc(0) is oxidized to TcO_4^- while the remainder is present in the undissolved solids (epsilon phase).[2] After dissolution, Tc is

extracted along with uranium as $UO_2(NO_3)(TcO_4)\cdot 2TBP$ into the organic phase using a tributyl phosphate (TBP) (30% in n-dodecane). Following extraction, Tc is back-extracted in nitric acid and vitrified in glass.[23]

In the UREX process, Tc is extracted with U in an organic phase with TBP. Both Tc and U are back extracted in a dilute nitric acid solution as TcO_4^- and UO_2^{2+}. Following back extraction, TcO_4^- and UO_2^{2+} are separated using anionic exchange resin, Tc would be converted to the metal after thermal treatment and incorporated in a metallic waste form for disposal. A demonstration has been performed in 2007 but the process has not been upscaled to the industrial level.[22]
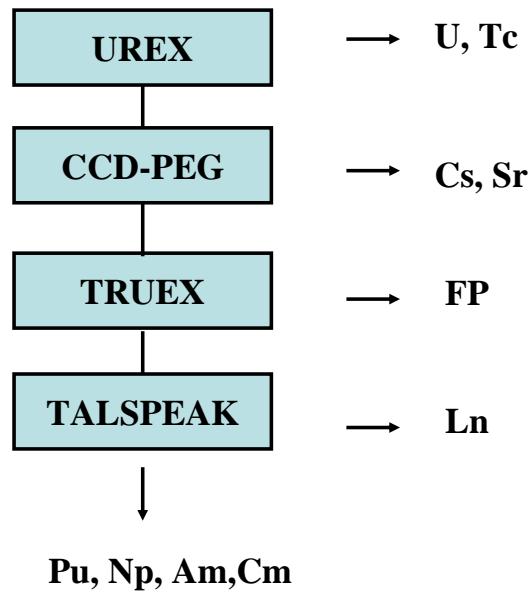
Figure 1.7. Flow sheet of the UREX +1 a process.

1.3.3 Technetium chemistry

The electronic configuration of Tc in the ground-state is $[Kr]4d^55s^2$. Technetium exhibits nine oxidation states from -1 to +7. A list of Tc compounds in various oxidation states is presented in Table 1.2. The most common geometries for Tc molecular complexes are octahedral and square pyramidal.

Table 1.2. Technetium compounds with oxidation states from -1 to +7, and their corresponding electron configuration in the d-shell.

ox	Tc config.	Compound
+7	d^0	$KTcO_4$
+6	d^1	$(TBA)TcNCl_4$
+5	d^2	$(TBA)TcOCl_4$
+4	d^3	K_2TcCl_6
+3	d^4	$(TBA)_3Tc(NCS)_6$
+2	d^5	$TcCl_2(PMe_3)_4$
+1	d^6	$K_5Tc(CN)_6$
0	d^7	$Tc_2(CO)_{10}$
-1	d^8	$[Tc(CO)_5]-$

Due to similar electronic configuration, group 7 elements exhibit similar chemical and physical properties, the chemistry of Tc resemble more to the chemistry of Re than the one of Mn.

Technetium exhibits three thermodynamically stable oxidation states : Tc(+7), Tc(+4) and Tc(0).

In aqueous solution, its chemistry is dominated by TcO_4^-, Tc(+4) hydroxo species and Tc metal

(Figure 1.8). In the following section, technetium compounds relevant to this study, are presented

and includes Tc metal, Tc binary oxides and pertechnetate salts.
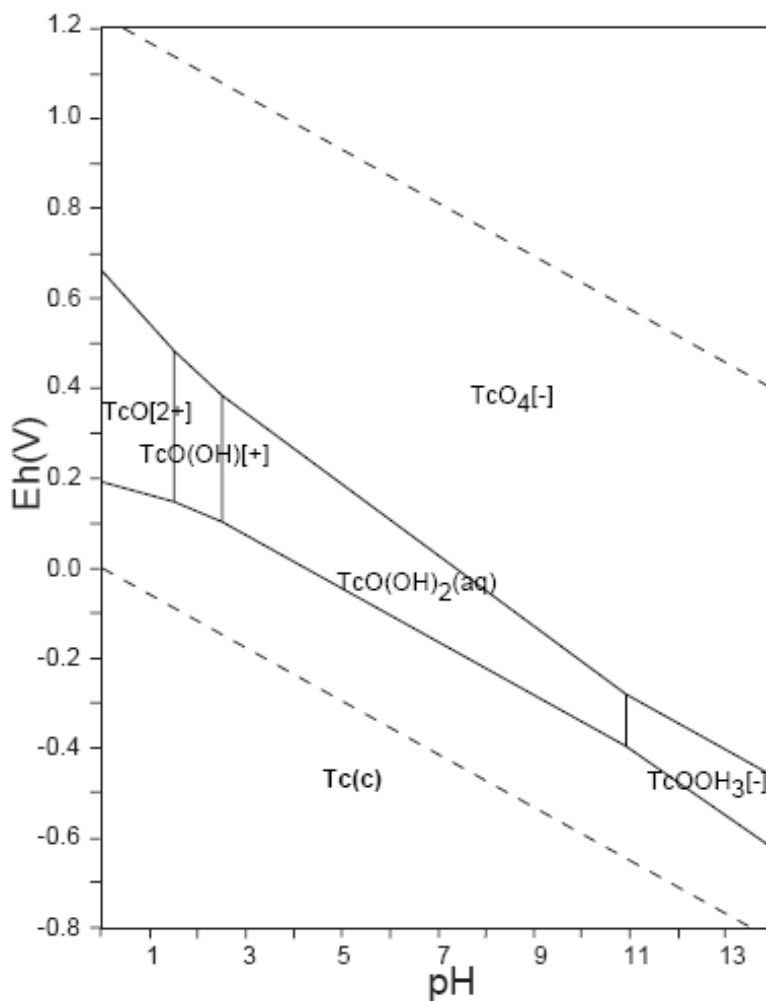
Figure 1.8. Eh-pH diagram of technetium in aqueous media.

1.4. Technetium compounds
1.4.1 Metallic technetium

Technetium metal can be prepared according 3 methods: hydrogen reduction of NH_4TcO_4 or TcO_2 at elevated temperatures, thermal decomposition of $(NH_4)_2TcX_6$ (X = Cl, Br) under inert atmosphere, and electroreduction of TcO_4^- in H_2SO_4.[24–27] The metal has a bright silvery grey color, it can be machined in different forms (rods, foils, plates, and wires).[28,29] Technetium metal crystallizes in the hexagonal close-packed space group P63/mmc (Figure 1.9), with a = 2.7364 Å and c = 4.3908 Å.[30] Technetium metal melts at 2167 °C, and boils at a temperature estimated to be 5173 °C. The metal has a density of 11.47 g/cm^3, its magnetic susceptibility at 298 K is 2.7 . 10^{-6} cm^3·g^{-1}.[31] Technetium metal is superconductor, its superconducting transition temperature (11.2 K) is the highest reported for a hexagonal metal.[32 ,33]
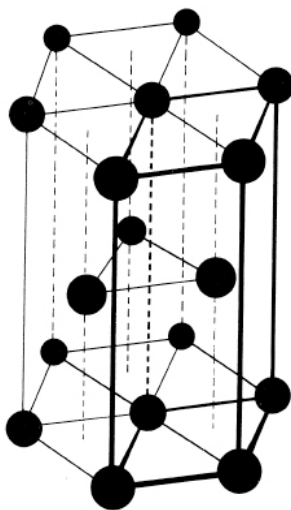
Figure 1.9. Ball and stick representation of the hcp structure of Tc metal.

Figure 1.10. Tc metal obtained after hydrogen reduction of NH_4TcO_4 (left) and electroreduction of TcO_4^- in H_2SO_4 on a Cu electrode (right).

1.4.2 Pertechnetate salts

Pertechnetate salts are most prevalent compounds for Tc in its highest oxidation state. The TcO_4^- anion exhibits a tetrahedral geometry (Figure 1.11), its UV-Visible (Figure 1.12) spectra displays two absorptions bands at 244 nm (ε = 5690 $M^{-1} \cdot cm^{-1}$) and 287 nm (ε = 2170 $M^{-1} \cdot cm^{-1}$) and resembles the spectra of its Re homologue.[34] A discussion of the pertechnetate salts is presented in the following section.

Kilogram quantities of NH_4TcO_4 can be obtained after treatment of spent nuclear fuel (Figure 1.11). Most of the ammonium pertechnetate used in the US is obtained from used nuclear fuel that has been treated at ORNL. The compound obtained from ORNL is black and needs to be purified (see Chapter 2).

Ammonium pertechnetate is a white solid, it crystallizes in the $I4_1/a$ space group with lattice parameters of a = 5.790 Å and c = 13.310 Å, [35] in TcO_4^- the average Tc-O bond distance is 1.702 Å . NH_4TcO_4 decomposes to TcO_2 after treatment at 700 °C under inert atmosphere.[36]
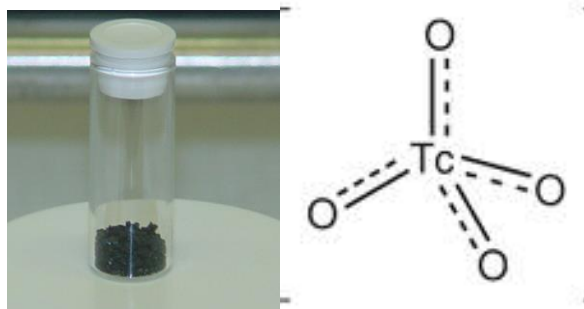
Figure 1.11. Impure NH_4TcO_4 from ORNL (left), schematic representation of TcO_4^- (right).
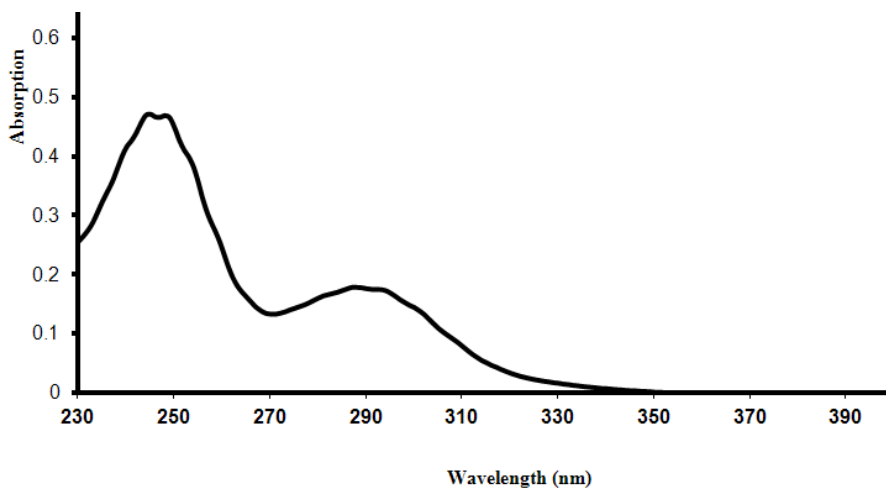
Figure 1.12. UV-Visible spectrum of TcO_4^- in H_2O.

Pertechnetate salts with the stoichiometry $MTcO_4$ (M = K, Rb, Cs) can be prepared after dissolution of NH_4TcO_4 in water and precipitation with MCl. The compound $NaTcO_4$ is prepared from the neutralization of $HTcO_4$ with NaOH or Na_2CO_3. Pertechnetic acid ($HTcO_4$) can be obtained after passing an aqueous NH_4TcO_4 solution through a cationic exchange resin.

The $MTcO_4$ (M = Na, NH_4, K, Rb) salts are isostructural and crystallize in the $I4_1/a$ space group. An increase of lattice parameter is observed when moving in the series NH_4, K and Rb (Table 1.3).[37,38,38,39] The lattice parameters for $KTcO_4$ are a = 5.654 Å and c = 13.030 Å. Potassium

14

pertechnetate melts at 540 °C and sublimes at 1000 °C without decomposition.[2] $CsTcO_4$ is orthorhombic with a = 5.718 Å, b = 5.918 Å, and c = 14.304 Å, and has a melting point of 790 °C.[40] Interestingly a linear relationship between the solubility and the polarizability (r/z) of the cation has been found for $MTcO_4$ (M = NH_4, K, Rb, Cs) (Figure 1.14).
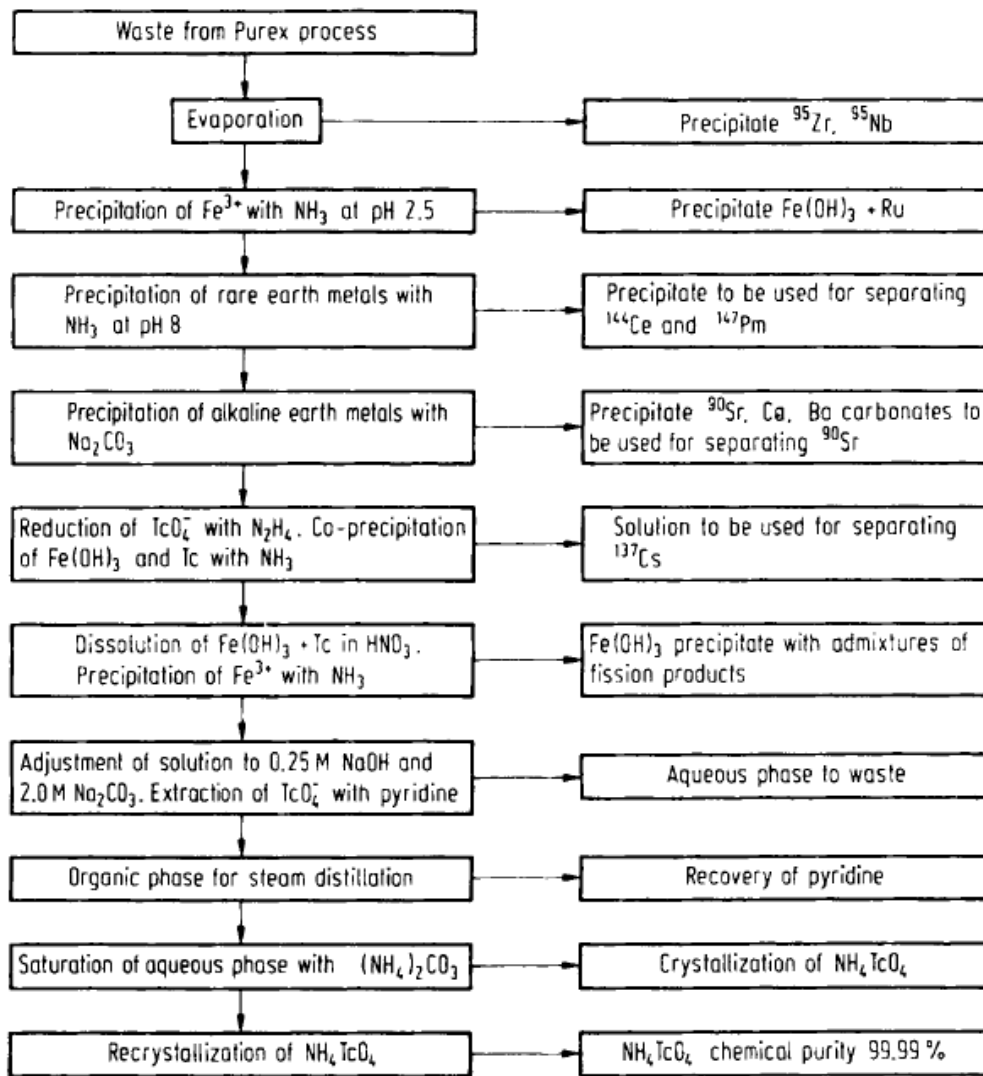
Figure 1.13. Production of NH_4TcO_4 from spent fuel reprocessing.[41]
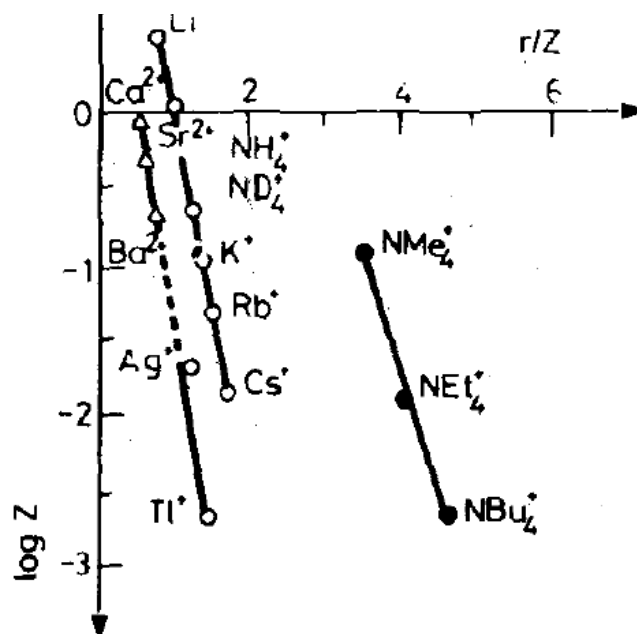
Figure 1.14. Log solubility versus cation polarizability (r/z) for $MTcO_4$ (M = NH_4, K, Rb, Cs).[1]

Table 1.3. Space group, lattice parameter and Tc=O distances in $MTcO_4$ (M= Na, K, Cs, NH_4) and melting point, solubility in water.

	$KTcO_4$	NH_4TcO_4	$CsTcO_4$	$NaTcO_4$
Space Group	$I4_1/a$	$I4_1/a$	P*nma*	$I4_1/a$
Tc = O (Å)	1.711	1.702	1.665, 1.763, 1.716	
Lattice Parameters	a = 5.630 c = 12/867	a = 5.775 c = 13.252	a = 5.726 b = 5.922, c = 14.36	a = 5.339 c = 11.869
Melt. Point (°C)	540	Decomp. 325	590	790
Solubility in Water per 100 g	2.13 g		0.412 g	67.7 g

1.4.3 Pertechnetic acid

Pertechnetic acid can be obtained by different methods: reaction of Tc_2O_7 with water, treatment of a $NaTcO_4$ solution through a cationic exchange resin or dilution of pertechnetate salts in concentrated sulfuric or perchloric acid. Diluted aqueous $HTcO_4$ solutions are colorless but a red color is observed upon concentration.[42] In a previous studies, it has been shown that the concentration of an $HTcO_4$ solution lead to the observation of a red color (for $Tc > 0.3$ M) and that the UV-visible spectra of the red solution exhibited a band centered at 585 nm.[42] Titration with Ce(IV) indicated that the red solution contained a reduced Tc species. It was shown that the red species is unstable in aqueous media and that brown solutions and precipitates were observed after addition of water and sodium hydroxide, respectively. It was proposed that the red solution contains Tc(VI) or Tc(V) species and that the reduction was due to the presence of dust, organic species, or natural contaminants in the reaction chamber.

Figure 1.15. Red compound obtained from the reaction of Tc_2O_7 and water.

Under oxidizing conditions and in the pH range 1-14, the aqueous chemistry of Tc(+7) is dominated by the pertechnetate anion. In high acid concentration, $[TcO_4]^-$ can be protonated and pertechnetic acid, $HTcO_4$, is formed. It has been shown that pertechnetic acid is formed above 7 M H_2SO_4 and 8 M $HClO_4$. The structure of $HTcO_4$ was studied by ^{99}Tc-NMR, UV-visible and XAFS spectroscopy. Experimental results and density functional calculations show pertechnetic acid to be an octahedral complex with the formula $[TcO_3(OH)(H_2O)_2]$ (Figure 1.16). The ^{99}Tc-NMR data were fit by allowing the pK_a and the chemical shifts of the unprotonated and protonated species to vary, $HTcO_4$ is a strong acid and its pKa was determined to be -4.9.
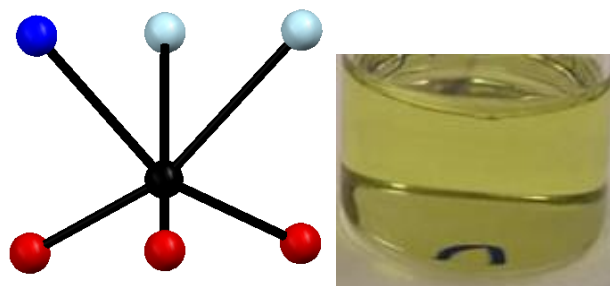
Figure 1.16. Ball and stick representation of $TcO_3(OH)(H_2O)_2$ (left) and solution of $TcO_3(OH)(H_2O)_2$ in 12M H_2SO_4 (right).

1.4.4 Technetium binary oxides
1.4.4.1 Ditechnetium heptoxide

Historically, Tc_2O_7 was first produced in 1952 from the reaction of Tc metal with dry oxygen at 400- 600 °C[43]; the reaction product, which consists of light yellow crystals, was first thought to be TcO_3, but it was confirmed that the compound contains Tc(+7).[43] Ditechnetium

heptoxide is a yellow hygroscopic solid, it melts at 119.5 °C [43] and boils at 310.6 °C, [44] its vapor

pressure was found to be 0.6 mm Hg at 100 °C.[44] Ditechnetium heptoxide is highly soluble in

water and forms $HTcO_4$ upon dissolution.[43]

The X-ray structure of Tc_2O_7 (determined at 293 K) was first reported in 1969 and found

to consist of centrosymetric $(O_{Ter})_3$-Tc-O_{Bri}-Tc-$(O_{Ter})_3$ linear molecules.[45] The structure of Tc_2O_7

has not been reported at low temperature and most of the theoretical work on Tc_2O_7 uses the room

temperature data to probe the accuracy of their theoretical methods. Other experimental methods

used to characterize Tc_2O_7 include gas, liquid and solid-phase Raman spectroscopy and [99]Tc- and

^{17}O solid-state NMR spectroscopy.[46,47,48] Interestingly, the Raman spectrum of Tc_2O_7 in the gas

phase was different than that of the one in the solid phase and indicated that Tc_2O_7 should exhibit

a bent structure in the vapor phase. Ditechnetium heptoxide has been also studied by theoretical

methods, but a comprehensive explanation why the Tc_2O_7 molecule is linear in the solid-state and

bent in the gas phase has not been reported.
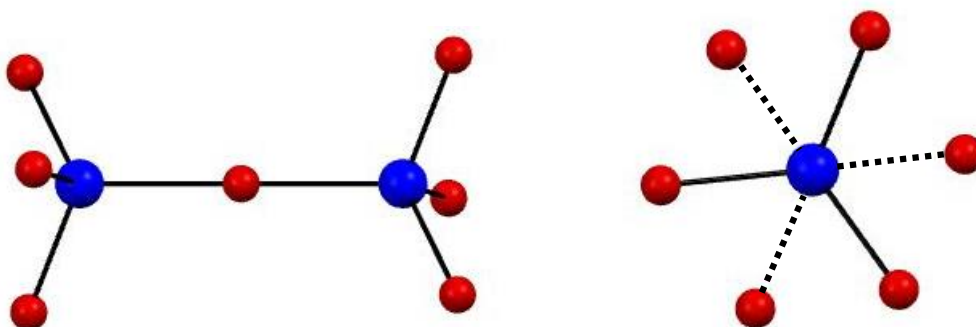
Figure 1.17. Left: ball and stick representation of Tc_2O_7 with a perpendicular view of the Tc-O_{Bri}-

Tc. Right: view along the Tc-O_{Bri}-Tc. Tc in blue and O in red.

Figure 1.18. From left to right are images of solid, liquid, and gaseous Tc_2O_7.

1.4.4.2 Technetium dioxide

Crystalline TcO_2 can be prepared by the thermal decomposition of NH_4TcO_4 under argon between 700 °C and 800 °C.[2,36] Technetium dioxide exhibits a distorted rutile structure and crystallizes in the monoclinic space group of *P2₁/c* with a = 5.689 Å, b = 4.754 Å, and c = 5.519 Å.[49] The structural unit in TcO_2 has three edge-sharing TcO_6 octahedra (Figure 1.19).[49] Tc-O bond lengths range from 1.96 Å to 2.01 Å and the Tc-Tc bond from 2.622 Å to 3.061 Å.[49,50] Technetium dioxide sublimes at 900 °C, and disproportionates to Tc metal and Tc_2O_7 above 1100 °C.[31,51] In the presence of oxygen, TcO_2 oxidizes to Tc_2O_7 and to TcO_4^- in aqueous acidic solution in the presence of Ce(IV) or alkaline / H_2O_2 solutions.[52] In water, the solubility of crystalline TcO_2 is 10^{-8} M.[53–55]
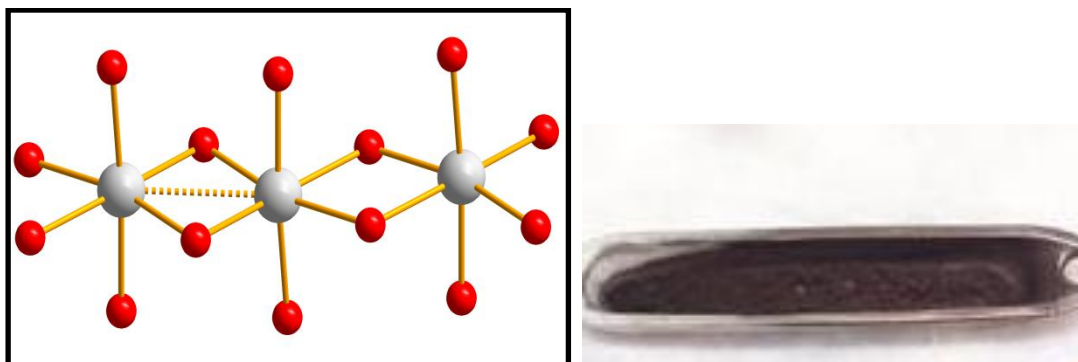
Figure 1.19. Ball and stick representation of TcO_2. (left). Image of crystalline TcO_2 in its reaction boat (right).

Hydrated technetium dioxide ($TcO_2 \cdot aq$) can be prepared from the electrochemical or chemical reduction of TcO_4^- in neutral and alkaline solutions.[52,56,57] Electrodeposits of $TcO_2 \cdot aq$ (Figure 1.20) were obtained by a cathodic reduction of neutral or alkaline pertechnetate solutions on platinum electrodes.[54] $TcO_2 \cdot aq$ has also been produced by the reduction of the TcO_4^- anion with hydrazine hydrate in a perchloric acid or with metallic zinc in hydrochloric acid.[58] Hydrated TcO_2 converted to crystalline TcO_2 in a nitrogen stream at 400 °C or at 250 °C under a vacuum.[2,59]
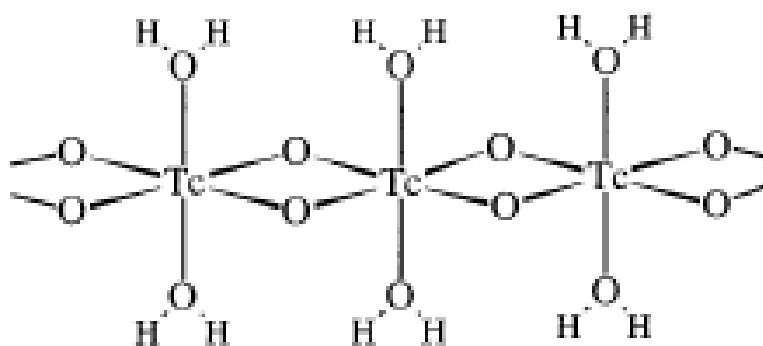
Figure 1.20. Structure of hydrated $TcO_2 \cdot xH_2O$.[54]

1.4.4.3 Ditechnetium pentaoxide

When Tc metal was burned in oxygen (400 °C - 600 °C), a red volatile Tc oxide and Tc_2O_7 were observed outside of the direct heating area of the furnace.[60] Based on the order of appearance of the species, it was thought that the red species was more volatile than Tc_2O_7. A sample of technetium metal was heated in oxygen for 3 months at 150 °C, and significant amounts of the red volatile oxide were obtained, and thought to be Tc_2O_5.[61] When technetium oxide of an unknown composition was treated to 900 °C in a Knudsen cell reactor, Tc_2O_5 was identified by mass spectrometry.[62] It was speculated that Tc_2O_5 should be stable in the solid-state.[62]

1.4.4.4 Technetium trioxide

Technetium trioxide was also reported to form as a volatile oxide at temperatures between 400 °C and 600 °C with no generation of Tc_2O_7.[60] It was attempted to produce TcO_3 by using sulphur dioxide to reduce Tc_2O_7, but only Tc metal formed. TcO_3 has been reported as a side product in the oxidation of Tc metal, and this appearance was black to reddish-purple color. It was then suggested that the darkening color of Tc_2O_7 is caused by the reaction of Tc_2O_7 with Tc_2O_5 impurity to form black TcO_3.[61] Gas chromatographic studies have been conducted and TcO_3 was reported to form in an oxygen stream at 1500 °C, but its chemical composition could not be proven.[63,64] Technetium trioxide was also observed from the mass spectra as a significant vapor species when technetium oxide was exposed to low pressure of oxygen at 900 °C.[62] Attempts to prepare TcO_3 using the method reported for the preparation of ReO_3 (i.e., decomposition of Re_2O_7 dioxane adduct) were unsuccessful.[49] The thermal treatment of Tc_2O_7 in dioxane produced TcO_2.
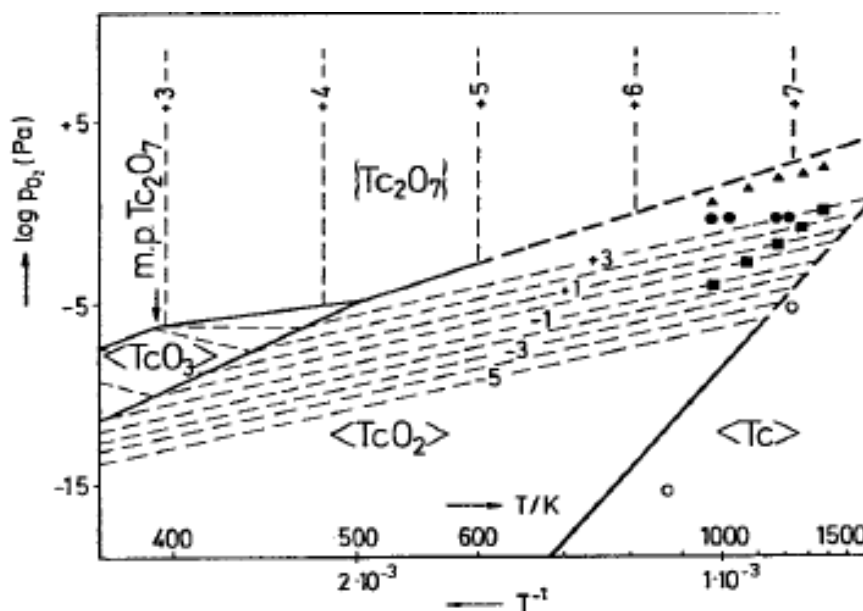
Figure 1.21. Theoretical Tc oxides temperature predominance diagram.[65] The dashed lines represent the vapor pressure of the heptoxide [$\log p(\text{Pa})$]. Note that TcO_3 has a very narrow domain of existence.

1.5   Synopsis

The isotope ^{99}Tc is a component of the low level radioactivity waste at the Hanford site. In the waste, it is primarily present in the heptavalent state as TcO_4^-. One option for the management Tc at the Hanford site is its vitrification into a borosilicate glass. The behavior of Tc during vitrification is problematic, as it volatizes and only a fraction is retained in the glass. Minimization of Tc volatility is a challenge for the development of safe vitrification processes. The nature of the volatile technetium species has been discussed and $HTcO_4$, Tc_2O_7 and alkali pertechnetate salts have been proposed. Until now, no characterization of the volatile technetium species has been performed. In this context, the vitrification of Tc in simulated borosilicate glass was performed

23

and the volatile Tc species characterized by X-ray absorption fine structure (XAFS) spectroscopy. In order to better understand the mechanism of formation of volatile Tc species, the chemistry of Tc_2O_7, $HTcO_4$ as well as the red volatile species were revisited.

The dissertation consists of the introduction, experimental methods (Chapter 2), results (Chapters 3 to 5) and a conclusion. In the experimental methods, the preparation of Tc precursors and glass samples, as well as the characterization techniques are presented.

In Chapter 3, the speciation of the volatile Tc species produced after vitrification of $NaTcO_4$ is studied. A volatile red species was obtained from the vitrification of technetium in glass, and was analyzed using XAFS spectroscopy. The nature of Tc in the glass was studied by scanning electron microscopy, XAFS, and sequential extraction.

In Chapter 4, the solid and gas-phase chemistry Tc_2O_7 is revisited. The structure of Tc_2O_7 has been studied by X-ray diffraction in temperature range 100 K and 275 K. The nature of the species in the gas phase after treatment of Tc_2O_7 at 450 °C was studied using electron-impact mass spectrometry. Density functional theory calculations were also conducted to compare the structure of Tc_2O_7 in the gas-phase and solid-phase.

In Chapter 5, the nature of the volatile red compound formed after oxidation of TcO_2 with O_2 and O_2/H_2O is studied. Crystalline TcO_2 was heated to 120 °C -250 °C and the resulting species was characterized by chemical titrations, UV-visible spectroscopy, mass-spectrometry and DFT methods.

Chapter 2: Experimental Methods

In this chapter, the materials, experimental methods and instrumentation used in this dissertation work are presented. Section 2.1 addresses chemicals and materials, and Section 2.2 focuses on experimental procedures that were employed for the syntheses of technetium precursors. Procedures that were used for the vitrification of technetium as well as the preparation of samples for GC-MS measurement are presented in Section 2.3. Characterization techniques are described in Section 2.4.

2.1   Chemicals and materials

All manipulations were performed in a laboratory designed for handling radioactive materials using efficient HEPA-filtered fume hoods, Schlenk techniques and following locally approved radiochemistry handling and monitoring procedures. Laboratory coats, disposable gloves, and protective eyewear were worn at all times. The chemicals and gases used during this dissertation work are presented in Table 2.1 and Table 2.2

Table 2.1 Gases used.

Gas	Purity (%)	Manufacturer
Argon	99.99	AirGas
20% O_2, 80% N_2	-	AirGas
10% O_2, 90% N_2	-	AirGas
Air	-	Praxair
Oxygen	99.99	AirGas

Pyrex tubes (L = 1 m, 10 mm outer diameter, 8 mm inner diameter) and quartz tubes (L = 1 m, 10 mm outer diameter, 8 mm inner diameter) were obtained from Chemglass. The composition of Pyrex was: SiO_2 (83.34%), B_2O_3 (11.19%), Na_2O (4.08%), Al_2O_3 (1.33%), K_2O (0.04%). The furnace used was a Thermo Fisher Scientific Lindberg/Blue M Mini-Mite Clamshell furnace ($T_{max} = 1100 °C$).

2.2   Preparation of technetium solutions and solid-state compounds

Several technetium compounds were used: $KTcO_4$, aqueous solutions of $NaTcO_4$ and binary oxides (TcO_2 and Tc_2O_7). The pertechnetate salts were used in Chapter 3 for the study of the nature of technetium species formed during the vitrification in borosilicate glass.

The binary oxides were used in Chapters 4 and 5 for the study of Tc_2O_7 and the nature of the volatile species formed during oxidation of TcO_2.

These compounds were prepared from ammonium pertechnetate that was obtained from Oak Ridge National Laboratory as an impure black solid. Radiolytic autoreduction of NH_4TcO_4 to TcO_2 was the likely reason of the black color. Prior any use, NH_4TcO_4 was purified (see 2.2.1).

2.2.1 Ammonium pertechnetate

In a typical purification procedure, black impure NH_4TcO_4 (550 mg, 3.05 mmol) was placed in the Erlenmeyer (50 mL) along with a Teflon stir bar. Deionized water (6 mL), NH_4OH (500 μL), and hydrogen peroxide (50% by volume) (500 μL) were added. The Erlenmeyer was placed on a hotplate; the suspension was stirred and heated to 110 °C. The solid began to dissolve and the color of the solution changed from brown to a light pale yellow. Once the solid had dissolved (15 minutes), the volume of the solution was reduced by blowing Argon over it; upon volume reduction, a white solid precipitates. After the volume was reduced nearly to dryness, the Erlenmeyer was removed from the hotplate, the solid (NH_4TcO_4) was then washed with isopropyl alcohol (2 x 2 mL) and diethyl ether (2 x 2 mL). The solid (534 mg, 2.96 mmol) was dried overnight and transferred to a glass scintillation vial for storage (97.05% yield).
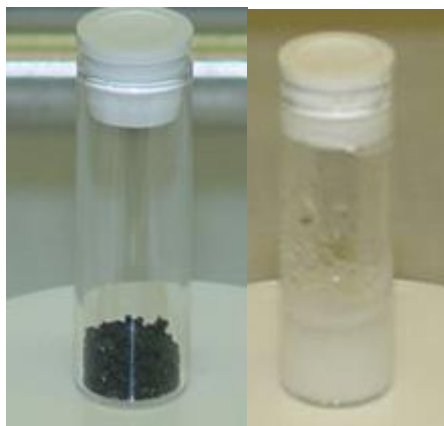
Figure 2.1. Impure ammonium pertechnetate (left) and purified ammonium pertechnetate (right).

2.2.2 Aqueous solution of sodium pertechnetate

A sodium pertechnetate aqueous solution was prepared by passing an aqueous solution of NH_4TcO_4 (534 mg in 6 mL of H_2O) through a cationic exchange resin (Dowex 50WX4-100). The column was 8 cm in height and 1 cm in diameter. The resin was initially washed with deionized water until the eluted product was clear and colorless. Afterwards, 30 mL of 1 M HNO_3 was added to the column and then eluted off with 50 mL of deionized water to remove the HNO_3. The NH_4TcO_4 solution (6 mL) was passed through to resin and eluted with H_2O (9 mL). The formation of $HTcO_4$ was followed with a pH paper and the elution was stopped when the pH was neutral. The resulting $HTcO_4$ solution was then neutralized with a saturated solution of sodium bicarbonate (1.8 mL, > 9g/100 mL) solution. The concentration of TcO_4^- (0.170 M) was determined by UV-Visible spectroscopy.

2.2.3 Potassium pertechnetate

In an Erlenmeyer flask, impure NH_4TcO_4 (628.6 mg, 3.47 mmol) was dissolved in 4.5 mL of deionized water. Potassium hydroxide (301.3 mg, 5.37 mmol), concentrated hydrogen peroxide (~ 60 μL) were added to the Erlenmeyer and the suspension heated to 110 °C on a hotplate. During the thermal treatment, a white solid ($KTcO_4$) precipitated. After 90 minutes, the Erlenmeyer was removed from the hotplate, the solution was allowed to cool to room temperature, and the supernatant was removed. The white solid was washed with isopropyl alcohol (3 x 2 mL), diethyl ether (3 x 2 mL) and then dried overnight in open air (638.8 mg, 3.16 mmol, 91.2% yield).

2.2.4 Technetium dioxide

Technetium dioxide was prepared according the method reported in the literature.[36] In a typical preparation, ammonium pertechnetate (2.72 g, 15.02 mmol) was evenly distributed in an 8 cm-long quartz boat using a disposable paper funnel. The quartz boat was placed in the middle of a 50 cm-long quartz tube that was fitted with O-ring joints. The quartz tube had previously been placed in a clamshell furnace. In the flowing gas setup, a water trap using an Erlenmeyer flask was set up to insure no excess technetium would escape from the system (Figure 2.4). After O-ring joints had been attached to the quartz tube, Argon was allowed to flow in the reaction tube for 15 minutes, the furnace was ramped to 700 °C (10 °C per minute) and the temperature hold at 700 °C for 2 hours before allowing the sample to cool to room temperature. During the ramping up, water was observed on the stopcock at ~ 350 °C; this phenomena was due to the thermal decomposition of NH_4TcO_4 (equation 2.1) The resulting black product (TcO_2) was collected and placed in a glass scintillation vial using a paper funnel (1.541 g, 11.77 mmol, 78.3% yield).

$$\textbf{Eq. 2.1.}\ NH_4TcO_4 \rightarrow TcO_2 + 2\ H_2O + 0.5\ N_2$$
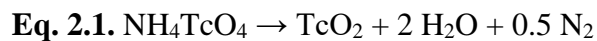
Figure 2.2. Technetium dioxide stored in a scintillation vial.

2.2.5 Ditechnetium heptoxide

Ditechnetium heptoxide was prepared in a sealed tube from the oxidation of TcO_2 with dry O_2 at 450 °C.[66] Using a long stem glass funnel, TcO_2 (23.4 mg) was placed in the sealed end of a 33 cm long Pyrex tube. The tube was connected to a Schlenk line (Figure 2.3) by thick wall Tygon tubing, evacuated, and gently flamed under vacuum to remove any residual moisture. The tube was backfilled with dry oxygen and evacuated and backfilled three additional times. After the last backfill, the end of the tube was immersed in liquid nitrogen. After 3 minutes of condensing oxygen, the tube containing TcO_2 was flamed sealed and allowed to reach room temperature. The tube was placed in the furnace, treated at 450 °C for 90 minutes and allowed to cool to room temperature. After the experiment, a yellow solid (Tc_2O_7) along with Tc_2O_7 crystals were observed on the tube (Figure 2.3). The crystals were used for the single crystal X-ray diffraction (SCXRD) measurements (See Chapter 3). Ditechnetium heptoxide is a highly hygroscopic compound; it can be kept only 5 minutes in air without apparent decomposition. Tc_2O_7 single crystals are stable up to 20 minutes in fluorinated oil (DuPont Krytox GPL106).

Figure 2.3. Single crystals of Tc_2O_7.

30

Figure 2.4. Experimental set-up used for the condensation of liquid O_2 into a glass tube.

2.3   Experimental procedures
2.3.1 Vitrification of technetium in borosilicate glass

The composition of the borosilicate glass used for the vitrification of technetium (Table 2.2) was provided by Pacific Northwest National Laboratory. In a typical vitrification experiment, the metal oxide mixture was placed in a platinum boat with a disposable wax paper funnel and distributed evenly throughout the boat. Then, a $NaTcO_4$ solution (0.170 M) was added to the glass mixture in the boat. The platinum boat was carefully placed in the middle of the quartz reaction tube; the experimental set-up is presented in Figure 2.6. A quartz wool trap was placed at the end of the reaction tube in order to capture the volatile Tc produced during experiment. The system was purged with breathing air for 15 minutes; the temperature was increased to 1100 °C and held at this temperature for 30 min. The sample was then allowed to cool to room temperature under flowing air.

Table 2.2. Metal oxide batch composition.

Oxide	Weight %	Oxide	Weight %
SiO_2	44.50	ZnO	3.43
Na_2O	21.27	ZrO_2	2.94
B_2O_3	9.79	CaO	2.46
Al_2O_3	5.97	MgO	1.45
Fe_2O_3	5.38	TiO_2	1.37

Figure 2.5. Glass that was vitrified at 900 °C in a platinum boat.

Figure 2.6. Flowing glass setup used for the vitrification of Tc in glass.

2.3.2 Preparation of samples for gas chromatography-mass spectrometry

2.3.2.1 Preparation under dry atmosphere

The experimental set-up used to prepare samples for mass spectrometry (MS) under dry O_2 atmosphere is presented in Figure 2.7. In a general preparation, technetium dioxide was added to the sealed end of a custom made reaction tube made by Joe Gregar, glass blower at Argonne National Laboratory (Figure 2.8). The reaction tube was connected to a Schlenk line, evacuated and gently flamed to remove residual moisture. After backfilling 3 times with dry O_2, the end of the tube was submerged for 3 minutes in liquid nitrogen. The apparatus was flame-sealed at 37 cm, and placed in a clamshell tube furnace. The 1.96 mm OD capillary, protected with a glass sheath containing Helium gas, was located outside the tube furnace. The system was ramped to temperature in the range 150 -450 °C (10 °C.min^{-1}), and held at those temperature for 3 hours - 2 days before allowing the furnace to cool to room temperature. After reaching room temperature, the tube was cut at 35 cm, immediately reconnected to a Schlenk line, evacuated and sealed at 27 cm. The outer glass sheath was then scored with a glass knife, hot spotted and removed. The inner capillary was then flame-sealed (L = 7.5 cm). The capillary was checked for external contamination and sent to the University of Zurich. A detailed preparation for Tc_2O_7 and red volatile samples is presented in Chapters 4 and 5.
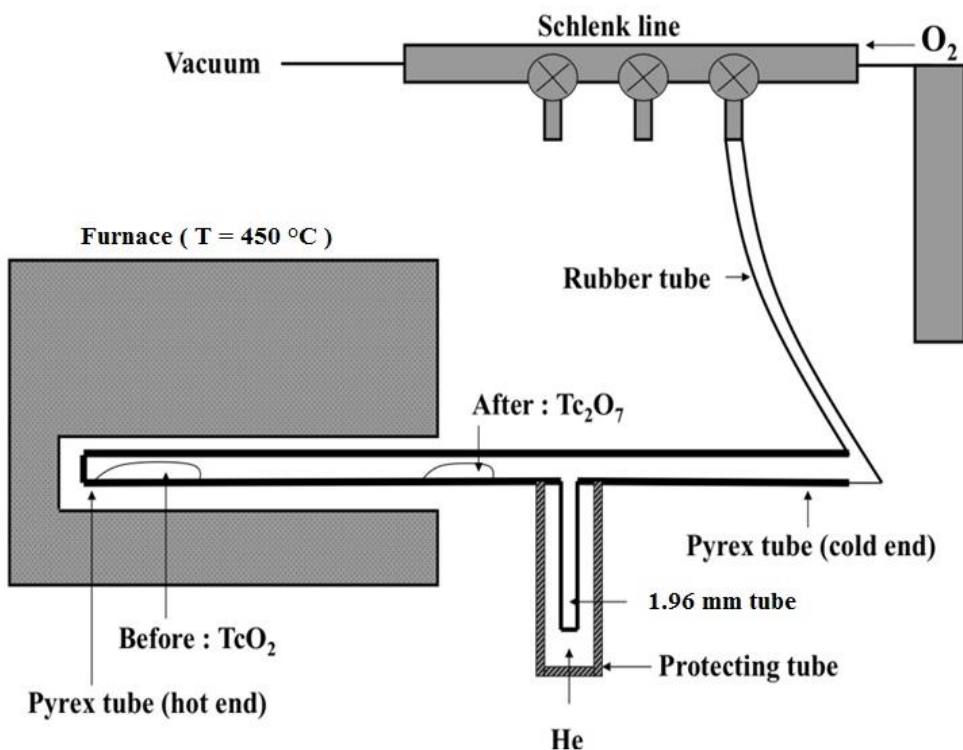
Figure 2.7 Schematic representation of the experimental setup used to prepare the Tc$_2$O$_7$ sample for MS measurement.

Figure 2.8. Specialty reaction tube with TcO$_2$(right) and the small capillary inside of Pyrex casing (left). The capillary was made from standard 2 mm outer diameter (OD) Pyrex tubing. The closed (test tube) end was submerged in 48% aqueous HF until the OD was reduced to 1.96 mm. This exactly matches the OD of the aluminum sample cups that fit into the MS probe.

2.3.3 Preparation under wet O$_2$ atmosphere

The experimental set-up for the preparation of sample under wet O$_2$ atmosphere was almost identical to the one under dry atmosphere with the exception of having a water bubbler placed in front of the line.

In a general procedure, technetium dioxide was added to the sealed end of the custom made tube. The reaction tube was connected to a Schlenk line and evacuated. After backfilling 3 times with wet O$_2$, the tube was placed in the furnace with the small capillary located outside the tube furnace. The system was ramped to temperature in the range 150 -450 °C (10 °C.min^{-1}), and held at those temperature for 3 hours - 2 days under flowing wet O$_2$ before allowing the furnace to cool to room temperature. After reaching room temperature, the tube was cut, immediately reconnected to the Schlenk line, evacuated and sealed. The outer glass sheath was scored with a glass knife, hot spotted and removed. The inner capillary was then flame-sealed, checked for external contamination and sent to the University of Zurich. A detailed preparation of red species for under wet atmosphere is presented in Chapter 5.

2.4 Instrumentation and techniques
2.4.1 X-ray absorption fine structure spectroscopy

X-ray absorption fine structure (XAFS) spectroscopy allows the determination of oxidation state, as well as the chemical environment (distance and number of atoms) of an absorbing atom.[67] This technique can be used on liquid, crystalline and amorphous solid-state samples. Usually, it requires 1-10 mg of sample diluted into a matrix (boron nitride). The sample holder used at UNLV (Figure 2.9) allows the measurement of XAFS spectra in fluorescence and transmission modes.

Figure 2.9. XAFS sample holder for solid-state compound.

The XAFS spectra can be divided in two regions: the X-ray absorption near edge structure (XANES) and the extended X-ray absorption fine structure (EXAFS). The XANES spectrum usually lies within 30 eV of the main absorption edge, and allows one to obtain information on formal oxidation state as well as the local geometry around the absorbing atom. The EXAFS spectrum allows the determination of bond distances, coordination numbers, and neighboring elements around the absorbing atom.

For technetium, XAFS spectroscopy has been widely used to characterize compounds with molecular or extended structures; it has been used in the study of Tc binary chlorides, oxides and metal-metal bonded dinuclear complexes.[68] A correlation between oxidation state and shift of the absorption edge has been determined and the correlation used to determine oxidation state of new samples.[68] The absorption K-edge for Tc species in various oxidization states is presented in Table 2.2.

Table 2.3. Technetium K -edge relative shift (eV) to NH_4TcO_4 of Technetium compounds.[68]

Compound	K-edge shift	δ ox.	Compound	K-edge shift	δ ox
NH_4TcO_4	0	7	$Tc_2(CO)_{10}$	-9.55	0
$[Tc(ArN)_3]_2Hg$	-4.61	5	$TcCl_2(py)_4$	-11.21	2
$Tc(ArN)_3I$	-5.57	7	$[TcCl_2(PMe_2Ph)_2]_2$	-13.24	2
TcO_2	-6.95	4	Tc metal	-19.85	0

In this dissertation, XAFS spectroscopy has been used to study the nature of the species formed during the vitrification of Tc in borosilicate glass (Chapter 3) as well as the nature of the red species formed during oxidation of TcO_2 with O_2 at 180 °C (Chapter 5).
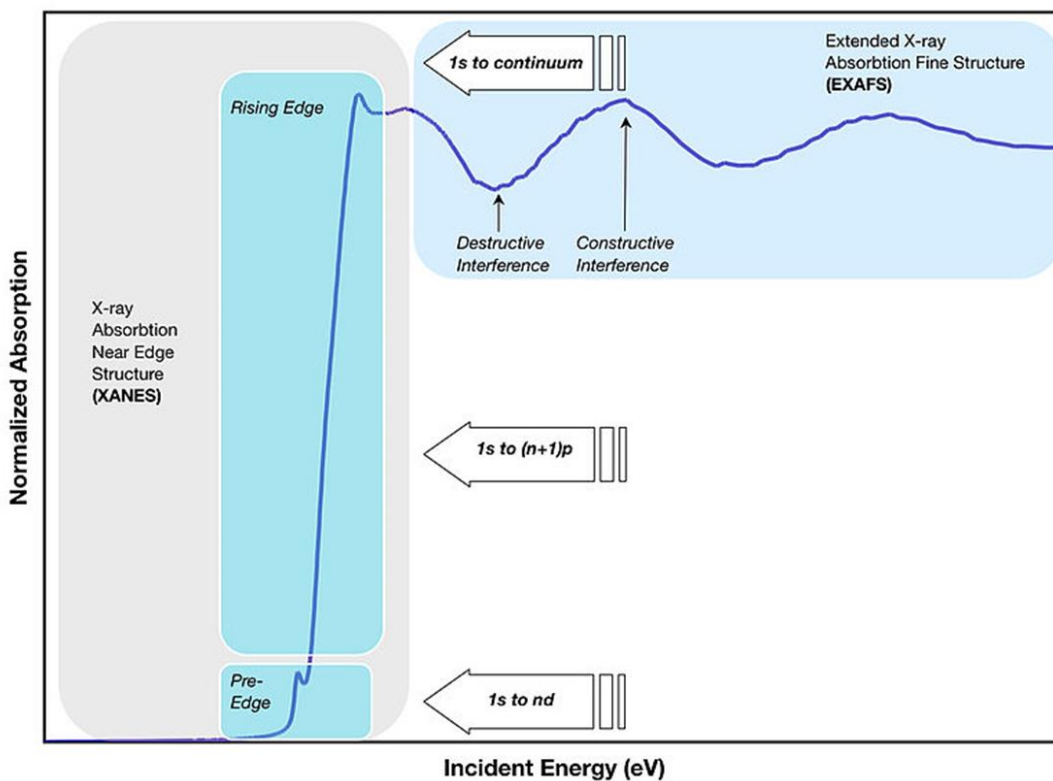
Figure 2.10. Illustration of XANES and EXAFS regions

The XAFS measurements were performed at the Advanced Photon Source at the BESSRC-CAT 12 BM station at Argonne National Laboratory in collaboration with Dr. Frederic Poineau (UNLV) and Dr. Sungsik Lee (Argonne National Laboratory). The samples were placed in aluminum holders with Kapton windows. The XAFS spectra were recorded at the Tc-K edge (21,044 eV) in transmission and/or fluorescence mode at room temperature using a 13 element germanium detector. A double crystal of Si (111) was used as a monochromator. The energy was calibrated using a molybdenum foil (Mo-K edge = 20,000 eV). The EXAFS spectra were extracted using Athena software,[69] and data analysis was performed using Winxas.[70] For the fitting procedure, the amplitude and phase shift functions were calculated by FEFF 8.2.[71] Input files were generated by Atoms.[72] Adjustments of the k^3-weighted EXAFS spectra were performed under the constraints $S_0^2 = 0.9$. For the XANES, the energy of the absorption edge was determined using the first derivative method.

2.4.2 Mass spectrometry

A mass spectrometer is an instrument that analyzes chemical species based on ions that are created by electron impact or chemical ionization and spectra that produce a mass to charge ratio. A heater vaporizes the samples and ions are accelerated through a magnetic field. This allows different masses to be observed by the detector and output a spectrum based on ion intensities. Pure samples and complex mixtures can be analyzed using this technique.

Electron ionization was one form of ionization used in these experiments. Molecules enter the mass spectrometer where they are bombarded with electrons of desired energy (eV). When the electrons interact with the molecule, the molecule M ionizes to M^+ and fragments and other

characteristic molecular ions of a lower mass to charge ratio (m/z) are created. Figure 2.11 illustrates the experimental set-up of a mass spectrometer. Data output for EI-MS are reported in relative intensity vs m/z. Mass spectrometry has already been use to determine the nature of other Tc species in the gas-phase. In those studies, Tc oxides or Tc metal were treated under various gaseous atmospheres (e.g., O_2, Cl_2, F_2) and new binary species (e.g., Tc_2O_5) were detected in the gase-phase.[73]

Chemical ionization is a lower energy process than EI that reduces the fragmentation. This technique requires a reaction gas which can produce ions that do not react with the gas of choice or have a very low reactivity.[74] Methane is the most common gas used
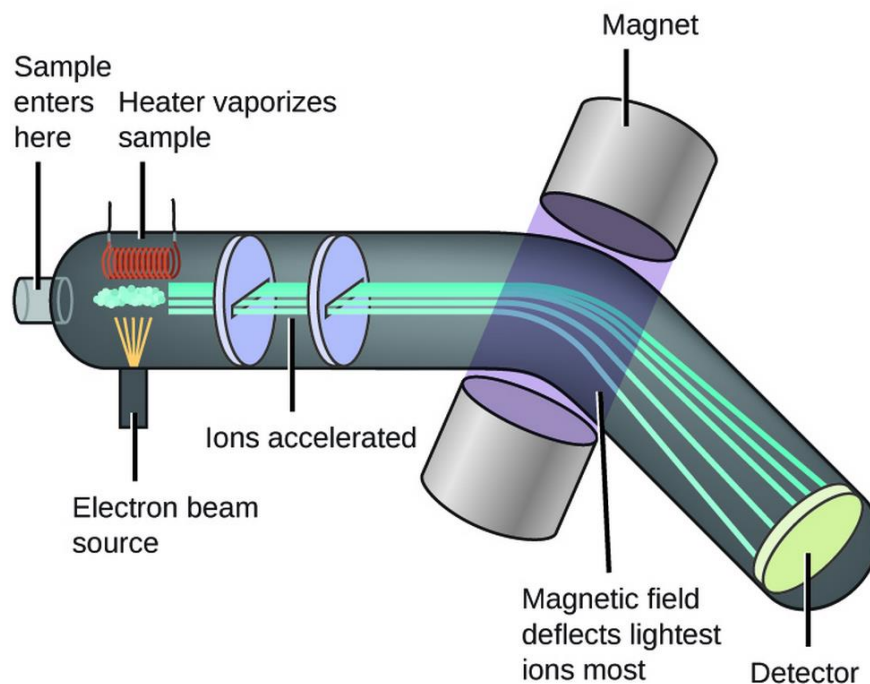
Figure 2.11 Schematic representation of mass spectrometry.

Mass spectrometry measurements were performed at the University of Zurich on a Thermo DFS (ThermoFisher Scientific, Bremen, Germany) double-focusing magnetic sector mass spectrometer (geometry BE). For EI-MS, mass spectra were measured in electron impact (EI) mode at 70 eV, with solid probe inlet, source temperature of 200 °C, acceleration voltage of 5 kV, and resolution of 7000. The instrument was scanned between m/z 30 and 800 at a scan rate of 2 s per decade in the magnetic scan mode. For CI-MS, mass spectra were measured in chemical ionization (CI) mode with iso-butane reactant gas at 130-200 eV, with solid probe inlet, a source temperature of 200 °C, an acceleration voltage of 5 kV, and a resolution of 2500. The instrument was scanned between m/z 30 and 900 at a scan rate of 2 s / decade in the magnetic scan mode. Perfluorokerosene (PFK, Fluorochem, Derbyshire, UK) was used for mass calibration. Before the mass spectrometry measurements, the small capillary was scored at the right length (~8.5 mm above test tube end), and opened. The capillary fragment was directly used as the sample holder for the EI-MS measurements. It was transferred to the mass spectrometer in tightly closed vials. The sample was introduced into a glove bag system, which was installed in front of the mass spectrometer and included the sample inlet. The Tc_2O_7 sample was mounted on the probe, which was then inserted into the mass spectrometer and evacuated (1×10^{-5} torr).

2.4.3 Scanning electron microscopy

Scanning electron microscopy (SEM) reveals the morphology of samples at the micrometric scales. In SEM, a beam of electrons interacts with sample causing electrons to lose energy. This energy exchange allows for the reflection of high energy electrons by way of elastic scattering and secondary electrons are produced by inelastic scattering. Energy dispersive X-ray

(EDX) spectroscopy provides elemental analysis by way of characteristic X-ray excitation. The SEM and EDX measurements were performed at UNLV in the microscopy laboratory on a JEOL model JSM-5610 scanning electron microscope that is equipped with secondary-electron and backscattered-electron detectors. Samples were prepared by placing glass pieces on carbon tape for conductivity. Samples were gold-coated to insure conductivity and placed in the evacuation chamber for analysis.

2.5.   Other techniques

Single crystal-ray diffraction was used to study the crystallographic structure of Tc_2O_7 (Chapter 5). Single crystal XRD data were collected on a Bruker Apex II system equipped with an Oxford nitrogen cryostream operating at 100 K. In the Apex II suite, data processing was performed using SAINT, the structure was solved with ShelXT and an absorption correction performed with SADABS. Structure refinements against F^2 were carried out using the SHELXL[75] refinement package in OLEX2-1.2.[76]

UV-Visible spectroscopy measurements were performed on a Cary 50 double beam spectrophotometer. Quartz cell with optical pathway between from 10 mm to 10 µm were used. UV-Visible spectroscopy is used as a speciation technique; technetium compounds in acid solution have characteristic spectra that allow one to estimate oxidation state. Absorption bands for TcO_4^- are presented in Table 2.4.

Table 2.4. Absorption maxima and molar absorbances of TcO$_4^-$ in aqueous solution.[34] Shoulders are given in parentheses.

λ [nm]	ε [M$^{-1} \cdot$cm^{-1}]	λ [nm]	ε [M$^{-1} \cdot$cm^{-1}]
292	2130	(258)	3380
287	2170	(253)	4830
(281)	2010	248	5690
(276)	1760	244	5690
(264)	2070	(240)	4990

In the present work, this technique has been used to quantify the TcO$_4^-$ and Ce(IV) in the chemical titrations and to perform the speciation of the red Tc species (Chapter 5). For TcO$_4^-$, (Table 2.4 and Figure 1.12) the extinction coefficients are respectively 2170 M^{-1}.cm^{-1} at 287 nm and 5690 M^{-1}.cm^{-1} at 244 nm. For Ce(IV) (Figure 2.12), the extinction coefficient is 2998 M^{-1}.cm^{-1} at 365 nm.
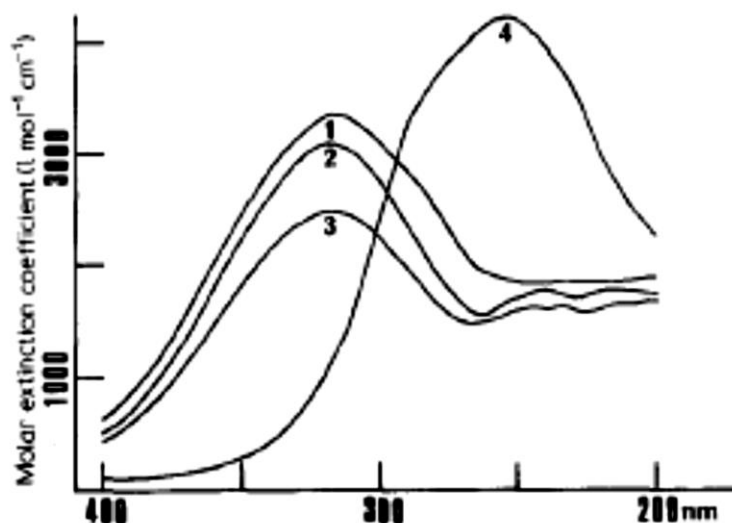
Figure 2.12. UV-Visible spectrum of Ce(IV) in different aqueous acidic solutions. Curve 1: 36N H_2SO_4; curve 2: 1N H_2SO_4; curve 3: 80% $HClO_4$; curve 4: 4 N H_3PO_4.[77]

Cerium titrations are used to determine the oxidation state of an element. In a typical Ce titration, the UV-Visible spectra of Ce^{4+} solution in 2M H_2SO_4 (4N) was recorded before and after reaction with the metallic species, the amount of Ce^{4+} consumed in the redox reaction ($Ce^{4+}c$) was used to calculate the oxidation state (n) of the Tc species (Eq. 2.2 and Eq. 2.3). In Eq. 2.3, Tc(7+) is the number of moles of TcO_4^- in solution after the reaction.

$$\text{Eq. 2.2. } nCe^{4+} + Tc^{n+} \rightarrow Tc^{7+} + nCe^{3+}$$
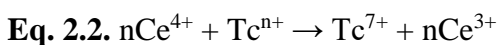
$$\text{Eq.2.3. } n = 7 - Ce^{4+}_c / Tc^{7+}$$

Raman spectroscopy has been widely used to characterize technetium oxides and pertechnetates.[78] In those experiments, the presence of bands at 910-956 cm^{-1} is a signature of Tc=O.[79] The vibrational frequencies for pertechnetate salts and Tc_2O_7 are presented in Table 2.3.

In the present work, Raman spectroscopy has been used to study the nature of the species formed after oxidization of TcO_2 (Chapter 5).

Figure 2.13. Jobin-Yvon Horiba T-64000 Raman Spectrometer (UNLV).
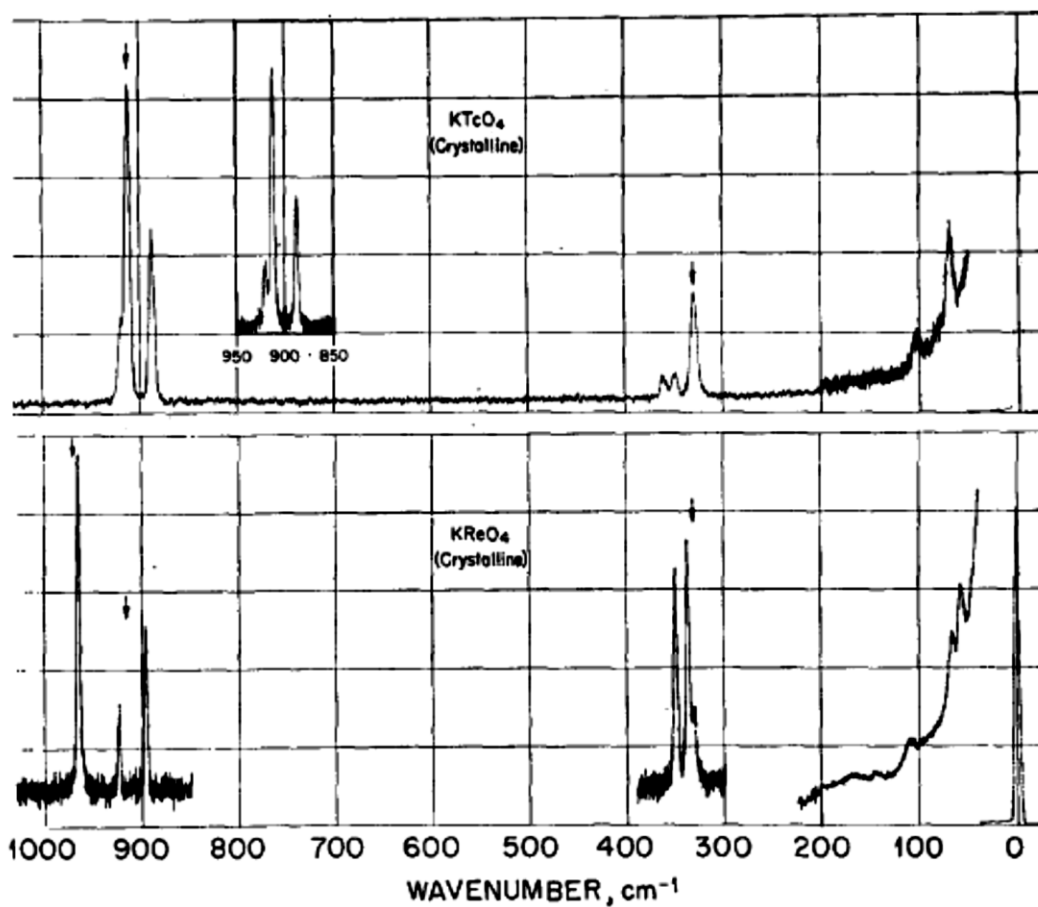
Figure 2.14. Raman spectrum of KTcO₄ (top) and KReO₄ (bottom).[79]
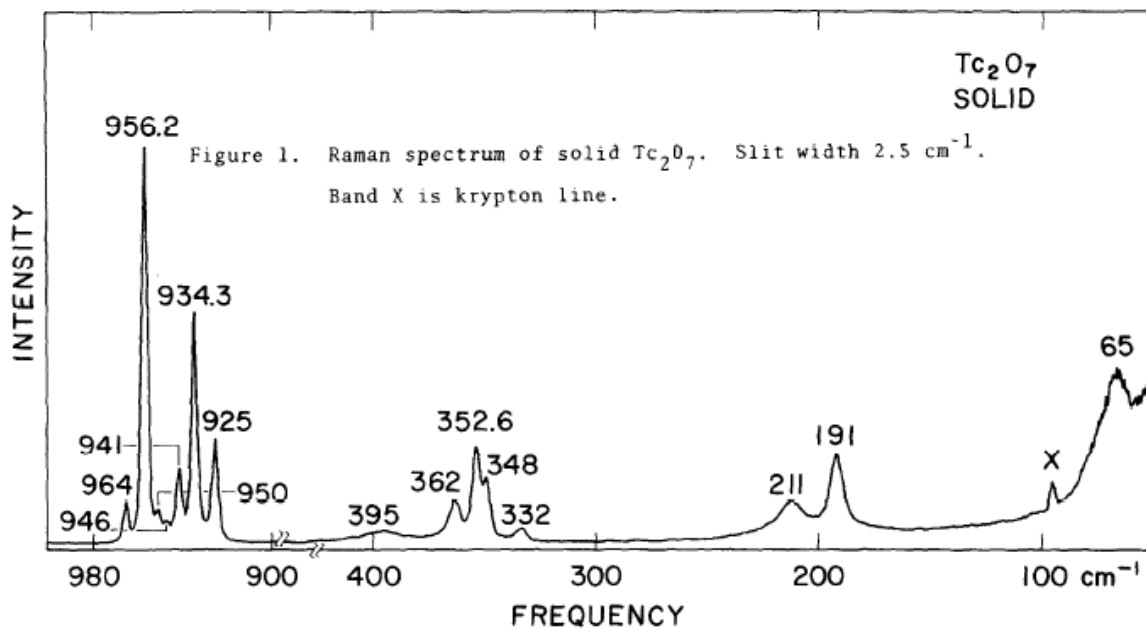
Figure 2.15. Raman spectra of solid Tc_2O_7.[47]

Table 2.5. Vibrational frequencies for NH_4TcO_4, $KTcO_4$, $Tc_2O_7(s)$, and $Tc_2O_7(g)$.

NH_4TcO_4 (cm^{-1})	$KTcO_4$ (cm^{-1})	Tc_2O_7(solid)(cm^{-1})	Tc_2O_7(gas)(cm^{-1})
912	920	956.2	957.3
325	913	934.3	955
	887	925	357
	360	352.6	340
	348	191	185
	327	211	178

Liquid scintillation counting (LSC) has been used for the determination of technetium concentration in solutions.[80] Samples were prepared by taking 100 µL of a given solution and added to 10 mL of ULTIME GOLD ABTM (Packard) scintillation cocktail. Analysis was conducted on a Perkin Elmer liquid scintillation counter Tri-Carb 3100TR with QuantaSmart software (Windows). A calibration curve was produced using $KTcO_4$ and used to compare results.

Theoretical calculations were used to analyze the solid-state and gas-phase structures of technetium binary oxides. Density Functional Theory (DFT) computational calculations were performed by Dr. Keith Lawler at UNLV. First-principles total energy calculations were performed using the plane-wave DFT as implemented in the Vienna *ab initio* simulation package (VASP) version 5.4.1.[81,82,83] Methods used involving this feature can be found in appendix section I. DFT calculations have already been used for the characterization of technetium species in solution, gas-phase and solid-state. At UNLV, the combination of DFT and spectroscopic techniques (XAFS and UV-Visible) have lead to major advances in understanding the chemistry of Tc(VII) in concentrated acids.[84,85,86]

Chapter 3: Nature of the Tc Volatile Species Formed During Synthesis of Borosilicate Glass

In this Chapter, the vitrification of $NaTcO_4$ in borosilicate glass under air in the temperature range of 600 °C to 1100 °C was performed. The nature of technetium in the glass as well as the nature of the volatile species has been studied. The speciation of Tc in the glass was studied by scanning electron microscopy, energy dispersive X-ray spectroscopy and XANES spectroscopy. The nature of the volatile species was studied by XANES and EXAFS spectroscopy. Using speciation data, the mechanism of formation of volatile species during vitrification is discussed.

3.1 Introduction

During the 1943-1987 time period, the Hanford site was the primary location for the production of plutonium for military applications in the United States. Decades of plutonium production have been accompanied by generation of large amounts of liquid and solid radioactive waste. There are over 55 million gallons of high level mixed waste located at the Hanford site. One of radioelements present in the Hanford site tanks is technetium, principally the isotope ^{99}Tc (~1500 kg).[87] In the waste, technetium is primarily present in the heptavalent state as TcO_4^-.[88] Waste tanks at the Hanford site contain ^{99}Tc that could potentially leak, and in the context of management of technetium, it is envisaged to incorporate Tc into a very resistant glass for long term storage.

The behavior of technetium during vitrification is problematic, as it volatizes (30% - 70%) and only a fraction is retained in the glass.[11] Minimization of technetium volatility is a challenge

for the development of safe vitrification processes. The nature of the volatile technetium species has been discussed; $HTcO_4$, Tc_2O_7 and alkali pertechnetate salts have been proposed.[6] Previous studies have focused on the speciation of technetium in the glass and until now, no characterization of the volatile technetium species has been performed.[13,14]

3.2 Speciation of Technetium in Borosilicate Glass
3.2.1 Preparation

A borosilicate glass with a composition similar to the one developed for vitrification of the low activity waste was used.[89] The compositions of the glass mixture have been taken from the literature and correspond to a glass mixture to be used at the Hanford site (Table 3.1).

A solution of sodium pertechnetate in H_2O ([Tc] = 0.170 M) was prepared after treatment of an $HTcO_4$ solution with Na_2CO_3 (see section 2.2.2) The vitrification experiments were performed under flowing air in a Lindberg Blue Mini-Mite tube furnace equipped with a 50 cm quartz tube. A representation of the experimental set-up is presented in Figure 2.6. The targeted temperatures for the studies were 600 °C, 700 °C, 800 °C, 900 °C and 1100 °C.

In a typical vitrification experiment, a glass mixture (~1.5 g) was put in a platinum boat and a solution of $NaTcO_4$ in water (470 µL, Tc = 8 mg) was added to the oxides mixture. The boat was placed in the 50 cm quartz tube and air was passed over the sample. The temperature was increased according to the ramping profile presented in Figure 3.1. The sample was kept for 30 minutes at the desired temperature after which it was cooled under flowing air. After reaching room temperature, the quartz boat was removed from the tube and the reaction product removed

from the boat. After the experiment, the glass samples were characterized using SEM, EDX and XANES spectroscopy.

Between 600 °C – 800 °C, two different products were obtained: a powdery material (Figure 3.2) and glassy material (Figure 3.2). For T > 900 °C, a single yellow-orange product was observed (Figure 3.2).
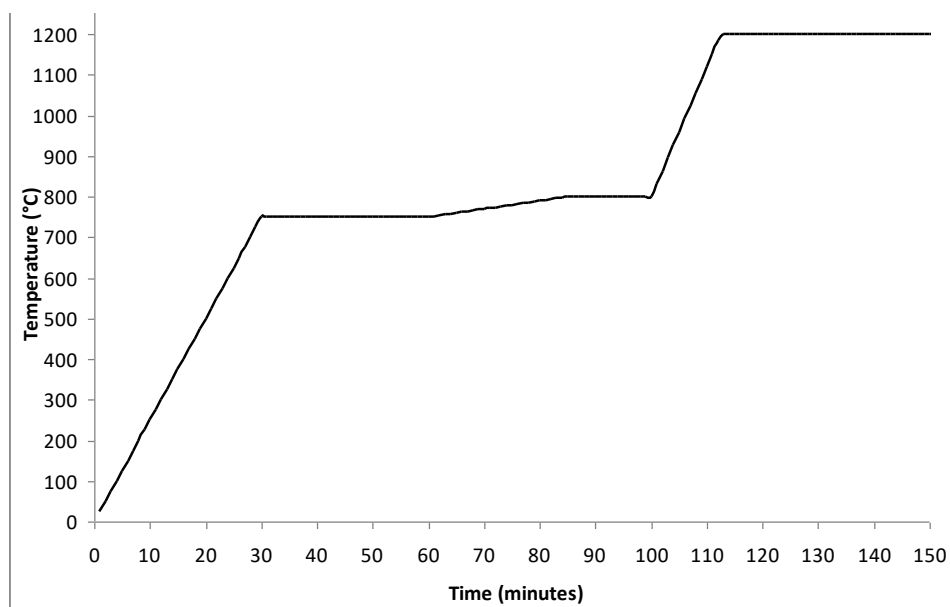
Figure 3.1. Heating profile temperature used to prepare sample.

Table 3.1. Mass (g) of the glass formers used to prepare borosilicate glass.

Compound	Al_2O_3	B_2O_3	CaO	Fe_2O_3	MgO	Na_2O	SiO_2	TiO_2	ZnO	ZrO_2
Mass (g)	5.97	9.79	2.46	5.38	1.45	21.27	44.5	1.37	3.43	2.94

Figure 3.2. Glass batch before (left) and after (right) adding the technetium solution.

Figure 3.3. Glass prepared under flowing air at 800 ° (right) and at 1100 °C (left).

3.2.2 Scanning Electron Microscopy/Energy Dispersive X-ray Spectroscopy

The distribution of technetium in the glass after vitrification at 1100 °C was studied by SEM and EDX. Figure 3.4 display SEM images of glass samples prepared at 1100 °C. The sample prepared at 1100 °C displays a smooth area (region A) over the majority of the glass surface as

well as a rough area (region B). EDX spectroscopy indicated that technetium is not uniformly distributed in the sample: Tc is absent on the smooth area (red) of the glass while it is present on the rough area (blue) (Figure 3.4). The Tc, Na, Si and O content (at. %) for the various areas is presented in Table 3.2.
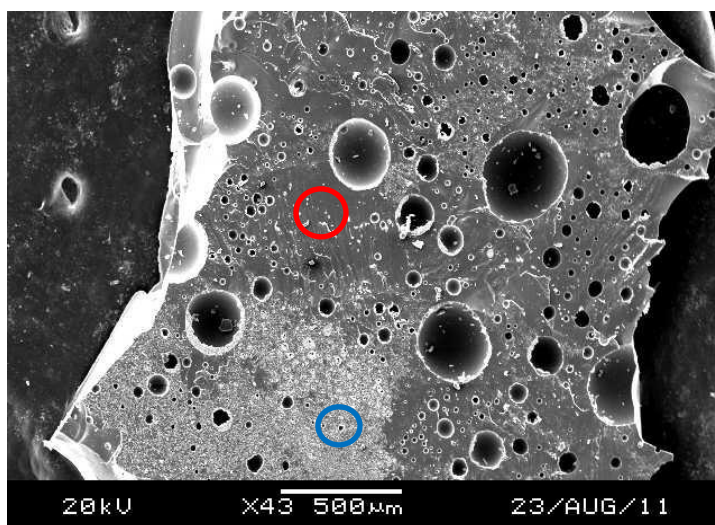
Figure 3.4 SEM image of glass product prepared at 1100 °C in air (x43). The red (region A) and blue circles (region B) indicate the areas where the EDX measurements were performed.

Figure 3.5 displays the SEM image of the sample prepared at 1100 °C at 2000 x magnification. EDX measurements show the presence of technetium (30%), oxygen (39%), sodium (19%) and silicon (8%); the Tc, O, and Na content are consistent with the presence of $NaTcO_4$.

Figure 3.5. SEM image of glass synthesized in air (x2000) at 1100 °C. The red circle (region C) indicates where the EDX measurement was performed.
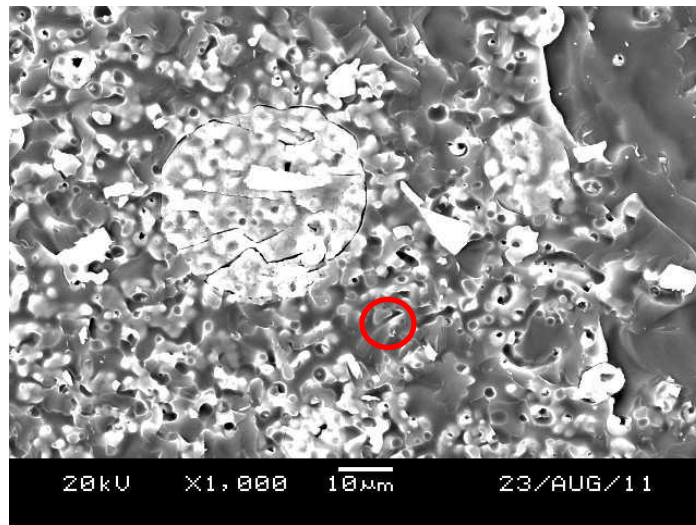
Figure 3.6. SEM image of glass synthesized in air (x1000) at 1100 °C. The red circle (region C) indicates where the EDX measurement was performed.

Another region of the glass sample prepared at 1100 °C was analyzed by EDX (Figure 3.7). The SEM/EDX analysis shows the presence of a small particle (10 µm) with a composition (27.5% oxygen, and 63.5% technetium) roughly consistent with that of TcO_2 (i.e., Tc = 75.5 w.t. %, O =

54

24.4 w.t %). This result indicates that some of the Tc(VII) has been reduced to Tc(IV) during the vitrification process. Those results are consistent with previous studies which show that the speciation of Tc in the glass after vitrification at 1000 °C under air consists of Tc(VII) (80 %) and Tc(IV) (20 %).[13]
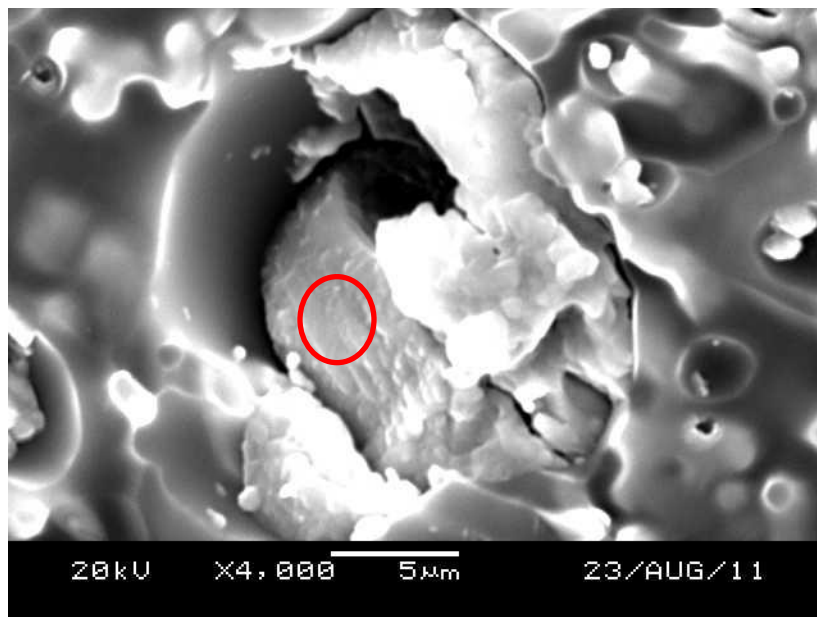
Figure 3.7. SEM image (x4000) and EDX spectrum of glass synthesized in air 1100 °C. The red circle (region D) indicates where the EDX measurement was performed.

3.2.3 XANES spectroscopy

In order to determine the speciation of Tc in the glass, samples were sent to the Advanced Photon Source for XANES measurements. Measurements were conducted on samples prepared

from the ranges of 600 °C to 1100 °C. The XANES spectra for the samples prepared at 600 and 800 °C are displayed in Figure 9. The XANES spectra of those 2 samples exhibit a strong pre-edge feature at 21,044 eV which is consistent with the presence of TcO_4^-.
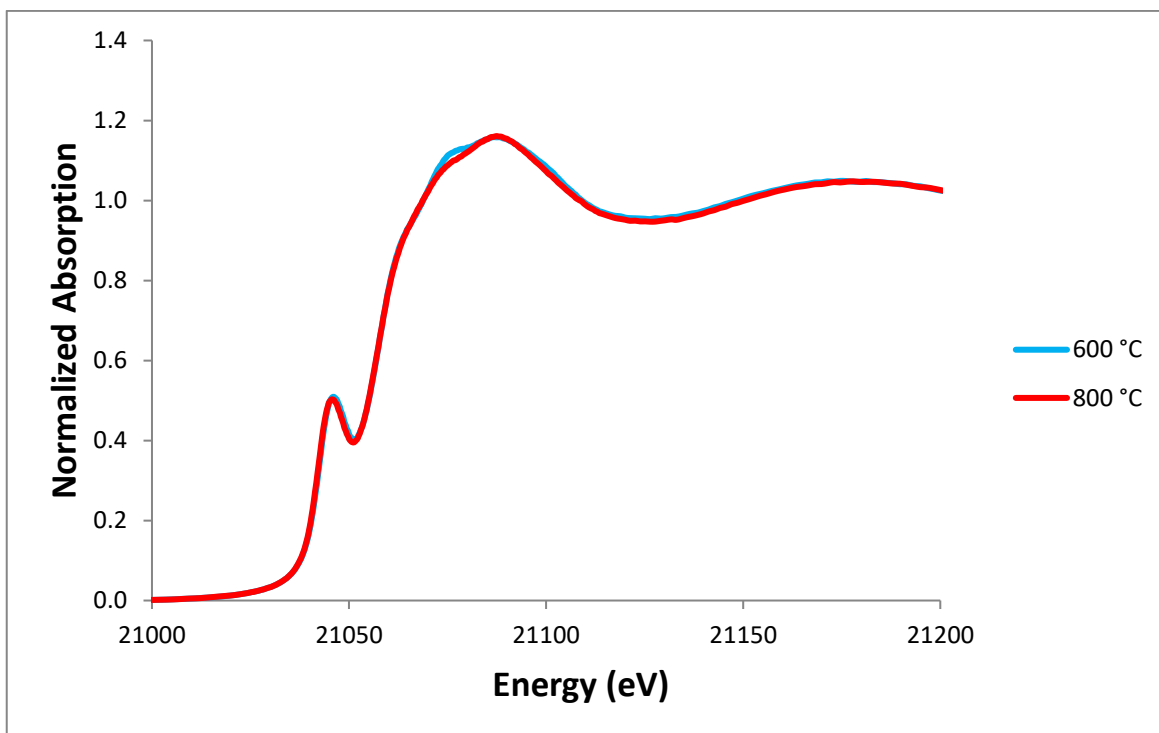
Figure 3.8. XANES spectra of the samples prepared at 600 °C and 800 °C.

The XANES spectra of the glass samples prepared at 900 °C, 1000 °C and 1100 °C are presented in Figure 3.9. The XANES spectra of those 3 samples, exhibit a pre-edge at 21,044 eV but the intensity of the pre-edge and the position of the edge absorption decrease when the preparation temperature increases. The XANES spectra of the sample prepared 1100 °C is consistent with the presence of both Tc(VII) and Tc(IV).
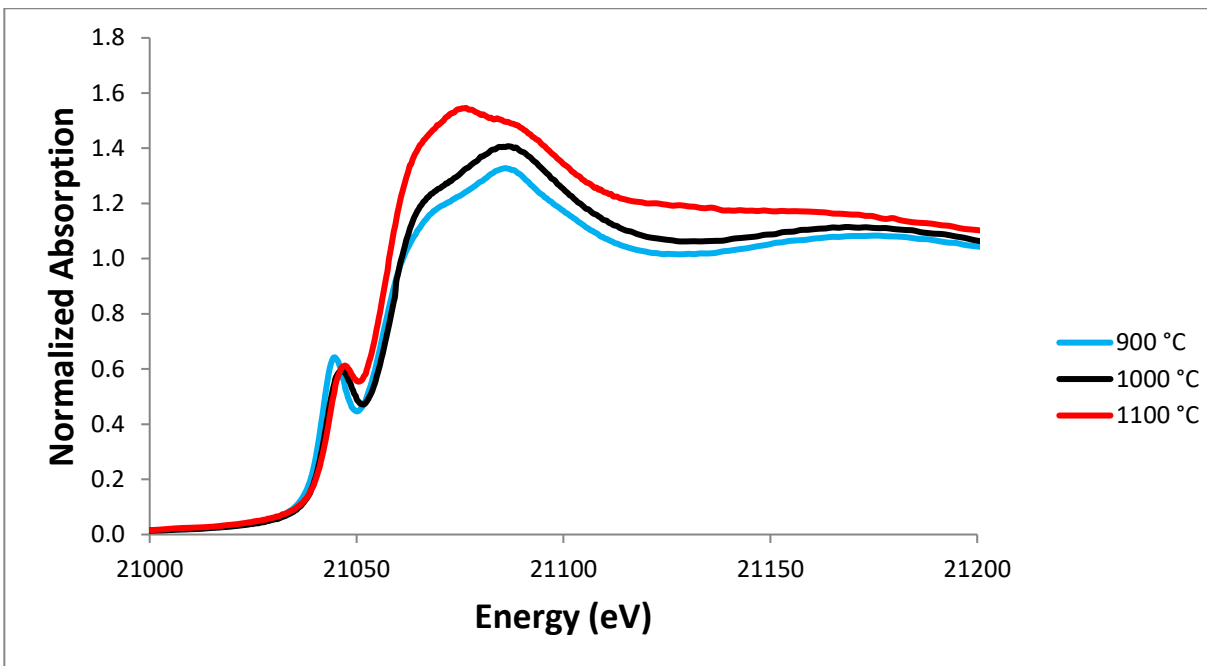
Figure 3.9. XANES spectra of the samples prepared at 900 °C, 1000 °C, and 1100 °C.

3.2.4 Extraction studies

Extraction studies using H_2O were performed on samples prepared after treatment of the glass mixture/NaTcO$_4$ samples between 600 °C to 1100 °C. Deionized water (15 mL) was added to the samples (1 gram) and placed on a shaker for 1 hour, 3 hours, 6 hours, and 12 hours. Afterwards 10 µL of the resulting solution was taken and placed in 10 mL liquid scintillation cocktail.

Samples prepared at T > 800 °C showed significantly lower activity than those prepared below 800 °C. This can be attributed to the morphology and surface area of the samples: samples

prepared above 800 °C are monolithic glass (small surface area) and while samples prepared at or below 800 °C are powdery and have large surface areas (Figure 3.2). The effect of contact time, preparation temperature, and morphology of sample on Tc retention is discussed.

3.2.4.1 Effect of contact time

The first variable that was monitored during extraction studies was contact time with water. The sample that was produced at 600 °C (Figure 3.10) had a gradual increase in activity as the contact time increased. This was expected, especially due to residual powder still on the sample. Activity in solution of the sample produced at 1100 °C decreased as contact time increased. This should have increased as well, especially since this was the first step in the extraction process. Uniformity of the sample could have contributed to mixed results. The activity of Tc in water as a function of the preparation contact time for glass sample prepared at 600 °C and 1100 °C is presented in Figure 3.10 and Figure 3.11.
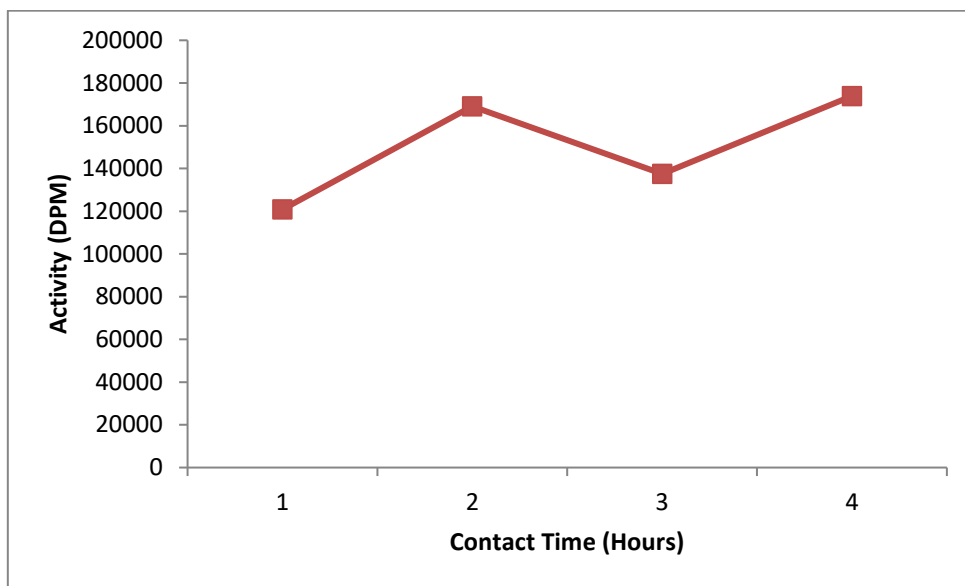
Figure 3.10. Activity of Tc in solution as a function of the contact time (1, 3, 6, and 12 hours) for the glass sample prepared at 600 °C.
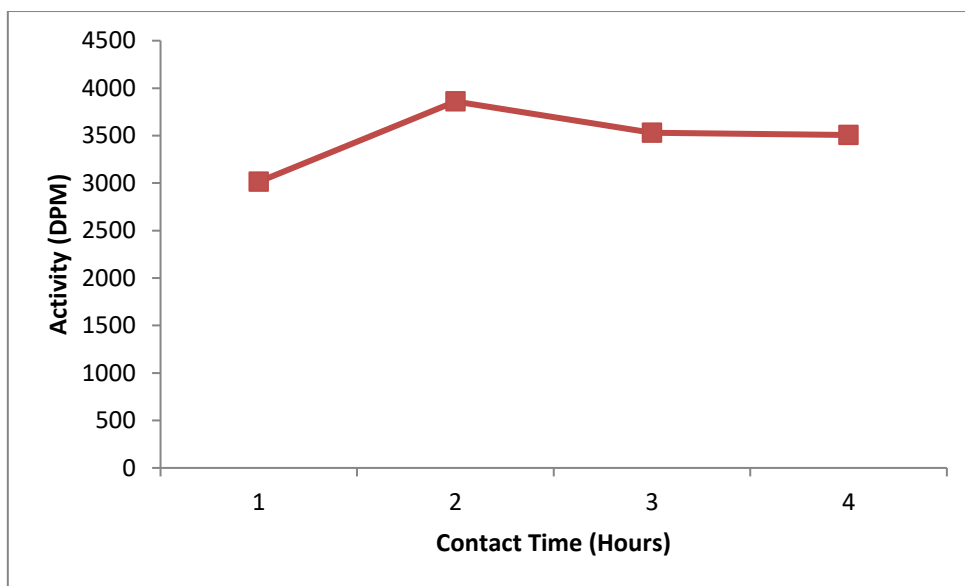
Figure 3.11. Activity of Tc in solution as a function of the contact time (1, 3, 6, and 12 hours) for the glass sample prepared at 1100 °C.

3.2.4.2 Effect of Preparation Temperature on Tc Retention in Glass.

The activity in solution decreased by two orders of magnitude from samples prepared at 600 °C to samples prepared at 1100 °C. The powdery samples prepared between 600 °C and 800 °C contain more activity than the glass samples synthesized at the same temperatures. The activity of Tc in water as a function of the preparation temperature after 1 and 12 hours of contact time are respectively presented in Figure 3.12 and Figure 3.13.
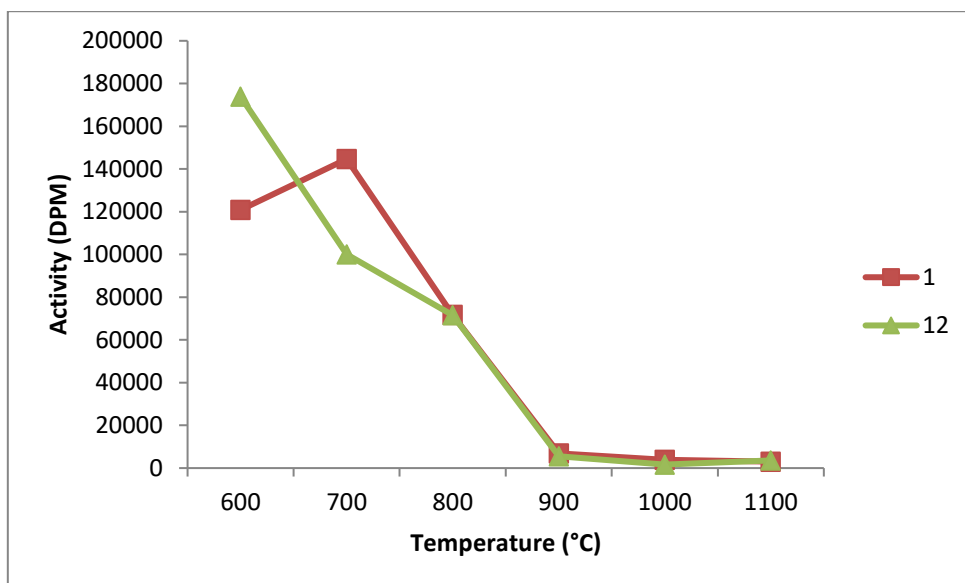
Figure 3.12. Activity of Tc in solution as a function of the preparation temperature (600 °C, 700 °C, 800 °C, 900 °C, 1000 °C, and 1100 °C) after treatment of glass sample with water. a) 1 hour and b) 12 hours.
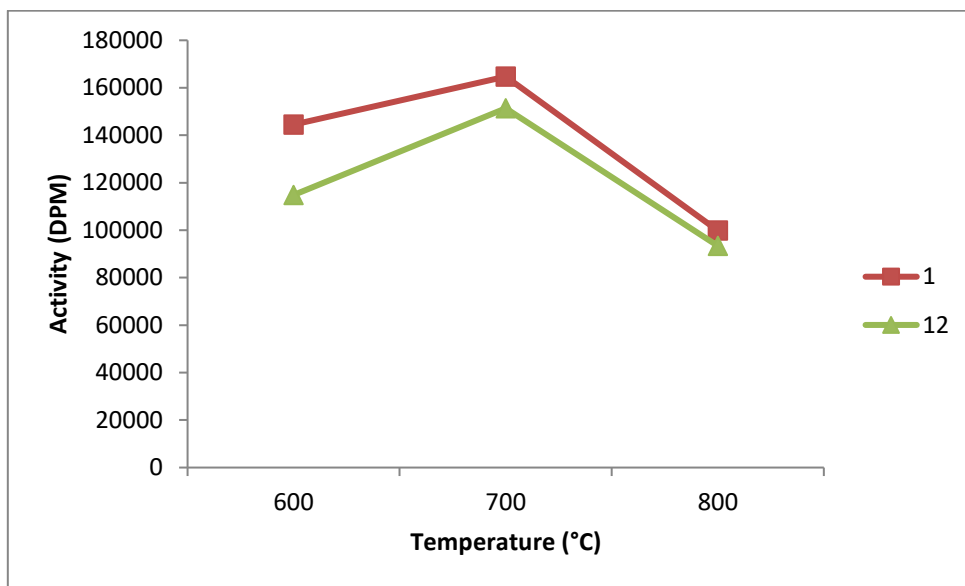
Figure 3.13. Activity of Tc in solution as a function of the preparation temperature (600 °C, 700 °C, and 800 °C) after treatment of powder sample with water. a) 1 hour and b) 12 hours.

The samples prepared at 800 °C and below are not homogenous and therefore had to be separated (Figure 3.3). Even in doing so, the activities of these samples at their synthesis temperatures was significantly higher for both the glass and the powder portions than any of the glass that made at temperatures of 900 °C and higher. There was not a significant change in activity between samples at 900 °C to 1100 °C.

3.2.4.3 Effect of sample morphology on Tc retention

Samples prepared between 600 °C and 800 °C, exhibit two phases (Figure 3.3). The activity of Tc in water after treatment of glass and powder sample as a function of the preparation temperature (600 °C, 700 °C, 800 °C) after 1 and 12 hours of contact are respectively presented in Figure 3.14 and Figure 3.15.

61
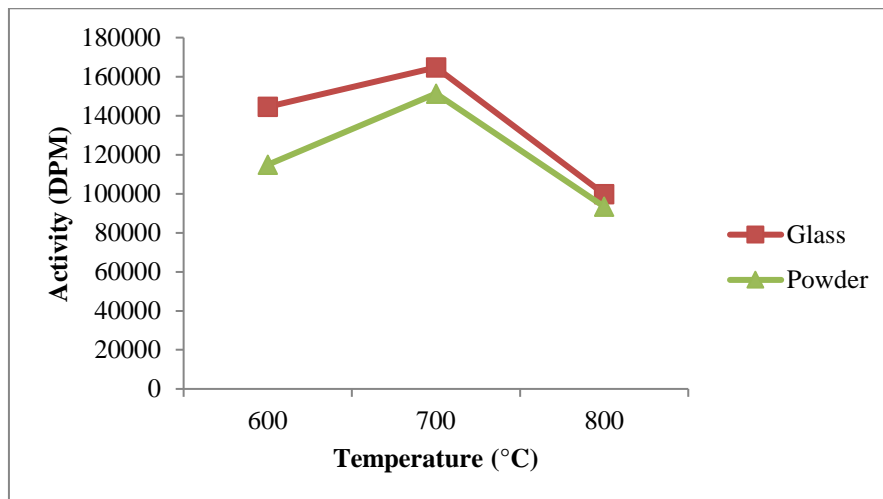
Figure 3.14. Activity of Tc in solution as a function of the preparation temperature (600 °C, 700 °C, 800 °C) after treatment of powder and glass samples with water after 1 hour of contact.
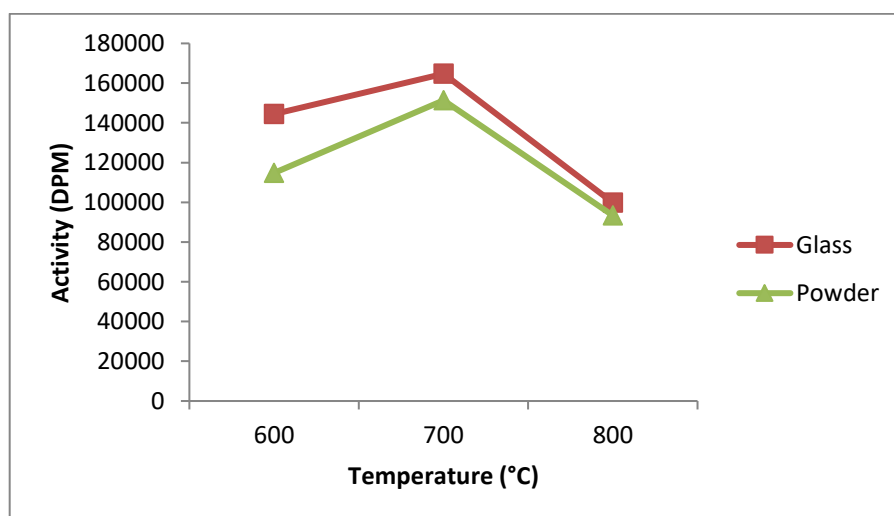
Figure 3.15. Activity of Tc in solution as a function of the preparation temperature (600 °C, 700 °C, 800 °C) after treatment of powder and glass samples with water after 12 hours of contact.

The morphology of these samples follows a similar trend with respect to activity versus

time. An increase in activity is observed from 600 °C to 700 °C, and then a decrease in activity is displayed at 800 °C. The powder has a lower activity than the glass portion of the sample, and this could be due to Tc preferentially incorporating in the glass portion of the sample.

3.3 Volatile Species Formed During Synthesis of Borosilicate Glass
3.3.1 Preparation of the sample.

The powder used for the glass preparation was prepared by the procedure presented previously (Table 3.1). The glass powder was weighed (1.477 grams) in a vial and the $NaTcO_4$ solution (470 µL, 0.0799 mmol) was added to the powder. The resulting powder/$NaTcO_4$ sample was dried at 90 °C for 12 hours and placed in a platinum crucible. The platinum crucible was placed in a 50 cm long quartz tube and positioned in a clamshell furnace so that crucible was located at the center of the furnace (Figure 3.16). A glass wool plug was placed inside the quartz tube in order to trap the volatile species. The apparatus was continuously purged with air from a cylinder that contained water (< 2 ppm). The temperature was slowly raised (10 °C per minute) to 1100 °C and held there for 30 minutes. No precautions were taken in the experiment to remove water from the system. During the thermal treatment, a red species (Figure 3.16) began to volatilize above 600 °C and condensed on the glass wool plug. After the experiment, the glass wool plug was removed from the tube and placed in an XAFS sample holder. This sample was then sent to the Advanced Photon Source for XAFS measurements.
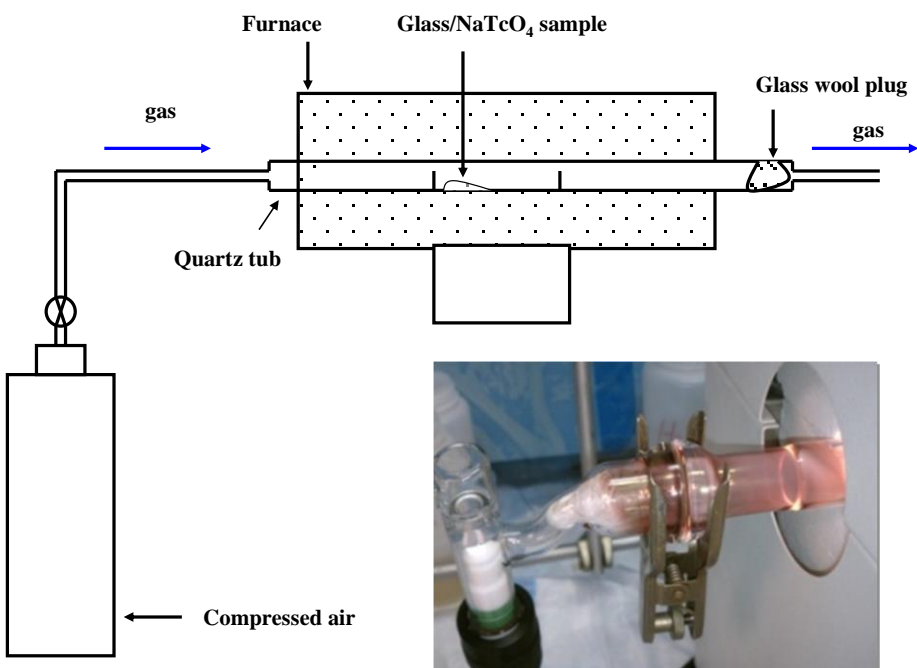
Figure 3.16. Experimental set-up used for volatility studies of technetium. Picture of the red volatile species obtained after treatment of the glass/NaTcO$_4$ sample at 1100 °C under air.

3.3.2 Characterization by XANES spectroscopy

The red volatile species that condensed on the glass wool was oily at room temperature, and its color was different from the one of alkali pertechnetate salts (white) and Tc$_2$O$_7$ (yellow). The nature of the red species was analyzed by XAFS spectroscopy. The XANES spectrum of the red species is presented in Figure 3.17. The position of the pre-edge (21,044 eV) is similar to the one of other Tc(VII) species (i.e., TcO$_4^-$ and TcO$_3$(H$_2$O)$_2$(OH)) and is consistent with the presence of Tc(VII) in the sample.[90]
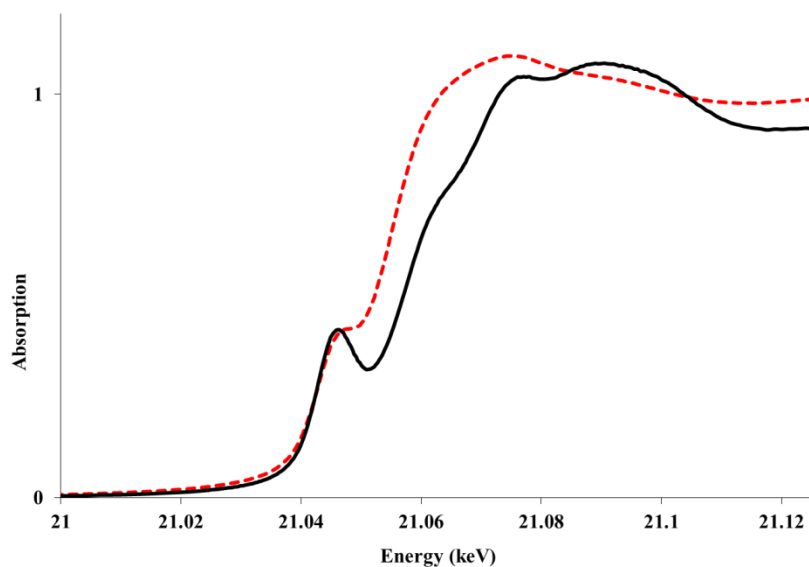
Figure 3.17. Normalized XANES spectrum of the red volatiles species (dashed line) and KTcO$_4$ (solid line).

3.3.3 Characterization by EXAFS Spectroscopy

The EXAFS portion of the spectrum was k^3-weighed and the Fourier transform (FT) performed in the k range [2-12] Å^{-1}. The FT shows one peak centred at R + Δ ~1.4 Å which is at the same position as in TcO$_4^-$ and indicates that the red species possesses Tc=O bonds. Further analysis of the FT indicates the absence of significant peaks above 2.5 Å, and indicates that dinuclear species such as Tc$_2$O$_7$ are unlikely. Simulated Fourier transforms of Tc$_2$O$_7$ exhibit an intense peak around 3.2 Å due to the Tc☐Tc and Tc☐O☐Tc scatterings.[90]

The EXAFS spectrum of the red species was fit using the scatterings calculated in $Tc_2O_7(H_2O)_2$.[90] The $Tc_2O_7(H_2O)_2$ species was modelled after the crystallographic structure of $Re_2O_7(H_2O)_2$ by replacing the Re atoms with Tc atoms. In order to determine the structure of the red species, various adjustments were performed considering: (1) Tc-O, (2) Tc=O, Tc-O, (3) Tc=O, Tc-O, Tc-Tc scatterings. The best adjustment, defined as a lower value of the reduced-chi^2, was obtained with the Tc=O and Tc-O scatterings. For the adjustment, the Debye-Waller factors of the Tc=O and Tc-O scatterings were fixed to the one determined in $TcO_3(OH)(H_2O)_2$ (i.e., σ^2Tc=O = 0.0022 Å^2, Å^{2}Tc-O = 0.004 Å^2). The $\Box$E$_0$ was constrained to be the same value for each wave; all the other parameters were allowed to vary.

The results of the adjustment (Figure 3.18, Table 3.2) indicate the environment of the absorbing atom to be constituted by 2.9(6) O atoms at 1.73(2) Å, 2.2(4) O atoms at 2.02(2) Å, and 0.8(2) O atoms at 2.18(2) Å. The results are consistent with the presence of an octahedral complex with a TcO_3^+ core coordinated to H_2O and/or OH ligands. The Tc=O and Tc-O distances found in the red species compare well with the one found in $TcO_3(OH)(H_2O)_2$ (i.e., 1.70(1) Å, 2.07(4) Å and 2.23(3) Å). The XAFS results indicate that a mononuclear species with a structure closely related to the one of $TcO_3(OH)(H_2O)_2$ is the dominant species formed during the volatilization of technetium.

Table 3.2. EXAFS fit parameters obtained for the red volatile species. $\Delta E_0 = 0.07$ eV.

scattering	C.N	Distance (Å)	σ^2 (Å^2)
Tc=O	2.9(6)	1.73(2)	0.0022
Tc-O	2.2(4)	2.02(2)	0.004
Tc-O	0.8(2)	2.18(2)	0.004
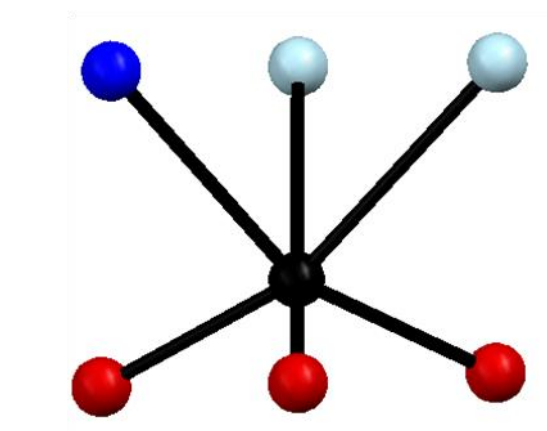
Figure 3.18. Ball and stick representation of $TcO_3(OH)(H_2O)_2$. Color of atom and ligands: Technetium in black, oxygen in red, OH in deep blue, H_2O in light blue.
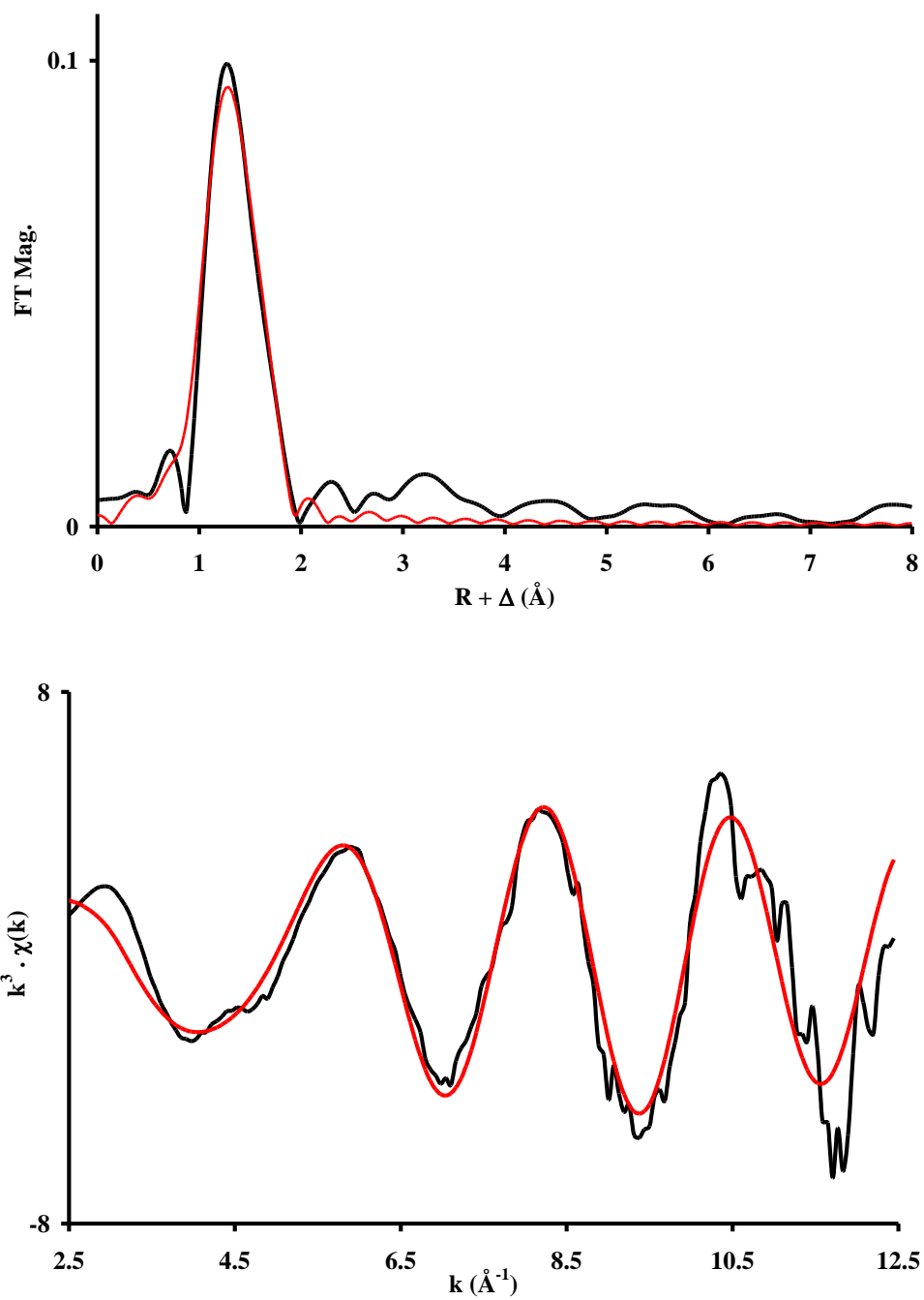
Figure 3.19. Fitted k^3-EXAFS (bottom) spectrum and Fourier transform (top) of the k^3–weighted EXAFS spectrum of the red species. Experimental data in black and fit in red.

The XAFS results are consistent with the one previously obtained from gas chromatography studies performed on Tc oxides or pertechnetate salts.[62,91] It was shown the treatment of Tc oxides or $KTcO_4$ with O_2/H_2O vapour at 950 °C produced mononuclear (i.e., TcO_3, $TcO_3(OH)$, $TcO_2(OH)_3$) and dinuclear species (i.e., Tc_2O_5 and Tc_2O_7). In those experiments, the predominant species was $TcO_3(OH)$ and dinuclear species coordinated to H_2O and OH ligands were not observed. In the gas phase, the $TcO_3(OH)$ consists of a TcO_3^+ core coordinated to an OH ligand, an arrangement also found in $TcO_3(OH)(H_2O)_2$. It is postulated that during vitrification, technetium is transported as $TcO_3(OH)$ in the gas phase and condenses in the presence of water as $TcO_3(OH)(H_2O)_2$ in the solid-state (Eq. 3.1).

Eq. 3.1. $\quad TcO_3(OH) + 2\ H_2O \rightarrow TcO_3(OH)(H_2O)_2$
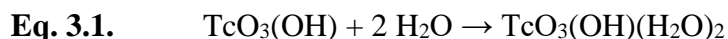
The formation of $TcO_3(OH)$ during vitrification can occur from different reactions:

a) Oxidation of Tc(IV) to Tc_2O_7 (Eq. 3.2) followed by the hydrolysis of Tc_2O_7 (Eq. 3.3). The presence of a mixture Tc(VII)/Tc(IV) in glasses synthesised at elevated temperature under air has been reported.[4]

Eq. 3.2. $\quad 2\ Tc(IV) + 7/2\ O_2 \rightarrow Tc_2O_7$

Eq. 3.3. $\quad Tc_2O_7 + H_2O \rightarrow 2\ TcO_3(OH)$
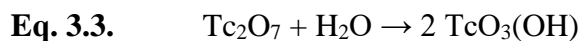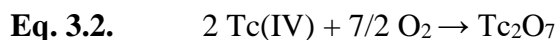
b) Reaction between $NaTcO_4$ and water (Eq. 3.4)

Eq. 3.4. $NaTcO_4 + H_2O \leftrightarrow TcO_3(OH) + NaOH$
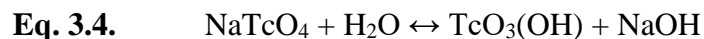
c) Thermal decomposition of $NaTcO_4$ (Eq. 3.5) followed by hydrolysis of Tc_2O_7 (Eq. 3.3)

Eq. 3.5. $2NaTcO_4 \rightarrow Na_2O + Tc_2O_7$

Because TcO_2 has been found in the sample prepared at 1100 °C and that treatment of pertechnetate salts in the temperature range 600-800 °C did not produce any red species. It is concluded that the formation of the volatile specie under air is due to the oxidation of Tc(IV) by O_2. The reaction products formed after the oxidation of TcO_2 by O_2 are presented in Chapter 4 and Chapter 5.

3.4   Conclusion

In this Chapter, the vitrification of sodium pertechnetate into borosilicate glass was performed under air at 600-1100 °C and the nature of Tc in the glass as well of the volatile species were characterized. SEM shows that technetium is not uniformly distributed in the glass and is present in the form of both Tc(VII) and Tc(IV). The cause of the heterogeneous distribution may be due to the nature of preparation of the sample, in which solution placed on batch materials and not mixed. Extraction studies indicated that a significant amount of technetium was not incorporated into the glass.

During the vitrifcation process, a red volatile species was observed above 600 °C. The nature of the red species was studied by XAS spectroscopy. The results were consistent with the presence of a mononuclear species with a structure closely related to the one of $TcO_3(OH)(H_2O)_2$. It was postulated that during vitrification, technetium was transported as $TcO_3(OH)$ in the gas phase and condensed as $TcO_3(OH)(H_2O)_2$ in the solid state. The formation of $TcO_3(OH)$ during vitrification can occur via different mechanisms, but all of them involve the reaction of a Tc(VII) species with water. The effect of temperature and water of the oxidation of TcO_2 under air are presented in Chapters 4 and 5.

Chapter 4: Ditechnetium Heptoxide Revisited: Solid-state, Gas-phase and First Principle studies

In this Chapter, the solid-state and gas-phase chemistry of Tc_2O_7 has been revisited. The X-ray structure of Tc_2O_7 has been measured at 100 K and the structural parameters compared with the ones previously obtained at 293 K. The mass spectrum of Tc_2O_7 has been recorded using EI-MS and the results compared with the ones previously obtained on Re_2O_7 and Tc oxide. Finally, the geometry of the Tc_2O_7 molecule in the solid-state and in the gas-phase was investigated by theoretical methods.

4.1   Introduction

Because ^{99}Tc is an important dose contributor in the Hanford waste and vitrification has been proposed as a method to immobilize high level nuclear waste, studies of the behavior of technetium during vitrification are of importance (see Chapter 1).[13] Previous studies have shown that Tc volatilizes during vitrification and various volatile species have been proposed,[6,92] one of them being Tc_2O_7. In this context, an understanding of the solid-state and gas-phase chemistry of Tc_2O_7 is of importance.

Transition metal binary oxides with the stoichiometry M_2O_7 are a rare family of compounds which are only encountered in Group 7.[93] The M_2O_7 oxides (M = Mn, Tc) crystallize as molecular solids while Re_2O_7 has a polymeric extended structure.[94,45,95]. Historically, Tc_2O_7 was first produced in 1952 from the reaction of Tc metal with dry oxygen at 400-600 °C;[43] the reaction product, which consists of light yellow crystals, was first thought to be TcO_3, but it was confirmed that the compound contains Tc(+7).[43] Ditechnetium heptoxide is a yellow hygroscopic solid, it

melts at 119.5 °C, [43] boils at 310.6 °C,[44] and its vapor pressure is 0.6 mm Hg at 100 °C.[44] Ditechnetium heptoxide is soluble in water and forms pertechnetic acid (HTcO$_4$) upon dissolution.[43]

The X-ray structure of Tc$_2$O$_7$ (determined at 293 K) was first reported in 1969 and found to consist of centrosymetric (O$_{Ter}$)$_3$-Tc-O$_{Bri}$-Tc-(O$_{Ter}$)$_3$ linear molecules.[45] The structure of Tc$_2$O$_7$ has not been measured at low temperature and most of the theoretical work on Tc$_2$O$_7$ uses the room temperature data to probe the accuracy of the theoretical methods. Other experimental techniques used to characterize Tc$_2$O$_7$ include gas, liquid and solid phase Raman spectroscopy, ^{99}Tc and ^{17}O solid-state NMR spectroscopy.[46,47,48] Interestingly, the Raman spectrum of Tc$_2$O$_7$ in the gas-phase is different than the one in the solid-state and indicates that Tc$_2$O$_7$ has a bent structure in the vapor phase. Ditechnetium heptoxide has been also studied by theoretical methods, but a comprehensive explanation why the Tc$_2$O$_7$ molecule is linear in the solid-state and bent in the gas-phase has not been reported. [96,97]

Because an understanding of the gas-phase chemistry of Tc$_2$O$_7$ is relevant to its behavior in the vitrification process, mass spectrometric studies are also of importance. In a previous study, the mass spectrum was recorded after reaction of a Tc oxide (presumably TcO$_2$) with O$_2$/H$_2$O at 950 °C.[73,62] The results showed that the main mononuclear species in the gas-phase was HTcO$_4$, while the main dinuclear species were Tc$_2$O$_5$ and Tc$_2$O$_7$. No mass spectrometric studies on pure Tc$_2$O$_7$ have been performed.

4.2   Single crystal X-ray diffraction study

The sample for SCXRD was prepared in a sealed tube from the oxidation of TcO_2 with O_2 at 450 °C. Using a long stem glass funnel, TcO_2 (22.6 mg) was placed in the sealed end of a 33 cm long Pyrex tube. The tube was connected to a Schlenk line by thick wall Tygon tubing, evacuated, and gently flamed under vacuum to remove any residual moisture. The tube was then backfilled with oxygen gas that was dried using Drierite column (28.9 cm in length and 6.65 cm in diameter) and evacuated and backfilled three additional times. After the last backfill, the stopcock was closed and a Dewar with liquid nitrogen was placed under the Pyrex tube and raised until 4 cm of the tube was submerged (3 minutes). This allows the oxygen to condense at the bottom of the tube and create a partial vacuum. The Pyrex tube (10 mm outer diameter, 9 mm inner diameter) was then sealed (L = 27 cm) and allowed to warm to room temperature. This yields an O_2:TcO_2 molar ratio of 6.6:1 respectively in the reaction tube. After reaching room temperature, the tube was placed in a Lindberg Blue Mini Mite clamshell tube furnace with the TcO_2 sample located over the thermocouple, the other end of the tube was located outside the furnace and glass wool was placed at both openings of the tube furnace. The furnace was slowly ramped to 450 °C (10 °C. min^{-1}) and held at this temperature for 3 hours before allowing the furnace to cool to room temperature without opening. After the reaction, all the TcO_2 was consumed and pale yellow needles (Tc_2O_7) were observed on the wall of the tube located outside the furnace (Figure 4.1), along with trace amounts of a volatile red species.

Figure 4.1 Tc_2O_7 crystals in sealed tube obtained after the oxidation of TcO_2 by O_2 at 450 °C.

The sealed tube containing Tc_2O_7 was taken out of the furnace and gently tapped on until multiple needles could be moved to one end of the tube. The tube was then scored using a glass cutter, and a heated glass rod was placed on the score to break the Pyrex tube. The pale yellow needles were immediately placed in fluorinated oil (DuPont Krytox GPL106), and a crystal was selected and mounted under the fluorinated oil on a Mitegen Micromount. The time between the opening of the Pyrex tube and the mounting of the Tc_2O_7 crystal on the diffractometer was approximately 20 minutes.

Refinement of the structure at 100 K indicates that Tc_2O_7 crystallizes in the orthorhombic space group Pbca with a = 7.312(3) Å, b = 5.562(2) Å, c = 13.707(5) Å, V = 557.5(3) Å^3. The lattice parameters and unit cell volume are smaller at 100 K than at 293 K (Table 4.1). Ditechnetium heptoxide is a molecular oxide consisting of centrosymmetric $(O_{Ter})_3$-Tc-O_{Bri}-Tc-$(O_{Ter})_3$ molecules with a Tc-O_{Bri}-Tc angle of 180°. The molecular species can be described as two corner-sharing distorted TcO_4 tetrahedra which are in a staggered (~D_{3d}) conformation (Figure 4.2). The Tc-O_{Bri} distance is 0.01 Å longer at 100 K than at 293 K (Table 4.1). The average Tc-O_{Ter} distances at 100 K and 293 K are 1.6872[6] Å and 1.672[6] Å, respectively. Further analysis indicates that the average O_{Bri}-Tc-O_{Ter} and O_{Ter}-Tc-O_{Ter} angles are comparable at both temperatures. Closer inspection of the Tc_2O_7 molecule reveals that the dihedral angles approach 60°, but are not equal. Binary transition metal oxides with the stoichiometry M_2O_7 are only found

75

for Group 7. The average $M-O_{Ter}$, $M-O_{Bri}$ distances and the $M-O_{Bri}-M$ angle for the M_2O_7 oxides

($M = Mn$, Tc, Re) are presented in Table 4.2. The reported structures of Re_2O_7 and Mn_2O_7 were

collected at 293 K and at 5 °C respectively. Analysis of Table 4.2, shows that an increase of the

$M-O_{Ter}$ distance occurs when moving down the series Mn, Tc, Re; a similar trend has been

observed for the MO_4^- anions ($M = Mn$, Tc, Re).[94,95]

In the solid-state, Tc_2O_7 adopts a staggered configuration approaching D_{3d} symmetry with

$Tc-O_{Bri}-Tc$ angle of 180°, while Mn_2O_7 has the C_{2v} structure with a $Mn-O_{Bri}-Mn$ angle of 120.7°.

The Mn_2O_7 molecule could be constructed from an *eclipsed* linear (D_{3h}) Mn_2O_7 molecule by

bending the $Mn-O_{Bri}-Mn$ angle to 120.7°. Previous studies indicated that in the gas-phase, M_2O_7

($M = Tc$, Re) should have non-linear structures and that in the solid-state the change of angle from

bent to linear when moving from Mn to Tc could be due to crystal packing effects.[94,45,95] The

packing of the Tc_2O_7 molecule in the unit cell is presented in Figure 4.3. The shortest distance

between two Tc_2O_7 molecules at 100 K (i.e., 4.594(2) Å) is shorter than the one at 293 K (i.e.,

4.661(2) Å). This is consistent with the expected thermal expansion behavior.
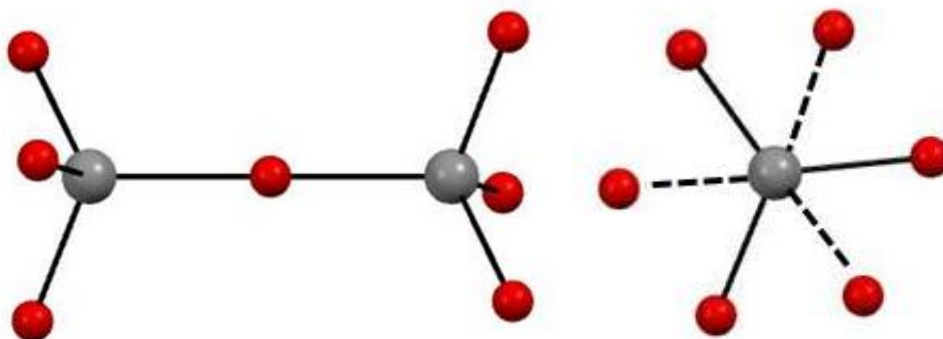
Figure 4.2 Ball and stick representations of Tc_2O_7. (Left) View perpendicular to the $Tc-O_{Bri}-Tc$

unit. (Right) View along the $Tc-O_{Bri}-Tc$ unit. Color of atoms: Tc in grey and O in red.

Table 4.1 Unit cell parameters (Å), Volume (Å^3), selected bond lengths (Å) and angles (°) in Tc_2O_7 obtained at 100 K and 293 K.[3]

	100 K	**293 K**
a	7.312(3)	7.439(4)
b	5.562(2)	5.617(3)
c	13.707(5)	13.756(7)
Volume	557.5(3)	574.8(5)
Tc-O$_{Bri}$	1.8488(5)	1.8403(9)
average: Tc-O$_{Ter}$	1.6872[6]	1.672[6]
Tc-O$_1$	1.6894(7)	1.649(6)
Tc-O$_2$	1.6791(5)	1.673(6)
Tc-O$_3$	1.6931(6)	1.695(6)
average: O$_{Bri}$-Tc-O$_{Ter}$	109.94[4]	109.7[2]
average: O$_{Ter}$-Tc-O$_{Ter}$	108.98[4]	109.2[3]

Table 4.2 Interatomic distances (Å) and angles (°) in M_2O_7 (M = Mn, Tc, Re)

	M-O$_{Ter}$	**M-O$_{Bri}$**	**M-O$_{Bri}$-M**	**Reference**
Mn$_2$O$_7$	1.587	1.761(3)	120.7	94
Tc$_2$O$_7$	1.6872[6]	1.8488(5)	180.0	This work
Re$_2$O$_7$	1.70	1.78	146.6 – 152.4	95
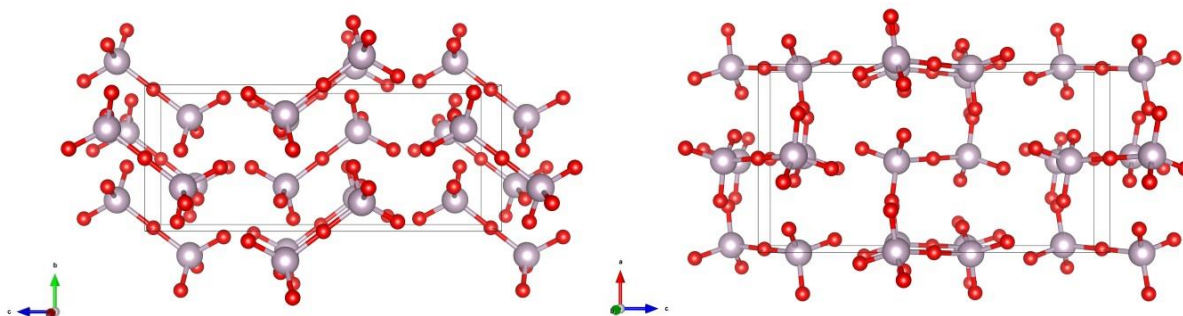
Figure 4.3 View of the crystal packing of Tc_2O_7 along the [100] (left) and [010]. (right) directions. Color of atoms: Tc in grey and O in red.

4.3 Mass spectrometry analysis.

The sample for electron impact mass spectrometry (EI-MS) and chemical ionization mass spectrometry (CI-MS) analysis were prepared in a custom-made glass apparatus designed and fabricated at Argonne National Laboratory. A schematic representation of the experimental setup was presented in Figure 2.12. Technetium dioxide (23.8 mg) was added to the sealed end of the apparatus. The reaction tube was connected to a Schlenk line, evacuated and gently flamed to remove residual moisture. After backfilling 3 times with dry O_2, the reaction vessel was isolated from the manifold by closing the stopcock and the end of the tube was submerged for 3 minutes in liquid nitrogen. The apparatus was then flame-sealed at 37 cm, and placed in a clamshell tube furnace. The 1.96 mm OD capillary, protected with a glass sheath containing helium gas, was located outside the tube furnace. The system was ramped to 450 °C (10 °C.min^{-1}), and held at this

temperature for 3 hours before allowing the furnace to cool to room temperature. Pale yellow needles along with a red film were observed (Figure 4.5) directly outside of the tube furnace. After reaching room temperature, the tube was cut at 35 cm, immediately reconnected to the Schlenk line, evacuated and sealed at 27 cm. By tapping the reaction tube, several Tc_2O_7 crystals (~0.5 mg) were moved into the small capillary. The outer glass sheath was then scored with a glass knife, hot-spotted and removed. The inner capillary was then flame-sealed (L = 7.5 cm). The sealed capillary was placed in an oven at 120 °C in order to melt and distribute the Tc_2O_7 throughout the tube. This would allow the Tc_2O_7 crystals to melt and adhere to the capillary walls and prevent contamination or sample loss upon opening. The capillary was checked for external contamination and sent to the University of Zurich.
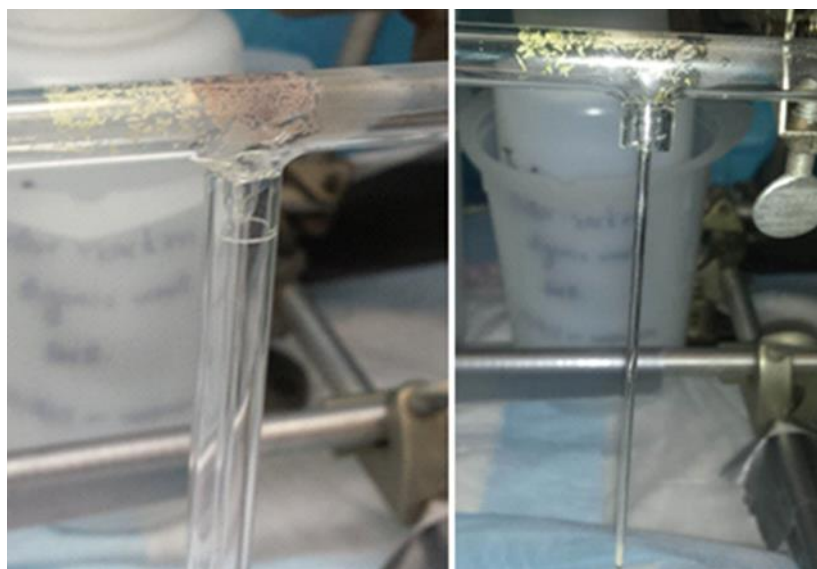
Figure 4.4 (Left) Crystals of Tc_2O_7 with a red film over the tube where Tc_2O_7 was collected. (Right) The protective tubing has been removed leaving only the 1.96 mm OD tube with Tc_2O_7 at the bottom.

Upon receipt at the University of Zurich, the capillary was stored in an N_2 atmosphere glove box. Shortly before the mass spectrometry measurements, the capillary was scored at the right length (~8.5 mm above test tube end), and opened. The capillary fragment was directly used as the sample holder for the EI-MS and CI-MS measurements. It was transferred to the mass spectrometer in tightly closed glass vials. The sample was introduced into a glove bag system, which was installed in front of the mass spectrometer and included the sample inlet. The Tc_2O_7 sample was mounted on the probe, which was then inserted into the mass spectrometer and evacuated (1 x 10^{-3}).

4.3.1 Electron Impact Mass Spectrometry

The EI-MS spectrum of Tc_2O_7 obtained by EI (70 eV) is presented in Figure 4.6. Analysis of the EI-MS data indicate that the gas-phase consists of both mononuclear and dinuclear species. The main dinuclear species are Tc_2O_7 and Tc_2O_5 while the main mononuclear species are TcO_3 and TcO_2. A small amount of $HTcO_4$ (~5%) is also detected and could be due to the presence of trace amounts of water in the system. The mass, species and relative ratio obtained for dinuclear and mononuclear species are presented in Table 4.3 and Table 4.4.

The species detected here are similar to the ones previously observed by Gibson after reaction of Tc oxide (presumably TcO_2[73]) with O_2/H_2O at 950 °C.[62] Nevertheless, some differences in the relative ratios are noticed between the two studies. In the earlier study, the main dinuclear species in the gas-phase was Tc_2O_5, while in our measurement it is Tc_2O_7. This difference could be due to the nature of the sample and can inform on the mechanism of formation of high valent Tc binary oxides. In the studies performed by Gibson, it is possible that the oxidation of TcO_2 by

80

O_2 leads first to Tc_2O_5 which is then further oxidized to Tc_2O_7. In our study, Tc_2O_7 is the main species in the gas-phase and Tc_2O_5 is an EI fragmentation product of Tc_2O_7.

Interestingly, the amount of Tc_2O_6 in both experiments is identical (~9 %) and suggests that Tc_2O_6 is primarily an EI fragmentation product of Tc_2O_7 and might not be involved in the formation of Tc_2O_7 from TcO_2. In his studies, Gibson mentioned that the electron potential has a slight influence on the Tc_2O_7/Tc_2O_5 ratio, while it has a large influence on the Tc_2O_7/Tc_2O_6 ratio. Concerning the mononuclear species, our study indicates that TcO_2 and TcO_3 are the main mononuclear species and a very small amount of $HTcO_4$ was detected. In the Gibson studies, $HTcO_4$ was the main mononuclear species and hydrolyses products (e.g., $TcO(OH)_3$) were also detected. In our experiments, precautions were taken to avoid contact with air/water, while the Gibson experiments, as noted above, were performed under an O_2/H_2O atmosphere.

Our results can also be compared with those obtained on Re_2O_7. A previous EI-MS study performed on Re_2O_7 has shown that Re_2O_7 and ReO_3 are the predominant species in the gas-phase. The species and relative ratios obtained for Re and Tc are presented in Table 4.5. In the Re experiment, it was mentioned that a change of color was observed after prolonged heating (T > 400 K) and that ReO_3 was also identified by XRD;[98] no explanation concerning the reduction of Re_2O_7 was provided. The difference between the relative ratios of the Tc and Re dinuclear species indicates that those elements exhibit different gas-phase chemistry during EI-MS. The main difference is observed with M_2O_5 where the ratio for Re is 1.7% and 57% for Tc.
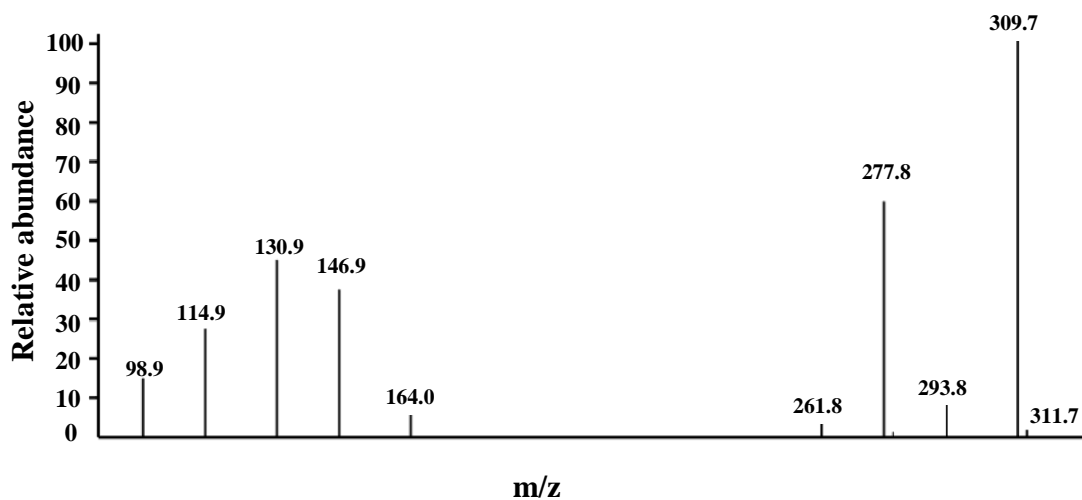
Figure 4.5 Electron impact mass spectrum (70 eV) of Tc_2O_7.

Table 4.3 Dinuclear species observed by EI-MS and relative peak intensities (%) for Tc_2O_7. Values in italics are those reported by Gibson.[62] Both measurements were performed by electron impact at 70 eV**.**

Mass	Species	Relative Intensity
261.8		4.3
262	$Tc_2O_4^+$	*4.5*
277.8		56.3
278	$Tc_2O_5^+$	*100*
293.8		9.6
294	$Tc_2O_6^+$	*9.4*
309.7		100
310	$Tc_2O_7^+$	*47.2*

Table 4.4 Mononuclear species and relative intensity (%) for Tc_2O_7.

Mass	Species	Relative Intensity
98.9	Tc^+	14.3
114.9	TcO^+	25.6
130.9	TcO_2^+	42.8
146.9	TcO_3^+	33.9
164	$HTcO_4^+$	5.2

Table 4.5 Species and relative intensities (%) identified in the spectra of M_2O_7 (M = Tc, Re). Both measurements were performed by electron impact at 70 eV.

Species	Relative intensity (M = Re)[98]	Relative intensity (M = Tc)
MO	-	25.6
MO_2	15.4	42.8
MO_3	27.6	33.9
$M_2O_5^+$	1.74	56.3
$M_2O_6^+$	9.1	7.9
$M_2O_7^+$	**100**	100

4.3.2 Chemical Ionization Mass Spectrometry

The spectrum of Tc_2O_7 obtained by chemical ionization is presented in Figure 4.7. Analysis of the CI-MS data indicate that the gas-phase consists of both mononuclear and dinuclear species

which is consistent with the EI-MS results. The first noticeable difference is the increased presence

of the mononuclear species: $HTcO_4$ (54.69%) and a species with a m/z ratio of 182.8 consistent

with $TcO_2(OH)_3$ (100 %). The dinuclear species is primarily Tc_2O_7, no Tc_2O_5 was observed in the

CI spectrum which confirms this species to be fragmentation product of Tc_2O_7 in the EI mode.
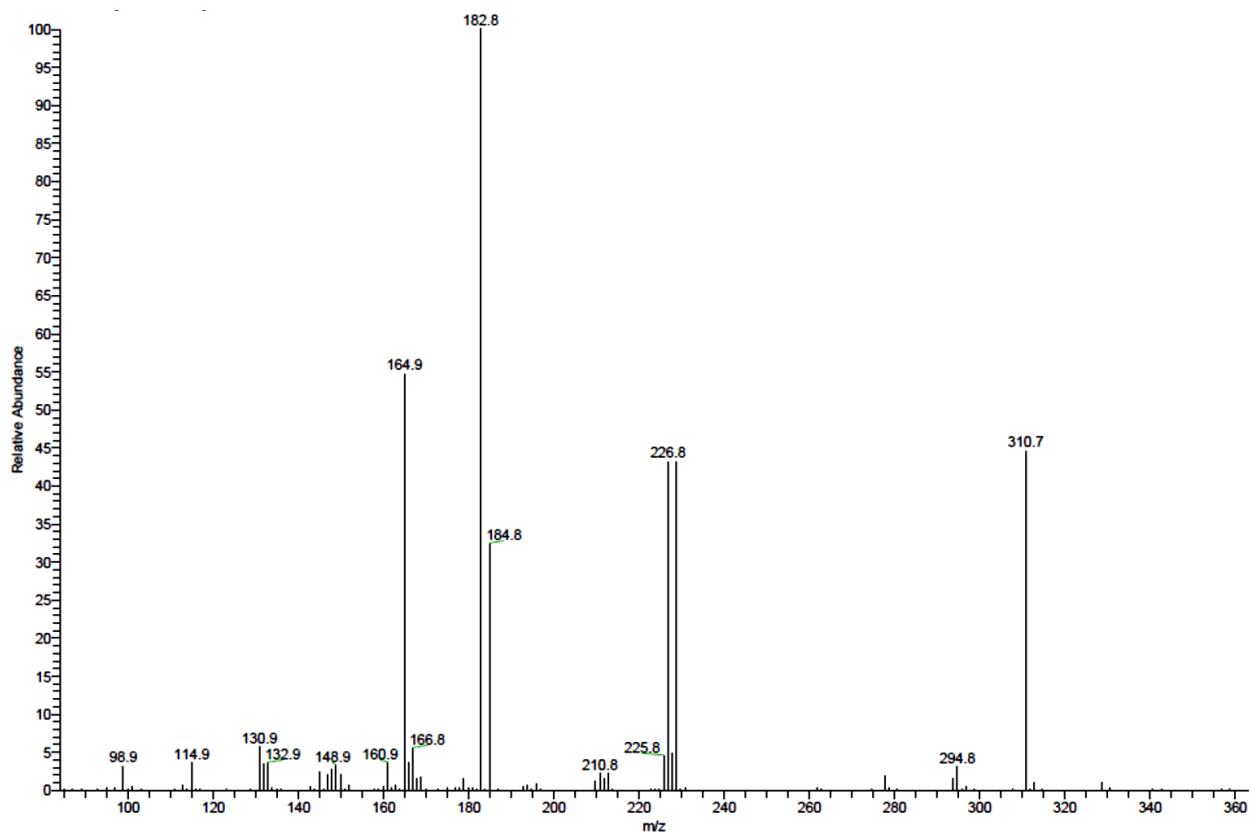
Figure 4.6 Chemical ionization mass spectrum of Tc_2O_7.
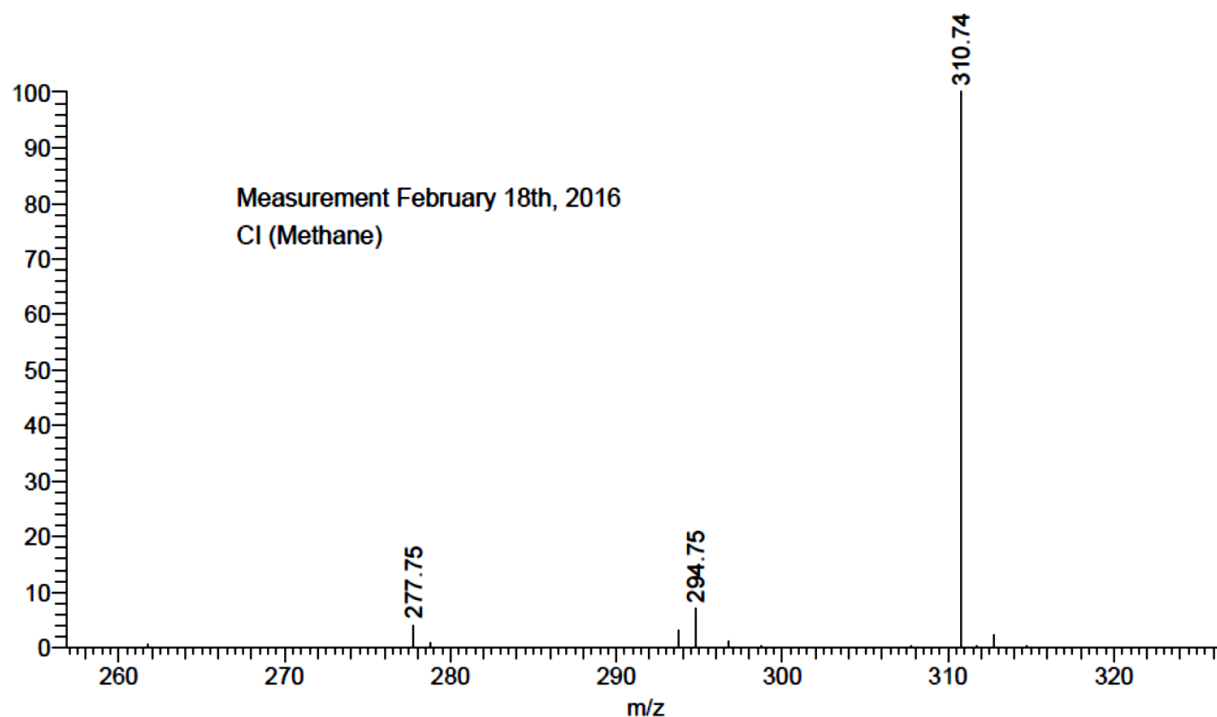
Figure 4.7 Chemical ionization mass spectrum of Tc_2O_7 in the region 250 - 320.

4.4   Theoretical methods.

The methods and an evaluation of the functional used for the theoretical calculation are

presented in Appendix I.

4.4.1 Gas-phase simulation

It has been demonstrated that while the Tc_2O_7 molecule is linear in the solid-state, it adopts

a bent structure in the gas-phase.[17] In order to determine the cause of these phenomena, potential

energy surfaces (PES) tracing the pathways between the high symmetry Tc_2O_7 conformers have

been calculated (Figure 4.10). Results show that the experimentally observed D_{3d} conformer is not

the lowest energy geometry. Both D_{3d} (staggered) and D_{3h} (eclipsed) linear geometries appear to be local minima along the twisting degree of freedom, but are in fact saddle points along the multi-dimensional potential energy surface. Frequency analysis confirms this with the presence of 3 imaginary vibrational modes for D_{3d} and 1 imaginary mode for each D_{3h} structure. The potential energy is dramatically lowered by allowing the Tc-O_{Bri}-Tc angle to bend away from a linear geometry with an optimal angle typically between 155-165º. For all of the local minima, the TcO_4 tetrahedra maintained largely the same internal geometry, and the only notable difference between the conformers were the mapped variables and a slight lengthening of the Tc-O_{Bri} bond length to upwards of 1.91 Å at a 120º Tc-O_{Bri}-Tc angle. While the PES looked very ragged with well-defined minima, the energy separation between each conformer is quite small and a free Tc_2O_7 molecule at 85 K should have enough thermal energy to access all of the reported conformers.

Scanning the potential energy pathways connecting the C_{2v} geometries (Figure AP4.1) indicates the presence of lower energy geometries closer to the $C_{2v(syn)}$ symmetry. When each of the identified minima was fully relaxed, the identified global minima is of $C_{s(eclipsed)}$ symmetry where the bridging oxygen is only 2.5º from $C_{2v\,(syn)}$ with a 156.5º Tc-O_{Bri}-Tc angle.[97] The relative energy differences observed here are somewhat different than those predicted by Amado, et al.,[97] but this is likely because of the inclusion of intra-molecular dispersion interactions and the constraints placed on the internal geometry when mapping the pathways for Figure 4.10.

4.4.2 Solid-state simulation

If the D_{3d} geometry is among the higher energy structures for a free molecule, the question remains as to why it is the one observed experimentally in the solid-state. To determine why this is the case, solid-state structures of Tc_2O_7 with the Mn_2O_7, Re_2O_7 and Tc_2O_7 (Tc_2O_7-D_{3d}) experimental structures, as well as a version of Tc_2O_7 (Tc_2O_7-D_{3h}) where half of the tetrahedra were rotated were optimized using PW-DFT. Table 4.7 displays the results for the each structure. Except for the Tc_2O_7-D_{3d} structure, the simulated packed Tc_2O_7 molecules adopted a twisted C_{2v} (anti) type geometry with a slightly elongated Tc-O_{Bri} bond length (1.868 Å) similarly to what was observed with the gas-phase simulations; in all of the simulated structures, the Tc-O_{Ter} bond length is 1.696 Å.

The calculated structures of Tc_2O_7 with the Mn_2O_7 structure and the Tc_2O_7-D_{3h} geometry retained a similar packing to their parent structures only having altered packed molecule geometries. In the manganese solid, the Mn_2O_7 are the most energetically favorable of the packed bent molecules; replacing Mn by Tc lead to significantly larger volume per molecule, less efficient packing and much less cohesive energy; which indicate that Tc_2O_7 with the Mn_2O_7 structure to be a less stable structurein the solid-state.

When replacing the Re atoms by Tc atoms in Re_2O_7, the structure migrated from extended polymeric to molecular with clearly identifiable Tc_2O_7 molecules with a packing similar to Tc_2O_7-D_{3h}. Despite the Tc_2O_7 molecules in the Re_2O_7 structure being lower in energy than the one in the Tc_2O_7-D_{3h} structure, their less efficient packing and higher cohesive energy make it a less favorable homologue.

Despite the Tc_2O_7 bent geometries being lower in energy in the gas-phase simulations, they have the highest energies in the solid-state. To verify that this energy ordering is not an artifact of the PW-DFT simulations, the molecules were allowed to relax in the large, empty box used to compute cohesive energies. The only significant change from the relaxation is an elongation of the $Tc-O_{Bri}$ bonds by ~0.1 Å, and the bent geometries returned to being the most favorable. Therefore, the D_{3d} structure is the most favorable geometry when compressed by the crystal packing forces. The stability with respect to compression combined with the most cohesive energy per molecule is why the linear D_{3d} geometry is observed experimentally.
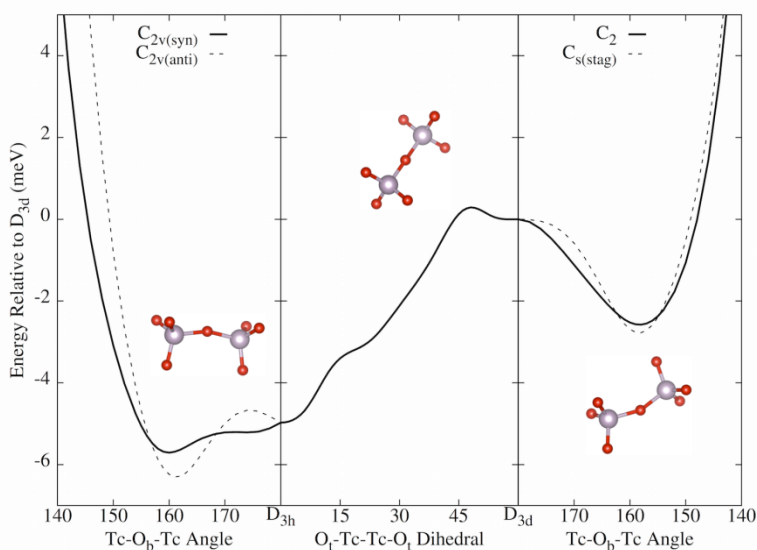
Figure 4.8 The potential energy surfaces connecting the highest symmetry conformers to the experimentally determined D_{3d} conformer via the central $Tc-O_{Bri}-Tc$ bending angle and the dihedral angle between the two TcO_4 tetrahedra. For each point the molecular geometries were optimized constraining only the $Tc-O_{Bri}-Tc$ bond angle and dihedral angles.

Table 4.6. Energetics and geometries of the lowest energy of the Tc_2O_7 structures with the Mn_2O_7, Re_2O_7 and Tc_2O_7 structure (Tc_2O_7-D_{3d}) as well as a version of Tc_2O_7 (Tc_2O_7-D_{3h}). Energies are in eV, volumes in Å^3, and angles in degrees.

Structure	Tc-O-Tc Angle	Twisting Dihedral Angle	Total Energy	Total Volume	Cohesive Energy	Single Molecule Energy	Relaxed Molecule Energy
Tc_2O_7-D_{3d}	180.0	60.0	-69.197	137.8	-1.541	0.000	0.000
Tc_2O_7-D_{3h}	155.6	20.6	-69.163	137.0	-1.539	0.030	-0.004
Mn_2O_7	148.0	11.4	-68.983	146.8	-1.339	0.011	-0.003
Re_2O_7	157.4	17.7	-69.154	138.2	-1.517	0.019	-0.004

4.5   Conclusion

In this Chapter, Tc_2O_7 was synthesized from the oxidation of TcO_2 with O_2 and its crystallographic structure determined at 100 K. The orthorhombic space group of Tc_2O_7 at 100 K is confirmed to be the same as determined previously at 293 K.

For the first time, the electron impact and chemical ionization mass spectra of Tc_2O_7 has been recorded. The main dinuclear species in the gas-phase are Tc_2O_7 and Tc_2O_5 while the main mononuclear species are TcO_3 and TcO_2. Here, Tc_2O_5 is obtained from the EI fragmentation of Tc_2O_7 while it is not observed in the CI mode. The fragmentation species derived from Tc_2O_7 are the same as those previously observed from the reaction of Tc oxide (probably TcO_2) with O_2/H_2O. Some differences on the relative intensity are noticed between the two studies. Starting from TcO_2,

the main dinuclear species was Tc_2O_5. It is possible that the oxidation of TcO_2 by O_2 leads to Tc_2O_5 which could be further oxidized to Tc_2O_7. In this context, it is noted that an intermediate red compound (possibly Tc_2O_5) was always observed during the preparation of Tc_2O_7 from TcO_2.[1] The EI mass spectrum of Tc_2O_7 was compared with the one of Re_2O_7 and both spectra show the presence of M_2O_5. The difference between the relative intensity of Tc_2O_5 and Re_2O_5 indicate that Tc and Re oxides exhibit different gas-phase chemistry. The CI-MS data confirms that Tc_2O_7 is present in the sample, and $HTcO_4$ increased significantly (~5% - 54%).The ratio between Tc_2O_7 and Tc_2O_5 also changed, which indicates that Tc_2O_5 is a fragmentation product of Tc_2O_7 in EI-MS.

The geometry of the Tc_2O_7 molecule was investigated in the gas-phase and in the solid-state by theoretical methods. The optimized geometry of the Tc_2O_7 molecule is in good agreement with the experimental one. Energetic calculations confirm the linear geometry to be the most favorable in the solid-state while a bent geometry is the most stable in the vapor phase.

Stability with respect to compression and high cohesive energy per molecule are possibly the reasons why the linear geometry is observed in the solid-state. Because Re_2O_5 is known[99] in the solid-state and Tc_2O_5 is the main species in the gas-phase when Tc oxide is oxidized by O_2, it can be anticipated that Tc_2O_5 can be produced in the solid-state; one method could involve the controlled oxidation of TcO_2 by O_2 (see Chapter 5).

Chapter 5: The Nature of the Technetium Species Formed During the Oxidation of Technetium Dioxide with Oxygen and Water.

In this Chapter, the oxidation of TcO_2 with O_2 in the presence of H_2O at 250 °C has been performed, after the reaction. Tc_2O_7 and a red product were observed. The products were characterized by UV-Visible measurement and chemical titration. The behavior of the reaction product of TcO_2 with O_2/ H_2O at 250 °C was studied by mass spectrometry. The reaction product of TcO_2 with O_2 at 180 °C was studied by Raman spectrometry. Finally, the molecular structure and electronic spectra of $HTcO_4$, $HTcO_4 \cdot H_2O$, $HTcO_4 \cdot 2H_2O$ and $Tc_2O_7 \cdot H_2O$ were studied by theoretical methods.

5.1   Introduction

The study of the high temperature chemistry of technetium is relevant to radiopharmaceutical applications. One of these radiopharmaceutical application is the production of ^{99m}Tc technegas which involves the heating of ^{99m}Tc in a carbon crucible to 2,750 °C.[100] Other nuclear applications include waste form development and environmental remediation such as the vitrification of low level and high level activity wastes at the Hanford site.

Over the last two decades, the vitrification of Tc for remediation at the Hanford site has been under investigation. Studies have shown that Tc volatilizes during vitrification and that its retention in the glass varies from 30% to 70%.[11]After vitrification under air, Tc was a present as a Tc(IV) /Tc(VII) mixture in the glass.[13] Concerning the nature of the volatile species, Tc_2O_7, pertechnetate salts and $HTcO_4$ were proposed.[6] In Chapter 3, it was shown that the volatile Tc product formed after vitrification of $NaTcO_4$ in borosilicate glass contains $TcO_3(OH)(H_2O)_2$. It

was proposed that $TcO_3(OH)(H_2O)_2$ was obtained from the reaction of Tc_2O_7 with water and that Tc_2O_7 was obtained from the oxidation of Tc(IV) in the glass by air.

An understanding of the formation of the volatile Tc species is of importance for the development of a reliable vitrification process. In order to better understand the mechanism of formation of Tc volatile species, a study on Tc_2O_7 has been initiated (Chapter 4). Technetium heptoxide was prepared from the oxidation of TcO_2 with O_2 and characterized by single-crystal X-ray diffraction and electron impact - mass spectrometry. The EI-MS analysis indicates that the main species in the gas phase were Tc_2O_7 and its fragmentation product, Tc_2O_5.

Because water can be present during the vitrification process, studying the effect of water on the nature of the volatile species is of importance. Previous works have shown that after oxidation of Tc oxide with O_2 and water at 950 °C, $HTcO_4$ was the main hydroxide species in the gas phase and it was formed from the reaction of Tc_2O_7 with H_2O.[62] In this previous study, where the nature of the starting species was unclear (probably TcO_2), it was mentioned that experimental set-up could have been contaminated with fluorine which lead to the presence of Tc oxyfluoride species. For a better understanding of the formation of volatile species, the determination of the conditions for the formation of Tc volatile species in the presence of water, as well as their nature in the gas phase is needed. In this Chapter, the oxidation of TcO_2 with O_2 /H_2O at 250 °C has been performed and the nature of the reaction products has been studied by EI-MS, UV-Visible spectroscopy and theoretical methods.

5.2   Formation and properties of the volatiles species

The oxidation of TcO_2 with O_2 /H_2O has been performed 250 °C. The samples were prepared by oxidation of TcO_2 with O_2/H_2O using a similar set-up as the used for the preparation of the EI-MS sample (Chapter 2); the specialty tube was replaced by a 33 cm long borosilicate tubes. For introduction of wet O_2 in the system, a bubbler of DI water was placed between the O_2 bottle and the glass tube.

Technetium dioxide (24.6 mg) was treated at 250 °C with O_2/H_2O atmosphere for 3 hours. At this temperature, red and yellow products were observed in the cold part of the tube after the reaction. While the yellow color is consistent with the presence of Tc_2O_7, the nature of the red product is still unclear. In order to know more about the red product, its UV-Visible spectra has been measured and its behavior studied in solution and in the solid-state.

The UV-Visible spectrum of the red product measured though the glass tube (Figure 5.1.b) exhibits a band a 509 nm and is similar to the one obtained after the reaction of Tc_2O_7 crystals with air (Figure 5.1a). A picture of the tube containing the red compound which has been measured in presented in the inset in Figure 5.1. This indicates that the red products obtained from the oxidation of TcO_2 with O_2 /H_2O might originate from Tc_2O_7.

The behavior of the red product was studied in the presence of Ce(IV) in 2 M H_2SO_4. After the reaction of TcO_2 and O_2/H_2O at 250 °C, the part of the tube containing the red product was cut and separated from the part containing Tc_2O_7. The portion of the tube containing the red species was placed in a glass vial, and 1 mL of solution Ce(IV) (0.5 mM in 2 M H_2SO_4) introduced in the tube and collected in the glass vial. The resulting solution was placed in small quartz cell (L = 1 mm) and its UV-Visible spectrum recorded (Figure 5.2).
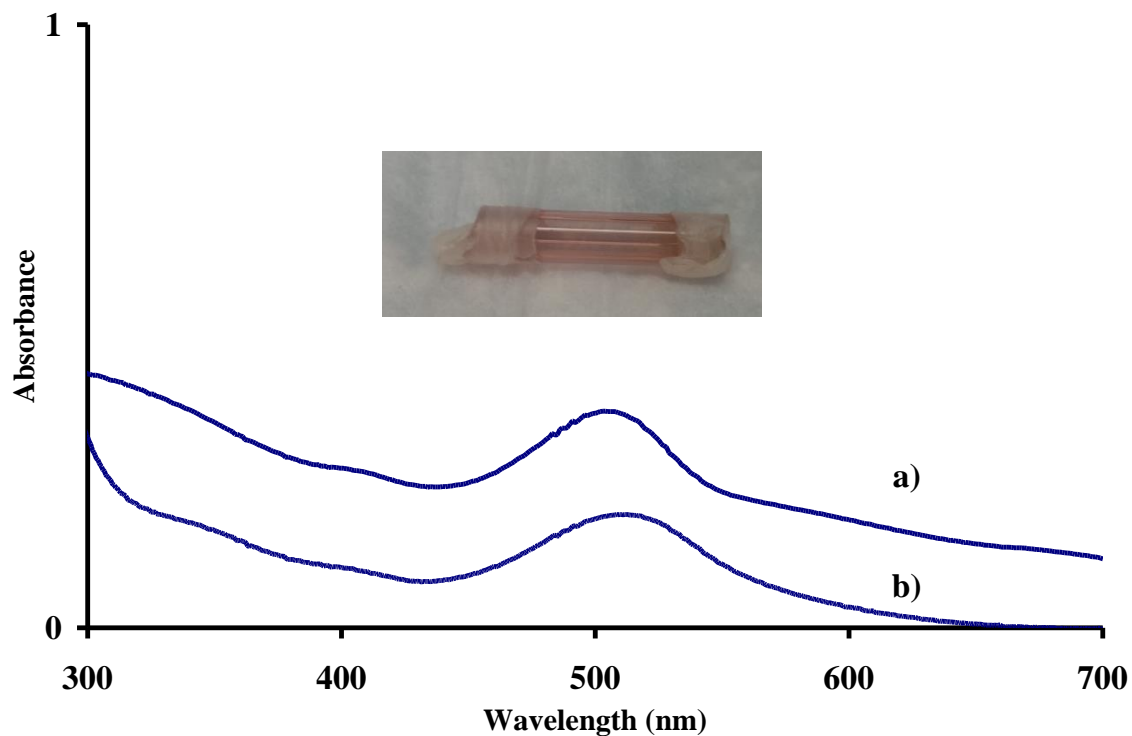
Figure 5.1. UV-Visible spectra of the red species formed from: a) the reaction of Tc_2O_7 crystal with water from the atmosphere (spectra recorded quartz cell); b) the reaction of TcO_2 with O_2/H_2O at 250 °C.

Analysis of the UV-Visible spectra after the reaction show the consumption of Ce(IV) and the observation of TcO_4^-. This indicates that a reduced Tc species (Tc^{x+}) was present in the red product and was oxidized with Ce(IV) according to Eq.5.1:

Eq.5.1. $Tc^{x+} + (7-x)Ce(IV) \rightarrow TcO_4^- + (7-x)Ce(III)$

The consumption of Ce(IV) was determined using the peak at 365 nm of Ce(IV) ($\Box = 300$ M^{-1}.mm^{-1}). Using Eq.5.1, the amount of Ce(IV) consumed ($1.0.10^{-4}$ mmol) and the amount of TcO$_4^-$ detected after the reaction ($1.38.10^{-4}$ mmol), the average oxidation state of Tc in the red solution (x = 7-[Ce(IV)]/[TcO$_4^-$]) was calculated to 6.27. The fraction of the reduced species in the red product was calculated assuming the presence of Tc(+7) and Tc(+x) with x = +6, +5 and +4. The results indicates either the presence of 73% for Tc(+6), 36.5% for Tc(+5) or 24.3% for Tc(+4).
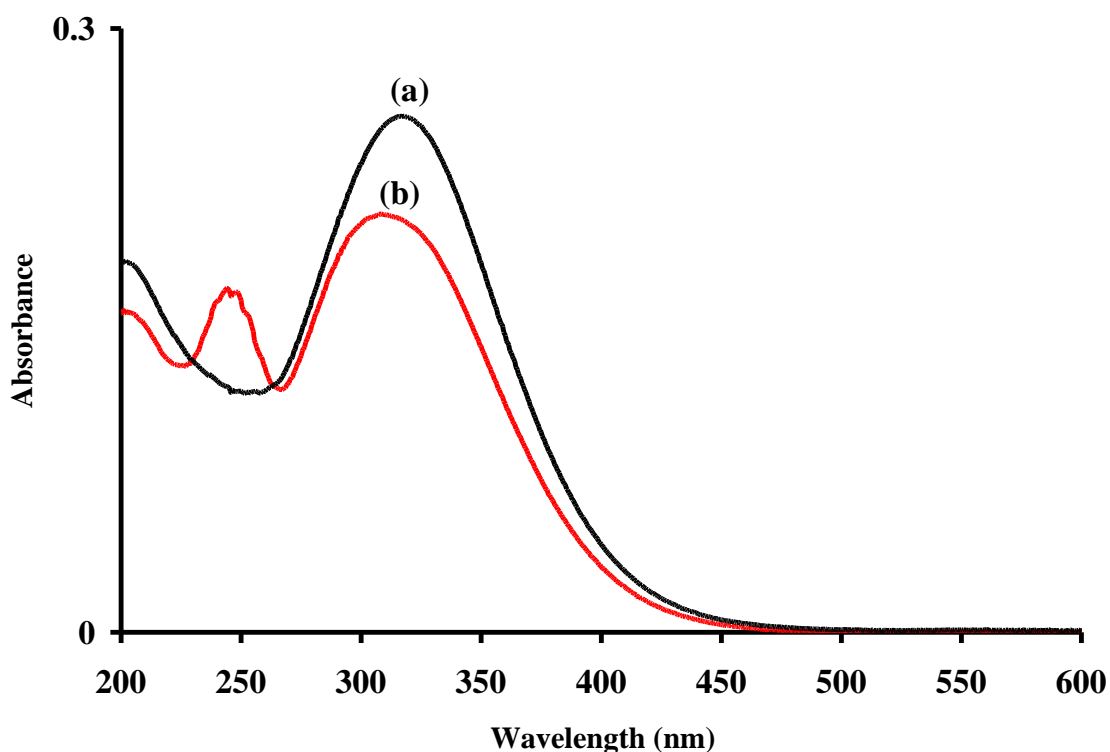
Figure 5.2. UV-Visible spectra the Ce(IV) solution: a) before and b) after the reaction with the red product. Spectra in recorded in 1 mm quartz cell.

The stability of the red product was also studied in a sealed tube under vacuum at 200 °C. Treatment at 200 °C leads to the formation of a black solid (presumably TcO_2) and is also consistent with the presence of a reduced species in the red product.

The results found here are consistent with those previously found on $HTcO_4$.[101] In their studies, Rulfs, et al. showed that the concentration of an $HTcO_4$ solution lead to the observation of a red color (for $Tc > 0.3$ M) and that the UV-Visible spectra of the red solution exhibited a band centered at 505 nm. Titration with Ce(IV) indicated that the red solution contained a reduced Tc species. It was shown that the red species in unstable in aqueous media and that brown solutions and brown precipitates were observed after addition of water and sodium hydroxide, respectively. Rulfs, et al. proposed that the red solution contains Tc(VI) or Tc(V) species and that the reduction was due to the presence of dust, organic species, or water according to Eq.5.2.[101]

$$\textbf{Eq. 5.2.} \quad 4\ HTcO_4 + 2\ H_2O \rightarrow 4\ H_2TcO_4 + O_2$$
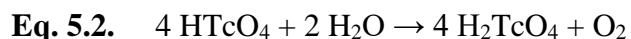
Here, it is proposed that the red product obtained from the oxidation of TcO_2 and water at 250 °C was produced stepwise according the following mechanisms:

1) Oxidation of TcO_2 to Tc_2O_7

2) Reaction of Tc_2O_7 with H_2O and formation of $HTcO_4$

3) Reduction of $HTcO_4$

Depending on the amount of water and the temperature, the reaction product of TcO_2 with O_2/H_2O can be described as a mixture of $HTcO_4$, Tc_2O_7 and a reduced Tc species. The behavior of the reaction product of TcO_2 with O_2/ H_2O at 250 °C was studied by mass spectrometry.

5.3   Mass spectrometry studies

The sample for EI-MS analysis was prepared in a custom-made glass apparatus, the experimental set-up used here is similar to the one used previously for the study of Tc_2O_7 (Chapter 4). Technetium dioxide (23.8 mg) was added to the sealed end of the apparatus. The reaction tube was connected to a Schlenk line, evacuated and wet O_2 was introduced in the system. The apparatus was placed in a clamshell tube furnace. The small capillary, protected with a glass sheath containing helium gas, was located outside the tube furnace. The system was ramped to 250 °C ($10\ °C.min^{-1}$), and held at this temperature for 3 hours before allowing the furnace to cool to room temperature. A yellow solid (Tc_2O_7) and red film were observed (Figure 5.3) outside of the tube furnace. After reaching room temperature, the tube was sealed at 27 cm. The outer glass was scored with a glass knife and removed. The inner capillary containing the red film was then flame-sealed and careful analysis of the reaction products in the small tube shows the presence of yellow and red products. The small tube was sent to the University of Zurich for the EI-MS measurements.
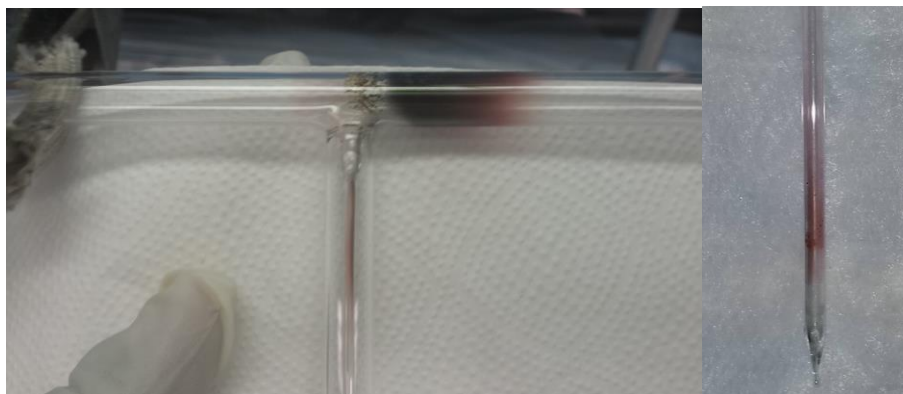
Figure 5.3. Left: red film and Tc_2O_7 produced during the oxidation of TcO_2 with O_2/H_2O. Right: the protective tubing has been removed.

The EI mass spectrum (70 eV) is presented in Figure 5.4. The EI-MS analysis indicates that the gas phase consists of both mononuclear and dinuclear binary oxide species, as well as mononuclear hydroxo species; dinuclear hydroxo or hydrated species (i.e., $Tc_2O_7 \cdot nH_2O$) were not detected.

The main dinuclear species are Tc_2O_7 (100 %) and Tc_2O_5 (~50 %), the main mononuclear binary oxide species is TcO_3 (~50 %) and the main hydroxo species is $HTcO_4$ (~72%). The mass, species and relative ratio for dinuclear and mononuclear species are respectively presented in Table 5.1.

In section 5.2, it was shown that the red product is thermally unstable and decomposes to TcO_2 at 200 °C. Under the experimental conditions used for the EI-MS analysis (200 °C, vacuum 10^{-7} Tor), it is expected that the red product will decompose and the sample analyzed will consist of a mixture $HTcO_4$, TcO_2 and Tc_2O_7; the EI mass spectrum of the sample will then logically consist of Tc_2O_7, $HTcO_4$ and their fragmentation products.
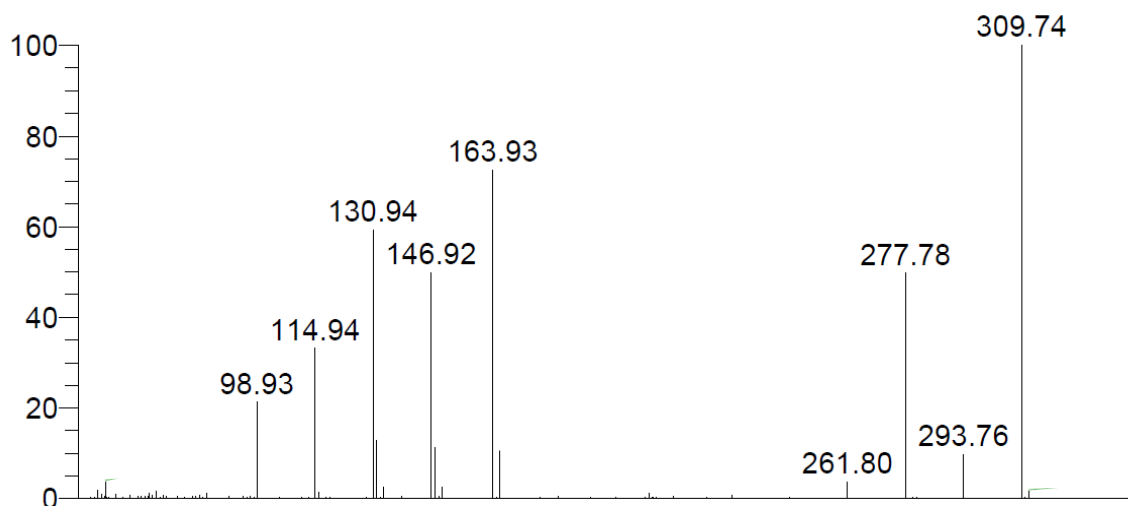
Figure 5.4. Electron impact mass spectrum (70 eV) of the product obtained after oxidation of TcO_2 with O_2/H_2O at 250 °C.

Previous studies on Re oxides have shown that the main hydroxo species obtained after sublimation of $ReO_3 + ReO_2$ was $HReO_4$, while the well-known $Re_2O_7 \cdot 2H_2O$ species was not detected. It was proposed that residual vapor in the vacuum system reacted with solid Re_2O_7 that had condensed on the spectrometer, formed $HReO_4$ and then vaporized.

The results were compared to the one previously obtained on Tc_2O_7 (Chapter 4). Analysis of the EI-mass spectra indicates that the nature of the binary oxides observed here is similar to the one previously observed on Tc_2O_7. In both cases, the main mononuclear binary oxide is TcO_3 while the main dinuclear species are Tc_2O_7 and its fragmentation product, Tc_2O_5. The abundance of $HTcO_4$ (~72 %) is much higher than the one previously obtained with Tc_2O_7 (~5 %). Also, the hydroxide species observed here ($TcO_2(OH)^+$, $TcO(OH)_3^+$ and $Tc(OH)_3^+$) were absent in the EI spectrum of Tc_2O_7. This is primarily due to the presence of water and of $HTcO_4$ in the sample while in the study of Tc_2O_7, precaution were taken in order to exclude water in the system.

Table 5.1. Dinuclear species observed by EI-MS and relative peak intensities (%) for Tc_2O_7. Values in parentheses are those previously reported for Tc_2O_7. Both measurements were performed by electron impact at 70 eV.

Mass	Species	Relative Intensity
98.9	Tc^+	21.1 (14.3)
114.9	TcO^+	33.0 (25.6)
130.9	TcO_2^+	59.25 (42.8)
131.9	$TcO(OH)^+$	12.68
146.9	TcO_3^+	49.78 (33.9)
147.9	$TcO_2(OH)^+$	11.22
163.9	$TcO_3(OH)^+$	72.45 (5.2)
165.9	$TcO(OH)_3^+$	10.62
261.8	$Tc_2O_4^+$	3.5 (4.3)
277.8	$Tc_2O_5^+$	49.68 (56.3)
293.8	$Tc_2O_6^+$	9.63 (9.6)
309.7	$Tc_2O_7^+$	100 (100)

The results were compared to the one previously obtained on the oxidation of Tc oxide with O_2 /H_2O at 950 °C,[62] and on the reaction $NaTcO_4$ with Ar/O_2 and Carbon at 2500 °C. Analysis of the EI-mass spectra indicates that the nature of the binary oxides species is similar to the one

obtained after oxidation at 950 °C. Concerning the hydroxides species, in both cases, $TcO_3(OH)$ is the main hydroxide species while $TcO_2(OH)_3$ (m = 182), which has been previously reported, was not detected here.

After treatment of $NaTcO_4$ at 2500 °C, $TcO_2(OH)_3$ and $TcO_3(OH)$ have been identified as the main gas phases species, it was proposed that those species were formed according after successive hydrolysis : $Tc_2O_7 \dashrightarrow TcO_3(OH) \dashrightarrow TcO_2(OH)_3$. From those results, it appears that the temperature of volatilization is driving the hydrolysis of $TcO_3(OH)$ to $TcO_2(OH)_3$: $TcO_2(OH)_3$ is not observed at 200 °C while it is observed at 950 °C and is the predominant species at 2500 °C.

5.4   Theoretical studies

Pertechnetic acid ($HTcO_4$) is the predominant mononuclear species in the gas phase after treatment TcO_2 with H_2O and O_2, but very few data on its gas phase chemistry are known. It was decided to revisit the molecular and electronic structure of $HTcO_4$ as well as its hydrates, one point of interest was to predict what should be the color of $HTcO_4$ and its hydrate; this could give some insight of the red color observed in concentrated $HTcO_4$ solution.

5.4.1 Study of HTcO₄

Pertechnetic acid ($HTcO_4$) adopts a C_s geometry with the hydroxyl staggered between two of the O atoms, and the Tc=O bond length opposite the hydroxyl being slightly shorter than the remaining Tc=O bonds (Figure 5.5). The Tc-OH distance is similar to the Tc-O_{Bri} in $Tc_2O_{7,}$ and

the double bonds are only elongated slightly.

The red compound exhibits an adsorption in the green at 509 nm (Figure 5.1). The predicted lowest energy adsorption bands for $HTcO_4$ (Figure 5.6) are in the UV range indicating that $HTcO_4$ should be colorless. The excited states are all singlets, as the computed triplet states have no oscillator strength. The strongest bands (i.e., 202, 208, 212, 225, 234, 236, 270, 271, and 284 nm) all correspond to excitations into the unoccupied Tc d orbitals (LUMO to LUMO+4, Table 5.2). These unoccupied Tc d states share some density with O p states confirming that there is covalency between the Tc and O atoms. The strongest band at 236 nm is composed of excitations from the highest occupied molecular orbital (HOMO) → LUMO+1, HOMO-1 → LUMO+1, HOMO-2 to LUMO+2, HOMO-2 to LUMO, and HOMO-3 to LUMO (Table 5.2).

The frontier band at 325 nm corresponds to a transition involving the HOMO to LUMO, HOMO-1 to LUMO, and HOMO-2 to LUMO+1, which again is O p states exciting into unoccupied states of predominant Tc d character. A lack of adsorption in the 500 nm region indicates that $HTcO_4$ should not be red.
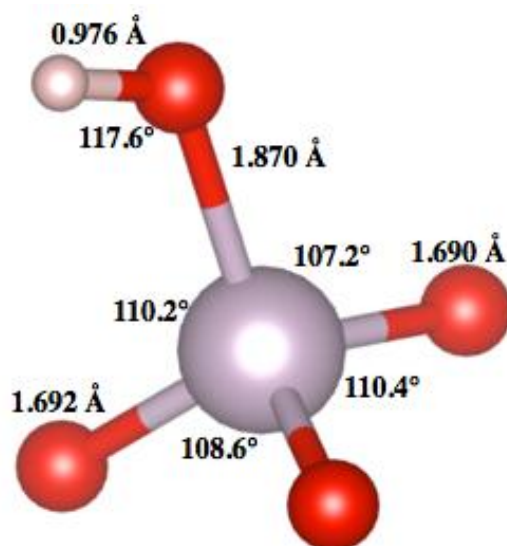
Figure 5.5. Ball and stick representation of the molecular structure of HTcO$_4$.
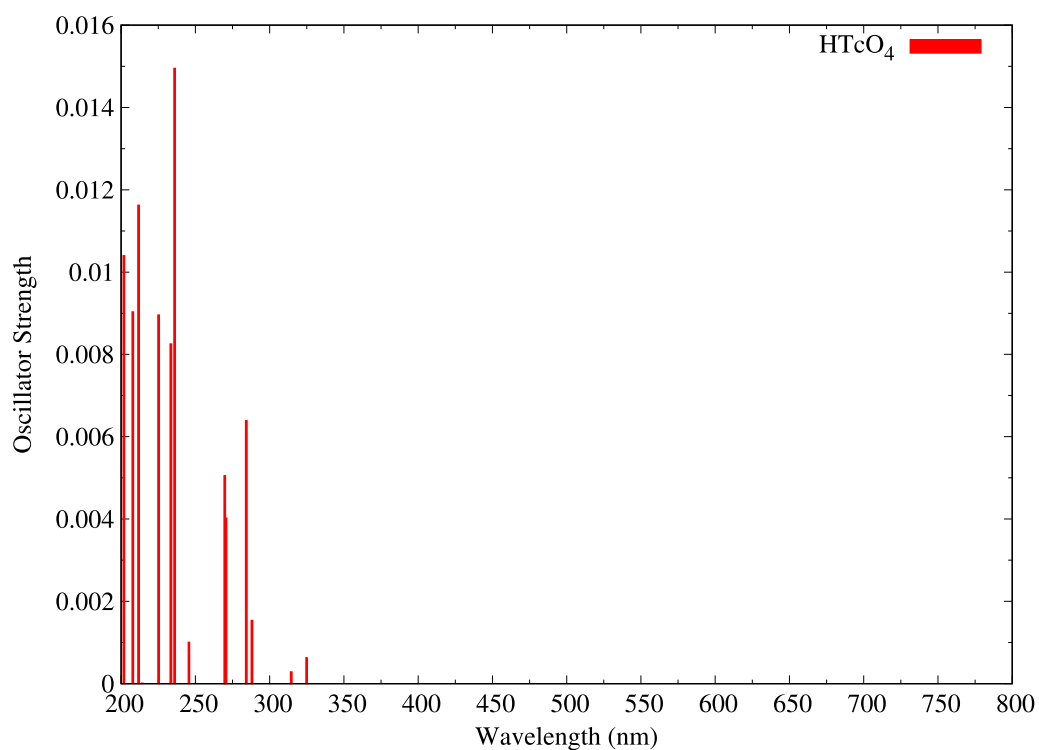
Figure 5.6. Calculated electronic spectra of HTcO$_4$.

Table 5.2. UV-Visible excitations of HTcO$_4$ and the compositions of the bands.

Wavelength (nm)	Oscillator Strength	Band Composition
325	0.0006	HOMO-2→LUMO+1, HOMO-1→LUMO, HOMO→LUMO
315	0.0003	HOMO-2→LUMO, HOMO-1→LUMO+1, HOMO→LUMO+1
288	0.0015	HOMO-2→LUMO+1, HOMO-1→LUMO, HOMO→LUMO
284	0.0064	HOMO-2→LUMO, HOMO-1→LUMO+1
271	0.0040	HOMO-3→LUMO, HOMO-2→LUMO, HOMO-1→LUMO+1, HOMO→LUMO+1
270	0.0051	HOMO-3→LUMO+1, HOMO-2→LUMO+1, HOMO-1→LUMO, HOMO→LUMO
246	0.0010	HOMO-4→LUMO
236	0.0149	HOMO-4→LUMO, HOMO-3→LUMO, HOMO-2→LUMO+2, HOMO-1→LUMO+1, HOMO→LUMO+1
234	0.0083	HOMO-3→LUMO+1, HOMO-2→LUMO+1, HOMO-1→LUMO+2
225	0.0090	HOMO-5→LUMO, HOMO-4→LUMO+1, HOMO-1→LUMO+1
212	0.0116	HOMO-6→LUMO, HOMO-5→LUMO, HOMO-4→LUMO+1
208	0.0090	HOMO-1→LUMO+2, HOMO→LUMO+3
202	0.0104	HOMO-3→LUMO+3, HOMO-2→LUMO+2, HOMO→LUMO+4

5.4.2 Study of HTcO$_4$-monohydrate

Several candidates with the TcO$_3$(OH)(H$_2$O) structure were studied via a combinatorial approach; the geometries included a 5-coordinate Tc with all possible placements of the water and hydroxide. Once optimized the initial structures only converged to 4 different solutions (Figure 5.7) whose uniqueness was determined by having an energy that differed by at least 1 mE$_h$. For the lowest energy structure (motif 1), the water is hydrogen bonded to HTcO$_4$ through an H$_2$-O···H-OTcO$_3$ interaction. The other structures more resemble a water molecule that has been associated to the Tc and rotated to overlap their H atoms with two of the other coordinated oxygens. The Tc-O distance (≥ 2.5 Å) is too large for a covalently coordinated ligand. The relative stabilities of the monohydrates compared to an isolated water and HTcO$_4$ (Table 5.3) also appear too small and are more reminiscent of values for a hydrogen bound complex, and the energy of those structures decreases as function of Tc-O distance. The hydrogen bound water of motif 1, while more energetically favorable, does not interact strongly with Tc as the one in motif 2, 3 and 4.

The water molecules in the other motifs are interacting more strongly with the Tc, as can be seen by the slight increase in the wavelength of the lowest energy excited state. Unfortunately, none of these wavelengths are in the visible part of the spectrum, so the compounds should all be colorless. Pertechnetic acid monohydrate with the structure TcO$_2$(OH)$_3$ was also tested, results indicate that this complex is less stable than an isolated HTcO$_4$ and water.
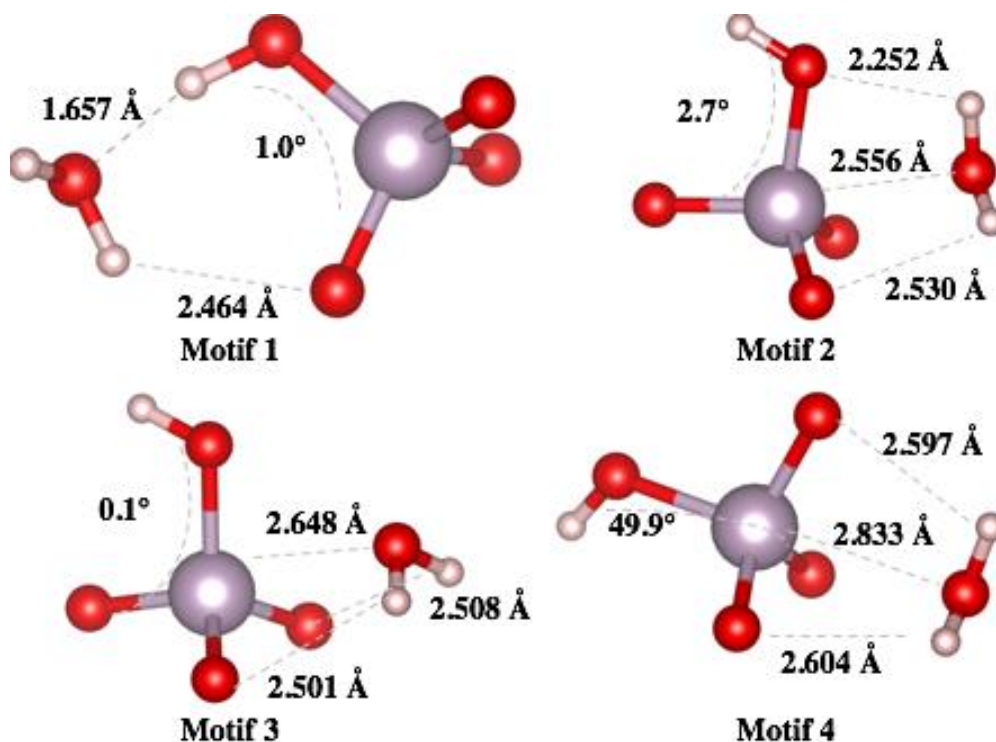
Figure 5.7. Lowest energy structures for HTcO$_4$ monohydrate. Relevant distances for the water are shown as well as the dihedral between the hydroxl group and a coordinated oxygen.

5.4.3 Study of HTcO$_4$-dihydrate

For the dihydrate species, the guess structures consisted of a Tc atom in an octahedral coordination. The lowest energy structure (figure 5.8) contains two waters molecules which are hydrogen bonded to HTcO$_4$ (i.e., the hydrogen-oxygen intermolecular distances being characteristic of a hydrogen bond). The structure of this complex is fairly distorted from an isolated HTcO$_4$ molecule: the hydroxyl bond stretched to 1.064 Å, the Tc-OH distance shortened to 1.817 Å, the hydroxyl group rotated towards the other HTcO$_4$ oxygen involved in the hydrogen bonding,

and the Tc=O distances extended to 1.716 Å. This complex is stable when compared to an isolated

HTcO$_4$ molecule and two H$_2$O, with a relative stability of ~10 kcal/mol per hydrogen bond.
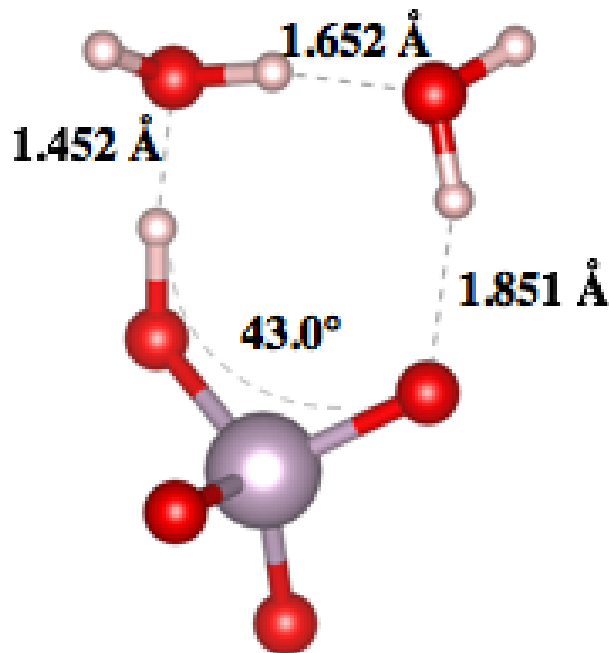
Figure 5.8. Lowest energy structures for HTcO$_4$ dihydrate. Relevant distances for the water are shown as well as the dihedral between the hydroxl group and a coordinated oxygen.

A previous study found the lowest energy structure of the dihydrate to have an overall C$_s$ symmetry with both waters coordinated to a nearly octahedral Tc and interestingly the structure shown in Figure 5.8 did come from a guess constructed from that C$_s$ structure. Several other randomly constructed geometries also converged to that structure. A plot of the energy of the system versus the geometry optimization iteration shows that the optimization passed through several local minima until finally converging to the structure in Figure 5.8. All the local minima are within 25 kcal/mol of complex presented in Figure 5.8. This means that although they are less stable than the hydrogen bonding complex, they would be stable compared to the isolated HTcO$_4$

and H_2O molecules. Optimization with B3LYP (the functional used in the previous study) also produced the structure shown in Figure 5.8. As the waters once again migrated away from the Tc to form a hydrogen bonding complex, it can be inferred that heptavalent Tc prefers to be 4-coordinate when three Tc=O bonds are present. Much like motif 1 of $HTcO_4(H_2O)$, the addition of hydrogen bound waters does not significantly lower the initial excitation energy of $HTcO_4.2H_2O$; The lowest excited state is still within the UV and should give a colorless complex.

Table 5.3. Relative stabilities and wavelength of the lowest energy excited state for the hydrated Tc species.

Structure	Relative Stability (kcal/mol)	Wavelength of Lowest Excited State (nm)
$HTcO_4 \cdot H_2O$: Motif 1	-13.35	324
$HTcO_4 \cdot H_2O$: Motif 2	-7.90	342
$HTcO_4 \cdot H_2O$: Motif 3	-7.37	337
$HTcO_4 \cdot H_2O$: Motif 4	-5.11	331
$TcO_2(OH)_3$	6.65	407
$HTcO_4 \cdot 2H_2O$	-29.79	318

5.4.4 Study of Tc$_2$O$_7$-monohydrate

In a previous study, it was mentioned that the red color obtained during the preparation of Tc$_2$O$_7$ could be due to the presence of Tc$_2$O$_7$·H$_2$O. The Tc$_2$O$_7$·H$_2$O species has not been reported experimentally. In order to determine if the color observed in the red product could come from Tc$_2$O$_7$·H$_2$O, the molecular and electronic structure of Tc$_2$O$_7$·H$_2$O has been studied.

Several guess structures were generated with a 4- and 5- coordinate Tc with varying twists between the polyhedral for both initially bent and linear molecules for each of the possibilities for coordinating water. Several solutions were found and each adopted a bent structure often with a greater bend than in the base Tc$_2$O$_7$ (~140° vs. 156.1°). The three lowest energy solutions are shown in Figure 5.9. The relative stability of these structures compared to an isolated Tc$_2$O$_7$ and water (Table 5.4) are similar to those of the HTcO$_4$.H$_2$O, which demonstrates that the association of H$_2$O molecules in Tc$_2$O$_7$·H$_2$O and HTcO$_4$.H$_2$O follow a similar mechanism.

All the structures are also more stable than two isolated HTcO$_4$ molecules (Table 5.4) which indicate that single water should not dissociate Tc$_2$O$_7$ into HTcO$_4$; however other contributions drive the dissociation reaction. For example, thermodynamic analysis predicts an entropy of 0.120 kcal/mol/K for motif 1 and 0.078 kcal/mol/K for HTcO$_4$. By 359 K, the entropy will outweigh the internal energy favoring two HTcO$_4$ molecules.

The search predicted several structures within 1 mE$_h$ of motif 3; each of these structures had a water molecule side-on-bound to the Tc$_2$O$_7$ molecule. The difference between these structures is the geometry of [Tc$_2$O$_7$] core and the orientations of the water molecule (Figure 5.9, motif 2, 3, and 4). In those motifs, the water molecule is not covalently coordinated to the Tc$_2$O$_7$ unit and no hydrogen bonding is observed. Calculations of the excitation energy indicate that none

of these structures have an excited state low enough in energy to adsorb in the visible. While the structure presented here may not have been exhaustive, it clearly shows that the hydration of Tc_2O_7 is not sufficient to lower the excitation energies into the green as is needed for the red compound.
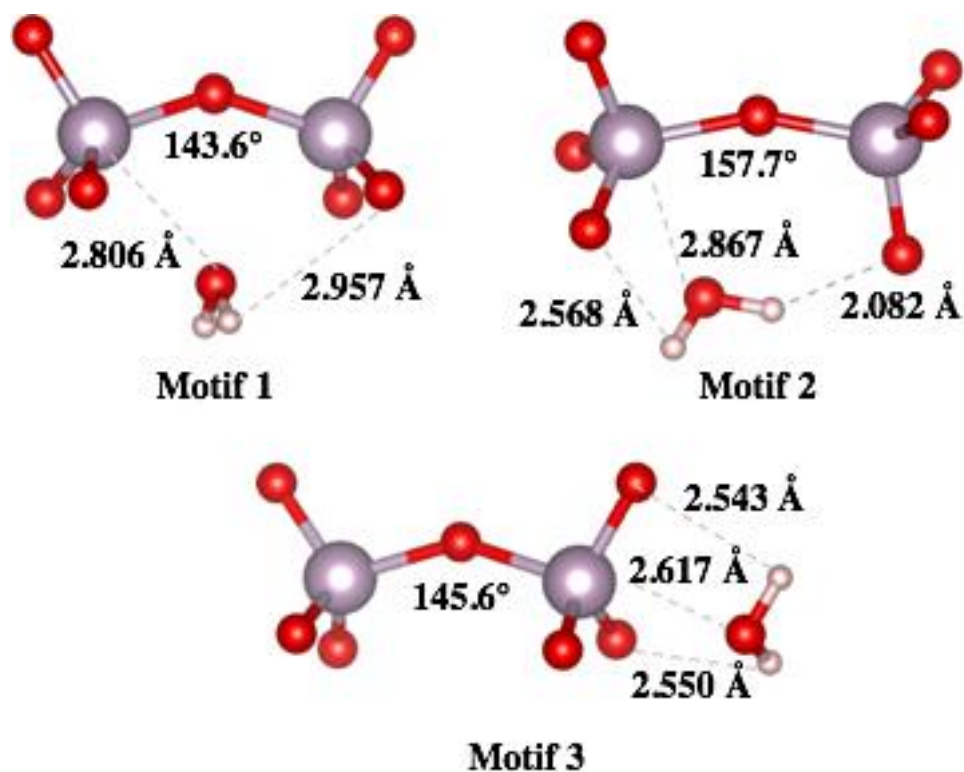
Figure 5.9. Lowest energy structures for $Tc_2O_7 \cdot H_2O$ complex.

Table 5.4. Relative stabilities and wavelength of the lowest energy excited state for the $Tc_2O_7 \cdot H_2O$ species.

Structure	Relative Stability (kcal/mol)	Wavelength of Lowest Excited State (nm)
$Tc_2O_7 \cdot H_2O$: Motif 1	-12.53 / -14.44	330
$Tc_2O_7 \cdot H_2O$: Motif 2	-9.92 / -11.83	343
$Tc_2O_7 \cdot H_2O$: Motif 3	-5.83 / -7.74	339

5.5 Oxidation of TcO₂ under dry Oxygen

The oxidation of TcO_2 with dry O_2 has been performed 180 °C. The samples were prepared by oxidation of TcO_2 with dry O_2 using a similar set-up as the used for the preparation of the EI-MS sample (Chapter 2). Under treatment of TcO_2 at 180 °C, a red product was also observed in the cold part of the tube. This red product might be different from the one obtained from the oxidation of TcO_2 with O_2/H_2O at 250 °C (see section 5.3).

In order to know more about the red product, its Raman spectra has been recorded and its behavior studied in the solid-state.

Initially, the stability of the red product was studied in a sealed tube under vacuum at 200 °C. Treatment at 200 °C leads to the formation of a black (presumably TcO_2) and yellow (Tc_2O_7) solids and is also consistent with the presence of a reduced species.

For the Raman study, technetium dioxide (26.4 mg, 0.201 mmol) was added to specialty reaction tube provided by Argonne National Laboratory. The tube was connected to the Schlenk line, evacuated and backfilled with dry oxygen. The reaction tube was then sealed at 43 cm and heated in a clamshell tube furnace for 21 days at 180 °C. After this time, a red color was observed in the small capillary. The capillary was sealed and the red product analyzed by Raman spectroscopy.

The Raman spectrum (Figure 5.10) differs from the one of Tc_2O_7 and pertechnetate salts. Current theoretical works focus on the calculations of Raman spectra of various oxides species (TcO_3, Tc_2O_5, TcO_2, ...); preliminary results indicate the calculated Raman spectra of molecular Tc_2O_5 to be similar to the experimental spectra of red products.

In order to determine the structure of the red species produced at 180 °C, a capillary containing the red compound prepared in similar conditions than the one for the Raman study was sent to the APS for XAFS spectroscopy analysis, unfortunately the small amount of compound collected in the capillary did not allow to observed XAFS signal.
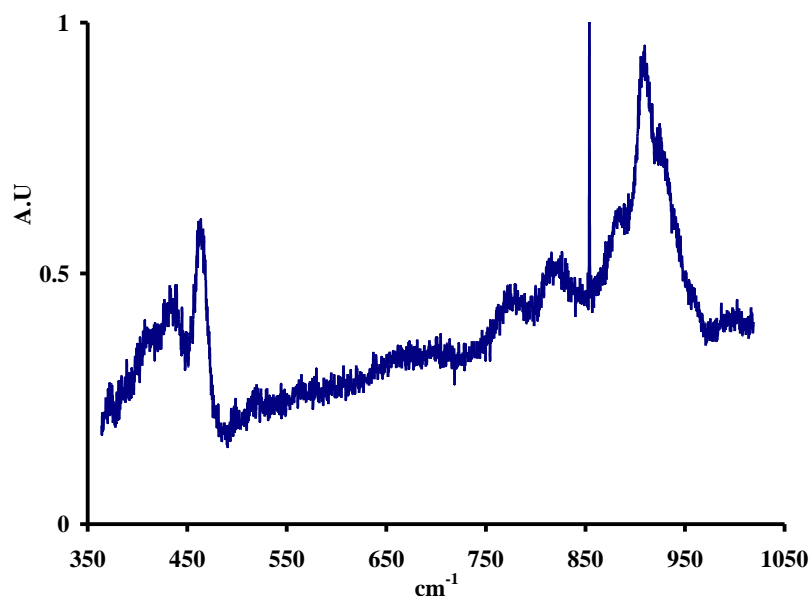
Figure 5.10. Raman spectra of the red species obtained after the oxidation of TcO_2 with dry O_2 at 180 °C.

5.6   Conclusion

In summary, the oxidation of TcO_2 with water and O_2 at 250 °C has been studied, and red and yellow (Tc_2O_7) products were observed after the reaction. The UV-Visible spectrum of the red product was similar to the one of $HTcO_4$ and to the one obtained after the reaction of Tc_2O_7 crystals with air. Cerium titration indicates that the red product contains a reduced Tc species. Treatment of the red product at 200 °C leads to the formation of a black powder, presumably TcO_2. It is proposed that the red product was produced from the oxidation of TcO_2 to Tc_2O_7, followed by the hydrolysis of Tc_2O_7 to $HTcO_4$ and the reduction of $HTcO_4$.

113

The behavior of the reaction product of TcO_2 with O_2/H_2O at 250 °C was studied by mass spectrometry. The main dinuclear species were Tc_2O_7 and Tc_2O_5, the main mononuclear binary oxide and hydroxo species were respectively TcO_3 and $HTcO_4$. Because the red product is thermally unstable and decomposed to TcO_2 and Tc_2O_7 at 200 °C, the sample analyzed by EI-MS probably consisted of a mixture $HTcO_4$, TcO_2 and Tc_2O_7.

The structure and electronic spectra of $HTcO_4$, $HTcO_4·H_2O$ and $HTcO_4·2H_2O$ and $Tc_2O_7·H_2O$ were studied by theoretical methods. For the $HTcO_4$ hydrates, results indicate the H_2O molecules to be hydrogen bonded to $HTcO_4$ and that covalent bonding does not occur between H_2O and $HTcO_4$. The calculated UV-Visible spectra of $HTcO_4$, $HTcO_4·H_2O$, $HTcO_4·2H_2O$ and $Tc_2O_7·H_2O$ do not exhibit bands at 500 nm, which indicates that the red color in the reaction product of TcO_2 with O_2/H_2O does not come from those species.

Chapter 6: Conclusion

From 1943 to 1987, the Hanford site was the primary location for the production of Pu for military applications in the United States. Decades of Pu production have been accompanied by generation of large amounts of liquid and solid radioactive waste. One radioelements present in the Hanford wastes is the isotope ^{99}Tc (~1500 kg). One option for the management of Tc at the Hanford site is its vitrification into a borosilicate glass. The behavior of Tc during vitrification is problematic, as it volatizes and only a fraction is retained in the glass. Minimization of Tc volatility is a challenge for the development of safe vitrification processes. The nature of the volatile Tc species is unclear and until now, no characterization of the volatile technetium species produced during vitrification of Tc has been performed.

In this dissertation, in order to better understand the mechanism of formation of volatile Tc species, the nature of the volatile species formed during vitrification and the solid-state and gas-phase chemistry of Tc_2O_7 and $HTcO_4$ was revisited.

In the first part of this work, the vitrification of Tc in borosilicate glass was conducted by using a flowing gas setup. Air was used as the flowing gas and $NaTcO_4$ was added a glass batch mixture to produce a Tc waste glass at 1100 °C. Glass samples were analyzed using SEM and EDX spectroscopy. Results indicate that Tc was not uniformly distributed throughout the glass product. Analysis of EDX spectra indicated that in some areas, $NaTcO_4$ was the dominant species, other parts of the glass contained particles with composition consistent with TcO_2. XAFS spectroscopy analysis indicated there was a mixed species in the glass as well, but mainly dominated by Tc(VII). A volatile red Tc species was identified during the vitrification of borosilicate glass by XAFS spectroscopy. The EXAFS results indicated the presence of

TcO$_3$(OH)(H$_2$O)$_2$. The mechanism of formation of volatile species were proposed and involved the oxidation of TcO$_2$ to Tc$_2$O$_7$ followed by the hydrolysis of Tc$_2$O$_7$ to HTcO$_4$ (or TcO$_3$(OH)(H$_2$O)$_2$).

As mentioned above, the mechanisms of volatilization of Tc during vitrifcation are likely to involve Tc$_2$O$_7$; in this context, the second part of this work focused on the study of the gas-phase and solid-state chemistry of Tc$_2$O$_7$. Here, Tc$_2$O$_7$ was synthesized from the oxidation of TcO$_2$ with O$_2$ and its crystallographic structure was determined at 100 K and the data compared with the previous structure elucidated in 1969. Refinement of the structure at 100 K indicates that Tc$_2$O$_7$ crystallizes as a molecular solid in the orthorhombic space group Pbca. The Tc$_2$O$_7$ molecule can be described by corner sharing TcO$_4$ tetrahedron with Tc$\cdots$Tc = 3.698(1) Å and Tc-O$_{Bri}$-Tc =180.0°. The electron impact-mass spectrum of Tc$_2$O$_7$ consists of both mononuclear and dinuclear species. The main dinuclear species in the gas-phase are Tc$_2$O$_7$ (100%) and Tc$_2$O$_5$ (56%), while the main mononuclear species are TcO$_3$ (33.9%) and TcO$_2$ (42.8%). The difference in the relative intensity of the M$_2$O$_5$ (M = Tc, Re) fragments (1.7 % for Re) indicate that these Group 7 elements exhibit different gas phase chemistry. The geometry of the Tc$_2$O$_7$ molecule was investigated in the gas-phase and in the solid-state by theoretical methods. The optimized structure of the Tc$_2$O$_7$ molecule was in good agreement with the experimental one. Energetic calculations confirm the linear structure to be the most favorable in the solid-state while the bent geometry is predicted to be the most stable in gas-phase. Stability with respect to compression and high cohesive energy per molecule are possibly the reason why the linear structure is observed in the solid-state.

Because water can be present during the vitrification process, studying the effect of water on the nature of the volatile species is of importance. In the last part of the dissertation, the effect of

water on the nature of the volatile species formed during oxidation of TcO_2 was studied. The oxidation of TcO_2 with water and O_2 was performed at 250 °C, after the reaction red and yellow (Tc_2O_7) products were observed. The UV-Visible spectrum of the red product was similar to the one of $HTcO_4$ and to the one obtained after the reaction of Tc_2O_7 crystals with air. It was proposed that the red product was produced from the oxidation of TcO_2 to Tc_2O_7, followed by the hydrolysis of Tc_2O_7 to $HTcO_4$ and the reduction of $HTcO_4$. The behavior of the reaction product of TcO_2 with O_2/H_2O at 250 °C was also studied by mass spectrometry. The main dinuclear species were Tc_2O_7 and Tc_2O_5, the main mononuclear binary oxide and hydroxo species were respectively TcO_3 and $HTcO_4$. Because the red product is thermally unstable and decomposed to TcO_2 and Tc_2O_7 at 200 °C, the sample analyzed by EI-MS probably consisted of a mixture $HTcO_4$, TcO_2 and Tc_2O_7. Because it was mentioned that $HTcO4$ was also involved in the mechanism of volatilization of Tc during the vitrification, its chemistry was also revisited by theoretical methods. The structure and electronic spectra of $HTcO_4$, $HTcO_4 \cdot H_2O$ and $HTcO_4 \cdot 2H_2O$ and $Tc_2O_7 \cdot H_2O$ were studied by theoretical methods. For the $HTcO_4$ hydrates, results indicated that the H_2O molecules were hydrogen bonded to $HTcO_4$ and that covalent bonding did not occur between H_2O and $HTcO_4$. The calculated UV-Visible spectra of $HTcO_4$, $HTcO_4 \cdot H_2O$, $HTcO_4 \cdot 2H_2O$ and $Tc_2O_7 \cdot H_2O$ did not exhibit bands at 500 nm, which indicates that the red color in the reaction product of TcO_2 with O_2/H_2O should not come from those species.

The oxidation of TcO_2 with dry O_2 has been performed 180 °C. Under treatment of TcO_2 at 180 °C, a red product was observed in the cold part of the tube. Treatment of the red products at 200 °C leads to the formation of a black (presumably TcO_2) and yellow (Tc_2O_7) solids. In order to know more about the red product, its Raman spectra has been recorded, The Raman spectra

117

differs from the one of Tc_2O_7 and pertechnetate salts. Current theoretical works focus on the calculations of Raman spectra of various oxides species (TcO_3. Tc_2O_5, TcO_2, ...); preliminary results indicate the calculated Raman spectra of molecular Tc_2O_5 to be similar to the experimental spectra of red products.

In regards to vitrification, a full understanding of the formation of volatile Tc-oxides would benefit in solving the issue of Tc retention in glass. The products and their order of formation could aid in the retention of glass if lower temperature were used in the vitrfication processes. Being able to establish periodic trends based on congeners, would not only help with the chemistry of Tc-oxides, but all other transition metal oxides.

Finally, in relation to binary Tc-oxides and their production, there remain many unanswered questions about the way to produce the red species in large quantities along with the physical properties that need to be analyzed. Ditechnetium heptoxide has the possibility to coordinate with ligands similarly as its Re_2O_7 congener and new $Tc_2O_7 \cdot 2L$ (L = pyridine, THF , etc.) complexes could be prepared. The thermal decomposition of $Tc_2O_7 \cdot 2L$ adduct could lead to the formation of TcO_3 and Tc_2O_5 in the solid-state.

Appendix I

The solid-state structure of Tc_2O_7 was modeled with plane-wave density functional theory (PW-DFT)[81,82] using the Vienna *ab initio* simulation package (VASP) version 5.4.1, and using the generalized gradient approximation (GGA) functional of Perdew, Burke, and Ernzerhof (PBE)[83] together with Grimme's -D3[102] semi-empirical dispersion correction. The projector augmented wave (PAW)[103] pseudopotentials formulated with PBE were used to represent the ionic cores, and the valence configurations were $4s^2 4p^6 5s^2 5d^5$ for Tc and $2s^2 2p^4$ for O. The first Brillouin zone was spanned by an automatically generated Γ-centered k-point mesh of size 4x6x2, corresponding to a grid spacing of roughly $0.035\ 2\pi\ Å^{-1}$. The plane waves were cut off at 600 eV. The Kohn-Sham[82] equations were solved using the blocked Davidson algorithm. Cell volumes were obtained through a fit to the Vinet equation of state (EOS)[104] from a series of 9 constant volume conjugate-gradient optimizations of the cell shape and atomic positions that spanned ±8% of our experimentally determined unit cell volume. To minimize the effect of Pulay stress, the constant volume optimizations were performed in 3 parts: 2 sequential optimizations and a final single point energy evaluation.[105,106,107,108] The convergence tolerance for total energies and forces were 10^{-6} eV and 10^{-5} eV, respectively. The structure optimizations used a Gaussian smearing scheme with a width of 0.05 eV, and single point energy evaluations used the tetrahedron method with Blöchl corrections.[109] A single molecule was extracted from the optimized unit cells and placed into an empty 20 Å cubic box; then a single point calculation was run with a Γ-centered k-point mesh of size 2x2x2 to compute the cohesive energies. In order to minimize the interaction with periodic images of the molecule, the empirical dispersion corrections were cut off at 7 Å.

Single Tc_2O_7 molecule PBE-D3 simulations were performed using the Q-Chem 4.0 package.[110] The ATZP all electron augmented triple-ζ valence with polarization basis set was employed.[111,112] The exchange-correlation functional was evaluated on an Euler-Maclaurin-Lebedev quadrature grid with 75 angular points and 302 radial points per atom. The energy convergence tolerance was 10^{-9} Hartree (2.7×10^{-8} eV) with an integral cutoff of 10^{-14} Hartree. Structures were optimized without symmetry considerations with a convergence criterion of a maximum gradient component of 10^{-4} Hartree/Å and a maximum atomic displacement of 10^{-4} Å. The initial guesses for the structures were taken from our experimental crystal structure and manually made to have broken symmetry.

AI.   Evaluation of functionals

A recent study examined the performance of several PW-DFT functionals in their ability to reproduce the original and predict compressed structures of Tc_2O_7 and to predict its compression;[96] yet their work was done with a full PW-DFT relaxation of cell volumes which has been shown in molecular or porous materials to produce erroneous volumes and potentially erroneous structures on account of the Pulay stress.[113] In general, our trends follow those of Feng, et al.[96] The pure generalized gradient approximation (GGA) functionals over-predicted the experimental volume by a large margin, which has been shown to be the case several times in the literature. Both vdW-DF[114,115,116,117] and vdW-DF2[118] over-predicted the cell volume, as has also been shown in previous works.[119] The vdW-DF functionals with optimized exchange functionals[119] and the dispersion corrected GGAs all predicted volumes that were within 6% of the experimentally measured volume. Surprisingly vdW-DF and vdW-DF2 over-predicted the Tc-O bond lengths by around the

same percentage that they over-predicted the cell volume. However, all the other functionals predicted roughly the same internal monomeric geometry. A full PW-DFT relaxation was performed for each of the functionals as an additional test (Table S7); the general observation is that Pulay stress led to a 2-5% under-estimation of cell volume for functionals that included dispersion and around a 10% under-estimation for the pure GGAs when compared to the cell volumes fit from an EOS. Hybrid and long range corrected functionals include some percent of the non-local exact exchange to the density functional, which tends to improve the description of charge transfer in systems. This usually provides more accurate predicted band gaps and optical properties, and it helps resolve the ordering of magnetic states in transition metals. Recently, both Taylor and Sa, et al. demonstrated that the GGA-PBE performed quite well at predicting the lattice vectors of the extended and more metallic TcO_2, and that the hybrid functionals and +U correction did not improve the structural description of TcO_2 and only slightly improved the description of some of the electronic features near the Fermi level.[120,121] Because of the large number of atoms in the Tc_2O_7 unit cell and the very large computational expense of exact exchange in plane-wave solid-state implementations, we found that each SCF iteration with exact exchange (PBE0-D3) cost more than fifty times that of a PBE-D3 iteration even with the Brillouin zone for the exact exchange sampled at only the Γ-point.[122,123] As Tc_2O_7 is far more molecular than TcO_2, functionals containing exact exchange were not included in this study.

As it appears, many of the functionals tested would be reasonable to study Tc_2O_7; then it must be determined which functional is the 'best'. Since PW-DFT relaxations are performed at 0 K, the 0 K cell volume (V_0) would be the best comparison. V_0 can be approximated as 549 $Å^3$ by evaluating the thermal expansion between the original 293 K structure[45] and the new 100 K structure; the

thermal expansion coefficient (α_V) obtained in this manner is 1.63 10^{-4} Å^3/K. PBE-D3 is the functional that best agrees with this value. The PBE-D3 bond lengths are also in great (0.54%) agreement with experiment (Table A1).

Table A1. Experimental and calculated bond distances (Å) in Tc_2O_7. The value in bracket is the variance on the $Tc\text{-}O_{Ter}$ distance.

Bond length	Experimental value	Periodic solid	Single molecule
$Tc\text{-}O_{Ter}$	1.6872[6]	1.696	1.695
$Tc\text{-}O_{Bri}$	1.8488(5)	1.859	1.875
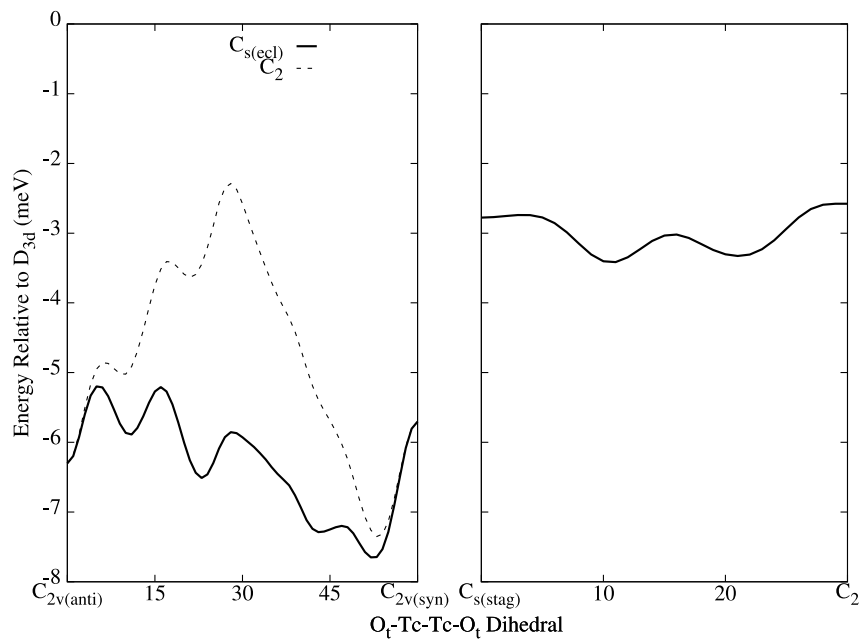
Figure AP4.1. The potential energy surfaces along low symmetries connecting the conformers without D_3 symmetry. For each point the molecular geometries were optimized constraining only the necessary dihedral angles to preserve symmetry. The left curves are denoted by which conformer is the 30° intermediate.

References

(1)   German, K. E.; Kriuchkov, S. V; Belyaeva, L. L. *J. Radioanal. Nucl. Chem.* **1988**, *121*, 515.

(2)   Schwochau, K. *Technetium: Chemistry and Radiopharmaceutical Applications*; Wiley-VCH: Weinheim, Germany, 2000.

(3)   Gerber, M. *Legend and Legacy: Fifty Years of Defense Production at the Hanford Site.*; Richland, WA, 1992.

(4)   Marceau, T. E.; Harvey, D. W.; Stapp, D. C.; Cannon, S. D.; Conway, C. A.; Deford, D. H.; Freer, B. J.; Gerber, M. S.; Keating, J. K.; Noonan, C. F.; Weisskopf, G. *History of the Plutonium Production Facilities at the Hanford Site Historic District*; Richland, WA, 2002.

(5)   Gaphart, R. E. *A Short History of Hanford Waste Generation, Storage, and Release*; Richland, WA, 2002.

(6)   Darab, J. G.; Smith, P. A. *Chem. Mater.* **1996**, *8* (5), 1004.

(7)   Lukens, W. W.; Bucher, J. J.; Edelstein, N. M.; Shuh, D. K. *J. Phys. Chem.* **2001**, *41* (32), 9611.

(8)   May, T. *Improved Technetium Retention in Hanford LAW Glass - Phase 1 Final Report*; Richland, WA, 2010.

(9)   Yoshihara, K. *Top. Curr. Chem.* **1996**, *176*, 17.

(10)   Lieser, K. H.; Bauscher, C. *Radiochim. Acta* **1987**, *42* (4), 205.

(11)   Langowski, M.; Darab, J.; Smith, P. *Volatility literature of chlorine, iodine, cesium, strontium, technetium and rhenium; technetium and rhenium volatility testing.*; Richland, WA, 1996.

(12)   Muller, I. S.; Viragh, C.; Gan, H.; Matlack, K. S.; Pegg, I. L. *Hyperfine Interact.* **2009**, *191* (1–3), 17.

(13)   Lukens, W. W.; McKeown, D. A.; Buechele, A. C.; Muller, I. S.; Shun, D. K.; Pegg, I. L. *Chem. Mater.* **2007**, *19* (3), 559.

(14)   Soderquist, C. Z.; Schweiger, M. J.; Kim, D. S.; Lukens, W. W.; McCloy, J. S. *J. Nucl. Mater.* **2014**, *449* (1–3), 173.

(15)   Perrier, C.; Segre, E. *Nature* **1937**, *140*, 193.

(16)   Icenhower, J. P.; Qafoku, N. P.; Martin, W. J.; Zachara, J. M. *The Geochemistry of*

Technetium: A Summary of the Behavior of an Artificial Element in the Natural Environment; Richland, WA, 2008.

(17)   Luykx, F. *Appl. Sci. Publ.* **1986**, 21.

(18)   Brookhaven National Lab: Brookhaven, NY 1973, p 325.

(19)   Tucker, W. D.; Greene, M. W.; Weiss, A. J.; Murrenhoff, A. J. *Trans. Am. Nucl. Soc.* **1958**, *1*, 160.

(20)   Utsunomiya, S.; Ewing, R. C. *Radiochim. Acta* **2006**, *94* (9–11), 749.

(21)   Salaria, G. B. S.; Rulfs, C. L.; Elving, P. J. *J. Chem. Soc.* **1963**, 2479.

(22)   Nakashima, T.; Lieser, K. H. *Radiochim. Acta* **1986**, *39* (3), 149.

(23)   Vida, J. *Chemical behavior of technetium during treatment of high-level radioactive waste*; Karlsruhe, 1989.

(24)   Schwochau, K. *The Analytical Chemistry of Technetium*; Brauer, G., Ed.;, 1981.

(25)   Eakins, J. D.; Humphries, D. G. *J. Inorg. Nucl. Chem.* **1963**, *77* (February), 1963.

(26)   Voltz, R. E.; Holt, M. L. *Electrochem. Soc.* **1967**, *114*, 128.

(27)   Box, W. D. *Nucl. Appl.* **1965**, *1*, 155.

(28)   Spitsyn, V. I. Z. *Chem. [Leipzig]* **1981**, *21*, 131.

(29)   Peacock, R. D. *The Chemisry of Technetium and Rhenium*; London, 1966.

(30)   Marples, J. A. C. **1972**, *41* (4), 307.

(31)   Nelson, C. M.; Boyd, G. E.; Smith, W. T. *J. Am. Chem. Soc.* **1954**, *76*, 348.

(32)   Daunt, J. G.; Cobble, J. W. *Phys. Rev.* **1953**, *92*, 507.

(33)   Compton, V. B.; Corenzwit, E.; Maita, J. P.; Matthias, B. T.; Morin, F. J. *Phys. Rev.* **1961**, *123* (5), 1567.

(34)   Mullen, P.; Schwochau, K.; Jorgensen, C. K. *Chem. Phys. Lett.* **1969**, *3*, 49.

(35)   Keller, C.; Kanellakopulos, B. *Radiochim. Acta* **1963**, *1*, 107.

(36)   Muller, O.; White, W. B.; Roy, R. *J. Inorg. Nucl. Chem.* **1964**, *26* (1962), 2075.

(37)   Krebs, B.; Hasse, K. D. *Acta Crystallogr. Sect. B.* **1976**, *32* (5), 1334.

(38)   Faggiani, B. Y. R.; Lock, C. J. L.; Poc, J. *Library (Lond).* **1980**, 231.

(39)   Meyer, G.; Hoppe, R. Z. *Anorg. Allg. Chem.* **1980**, *420*, 40.

(40)   German, K. E. *Bull. Acad. Sci, USSR* **1987**, *10*, 213.

(41)   Kotegove, K. V.; Pavlov, O. N.; Shvedov, V. P. *kotegov*; 1968; Vol. 2.

(42)   Pozdrowicz, U.; Krebs, B.; Schwochau, K. Master Thesis, University of Munster, 1984.

(43)   Boyd, G. E.; Cobble, J. W.; Nelson, C. M.; Smith, W. T., J. *J. Am. Chem. Soc.* **1952**, *74*, 556.

(44)   Smith, W. T.; Cobble, J. W.; Boyd, G. E. *J. Am. Chem. Soc.* **1953**, *75* (23), 5773.

(45)   Krebs, B. *Angew. Chemie Int. Ed.* **1969**, *8* (5), 381.

(46)   Cho, H.; de Jong, W. A.; Sattelberger, A. P.; Poineau, F.; Czerwinski, K. R. *J. Am. Chem. Soc.* **2010**, *132*, 13138.

(47)   Selig, H.; Fried, S. *Inorg. Nucl. Chem. Lett.* **1971**, *7* (5), 315.

(48)   Beattie, I. R.; Gilson, T. R.; Jones, P. J. *Inorg. Chem.* **1996**, *35* (5), 1301.

(49)   Rodriguez, E. E. Thesis dissertation. UC Santa Barbara 2009, p 236.

(50)   Bolzan, A. A.; Kennedy, B. J.; Howard, C. *Aust. J. Chem.* **1995**, *48*, 1473.

(51)   Lieser, K. H.; Bauscher, C.; Nakashima, T. *Radiochim. Acta* **1987**, *42*, 191.

(52)   Boyd, G. E. **1959**, *36* (1), 3.

(53)   Maes, A.; Geraedts, K.; Bruggeman, C.; Vancluysen, J.; Rossberg, A.; Hennig, C. *Environ. Sci. Technol.* **2004**, *38* (7), 2044.

(54)   Lukens, W. W.; Bucher, J. J.; Edelstein, N. M.; Shuh, D. K. *Environ. Sci. Technol.* **2002**, *36* (5), 1124.

(55)   Hanke, C.; Jahrling, B.; Lieser, K. H. *Technetium Environ.* **1984**, 179.

(56)   Mazzocchin, G. A.; Magno, K.; Bontempelli, G. *Inorg. Chim. Acta.* **1975**, *13*, 209.

(57)   Cartledge, G. H.; Smith, W. T. *J. Phys. Chem.* **1955**, *59*, 1111.

(58)   Gorksi, B.; Koch, H. *J. Inorg. Nucl. Chem* **1969**, *31*, 3565.

(59)   Kanellakopulos, B. *Dissolution of Technetium*; Karlsruhe, 1963.

(60)   Fried, S.; Jaffey, A. H.; Hall, N. F.; Glendemin, L. E. *Phys. Rev.* **1951**, *81* (5), 741.

(61)   Herrell, A. Y.; Busey, R. H.; Gayer, K. H.; Schwochau, K.; Gutzeit, S. *Inorg. Synth.* **1977**, *17*, 155.

(62)   Gibson, J. K. *Radiochim. Acta* **1993**, *60* (2–3), 121.

(63)   Steffen, A.; Bachmann, K. *Talanta* **1978**, *25*, 677.

(64)   Steffen, A.; Bachmann, K. *Talanta* **1978**, *25*, 551.

(65)   Migge, H. In *Mat. Res. Soc. symposia proceedings*; 1989; pp 205–213.

(66)   Childs, B. C.; Braband, H.; Lawler, K. V.; Mast, D. S.; Bigler, L.; Stadler, U.; Forster, P. M.; Czerwinski, K. R.; Alberto, R.; Sattelberger, A. P.; Poineau, F. *Inorg. Chem.* **2016**,

(67)   Denecke, M. A. *Coord. Chem. Rev.* **2006**, *250* (7–8), 730.

(68)   Almahamid, I.; Bryan, J. C.; Bucher, J. J.; Burrell, A. K.; Edelstein, N. M.; Hudson, E. A.; Kaltsoyannis, N.; Lukens, W. W.; Shuh, D. K.; Nitsche, H.; Reich, T. *Inorg. Chem.* **1995**, *34*, 193.

(69)   Ravel, B.; Newville, M. *J. Synchrotron Radiat.* **2005**, *12* (4), 537.

(70)   Ressler, T. *J. Synchrotron Radiat.* **1998**, *5* (Pt 2), 118.

(71)   Rehr, J. J.; Albers, R. C. C. *Rev. Mod. Phys.* **2000**, *72* (3), 621.

(72)   Ravel, B. *J. Synchrotron Radiat.* **2001**, *8* (2), 314.

(73)   Gibson, J. K. *J. Fluor. Chem.* **1991**, *55* (3), 299.

(74)   Fales, H. M.; Milne, G. W. A.; Vestal, M. L. *J. Am. Chem. Soc.* **1969**, *91*, 3682.

(75)   Sheldrick, G. M. *Acta Crystallogr. Sect. A.* **2008**, *64* (1), 112.

(76)   Dolomanov, O. V.; Bourhis, L. J.; Gildea, R. J.; Howard, J. A. K.; Puschmann, H. *J. Appl. Crystallogr.* **2009**, *42* (2), 339.

(77)   Paul, A.; Mulholland, M.; Zaman, M. S. *J. Mater. Sci.* **1976**, *11* (Iii), 2082.

(78)   Mueller, A.; Rittner, W. *Spectrochim. Acta* **1967**, *23*, 1831.

(79)   Busey, R. H.; Keller, O. L. *J. Chem. Phys.* **1964**, *41* (1), 215.

(80)   Elmer, P. Waltam, MA 2008, p .

(81)   Hohenberg, P.; Kohn, W. *Phys. Rev. B* **1964**, *136* (3B), 864.

(82)   Kohn, W.; Sham, L. J. *Phys. Rev. A* **1965**, *140* (4A), 1133.

(83)   Perdew, J. P.; Burke, K.; Ernzerhof, M. *Phys. Rev. Lett.* **1996**, *77* (18), 3865.

(84)   Poineau, F.; Sattelberger, A. P.; Conradson, S. D.; Czerwinski, K. R. *Inorg. Chem.* **2008**, *47* (6), 1991.

(85)   Poineau, F.; Weck, P. F.; Burton-Pye, B. P.; Kim, E.; Francesconi, L. C.; Sattelberger, A.

127

P.; German, K. E.; Czerwinski, K. R. *Eur. J. Inorg. Chem.* **2013**, No. 26, 4595.

(86)   Poineau, F.; Burton-Pye, B. P.; Maruk, A.; Kirakosyan, G.; Denden, I.; Rego, D. B.; Johnstone, E. V.; Sattelberger, A. P.; Fattahi, M.; Francesconi, L. C.; German, K. E.; Czerwinski, K. R. *Inorg. Chim. Acta* **2013**, *398*, 147.

(87)   Colby, S.; Peterson, C. Westinghouse Hanford Co.: Richland, WA 1995.

(88)   McGregor, D.; Burton-Pye, B. P.; Howell, R. C.; Mbomekalle, I. M.; Lukens, W. W.; Bian, F.; Mausolf, E.; Poineau, F.; Czerwinski, K. R.; Francesconi, L. C. *Inorg. Chem.* **2011**, *50* (5), 1670.

(89)   Kim, D. S.; Yeager, D. J.; Soderquist, C. Z.; Matyáš, J.; Icenhower, J. P.; Darnell, L. P.; Mcgrail, B. P.; Schaef, H. T.; Scheele, R. D.; Owen, A. T.;et al. . *Tc reductant chemistry and crucible melting studies with simulated Hanford low-activity waste*; 2005.

(90)   Poineau, F.; Weck, P. F.; German, K.; Maruk, A.; Kirakosyan, G.; Lukens, W.; Rego, D. B.; Sattelberger, A. P.; Czerwinski, K. R. *Dalton Trans.* **2010**, *39* (37), 8616.

(91)   Gibson, J. K. *Radiochim. Acta* **1993**, *62*, 127.

(92)   Childs, B. C.; Poineau, F.; Czerwinski, K. R.; Sattelberger, A. P. *J. Radioanal. Nucl. Chem.* **2015**, *306* (2), 417.

(93)   Cotton, F. A.; Wilkinson, G. *Advanced Inorganic Chemistry*, 3rd ed.; Wiley & Sons: New York, NY, 1972.

(94)   Simon, A.; Dronskowski, R.; Krebs, B. *Angew. Chem. Int. Ed. Engl.* **1987**, *24* (1979), 139.

(95)   Krebs, B.; Muller, A.; Beyer, H. H. *Inorg. Chem.* **1969**, *8* (3), 436.

(96)   Fang, Y.; Sa, B.; Miao, N.; Sun, Z.; Wu, B. *CrystEngComm* **2015**, 328.

(97)   Amado, A. M.; Ribeiro-claro, P. J. A. *J. Mol. Struct. THEOCHEM* **1999**, *469*, 191.

(98)   Skinner, B.; Searcy, A. W. *J. Phys. Chem.* **1973**, *77* (12), 1578.

(99)   Briscoe, H. V. A.; Robinson, P. L.; Rudge, A. J. *J. Chem. Soc.* **1929**, 3087.

(100) Mackey, D. W. J.; Jackson, P.; Baker, R. J.; Dasaklis, C.; Fisher, K. J.; Magee, M.; Bush, V.; Burch, W. M.; Wall, H. Van Der; Willeâ, G. D. *J. Nucl. Med.* **1997**, *38*, 163.

(101) Rulfs, C. .; Pacer, R. .; Hirsch, R. . *J. Inorg. Nucl. Chem.* **1967**, *29* (3), 681.

(102) Grimme, S.; Antony, J.; Ehrlich, S.; Krieg, H. *J. Chem. Phys.* **2010**, *132*, 1.

(103) Blöchl, P. E. *Phys. Rev. B* **1994**, *50* (24), 17953.

(104) P.Vinet; Smith, J. R.; Ferrante, J.; Rose, J. H. *Phys. Rev. B* **1987**, *35* (4), 1945.

(105) Froyen, S.; Cohen, M. *J. Phys. C Solid State Phys.* **1986**, *19*, 2623.

(106) Dacosta, P. G.; Nielsen, O. H.; Kunc, K. *J. Phys. C Solid State Phys.* **1986**, *19* (17), 3163.

(107) Vanderbilt, D. *Phys. Rev. Lett.* **1987**, *59* (13), 1456.

(108) Francis, G. P.; Payne, M. C. *J. Phys. Condens. Matter* **1990**, *2*, 4395.

(109) Blöchl, P. E.; Jepsen, O.; Andersen, O. K. *Phys. Rev. B* **1994**, *49* (23), 16223.

(110) Shao, Y.; Gan, Z.; Epifanovsky, E.; Gilbert, A. T. B.; Wormit, M.; Kussmann, J.; Lange, A. W.; Behn, A.; Deng, J.; Feng, X.; et al. *Mol. Phys.* **2015**, *113* (2), 184.

(111) Fantin, P. A.; Barbieri, P. L.; Canal Neto, A.; Jorge, F. E. *J. Mol. Struct. THEOCHEM* **2007**, *810* (1–3), 103.

(112) Martins, L. S. C.; de Souza, F. A. L.; Ceolin, G. A.; Jorge, F. E.; de Berredo, R. C.; Campos, C. T. *Comput. Theor. Chem.* **2013**, *1013*, 62.

(113) Vanpoucke, D. E. P.; Lejaeghere, K.; Van Speybroeck, V.; Waroquier, M.; Ghysels, A. *J. Phys. Chem. C* **2015**, *119* (41), 23752.

(114) Dion, M.; Rydberg, H.; Schröder, E.; Langreth, D. C.; Lundqvist, B. I. *Phys. Rev. Lett.* **2004**, *92* (24), 1.

(115) Román-Pérez, G.; Soler, J. M. *Phys. Rev. Lett.* **2009**, *103* (9), 1.

(116) Klimes, J.; Bowler, D. R.; Michaelides, A. *Phys. Rev. B* . **2011**, *83* (19), 1.

(117) Thonhauser, T.; Cooper, V. R.; Li, S.; Puzder, A.; Hyldgaard, P.; Langreth, D. C. *Phys. Rev. B* -. **2007**, *76* (12), 1.

(118) Lee, K.; Murray, É. D.; Kong, L.; Lundqvist, B. I.; Langreth, D. C. *Phys. Rev. B* . **2010**, *82*, 1.

(119) Klimeš, J.; Bowler, D. R.; Michaelides, A. *J. Phys. Condens. Matter* **2010**, *22* (2), 1.

(120) Taylor, C. D. *J. Phys. Chem. C* **2014**, *118* (19), 10017.

(121) Sa, B.; Miao, N.; Sun, Z.; Wu, B. *RSC Adv.* **2015**, *5* (3), 1690.

(122) Adamo, C.; Barone, V. *J. Chem. Phys.* **1999**, *110* (13), 6158.

(123) Paier, J.; Hirschl, R.; Marsman, M.; Kresse, G. *J. Chem. Phys.* **2005**, *122* (23).

Curriculum Vitae

Bradley C. Childs

Education
Ph.D. Radiochemistry   Expected Defense: Fall 2016
University of Nevada, Las Vegas

- Advisor: Dr. Frederic Poineau
- Dissertation work with fundamental technetium chemistry and waste forms.

B.S. Chemistry   5/2010
South Carolina State University   Orangeburg, South Carolina

- GPA: 3.61/4.0 (Magna Cum Laude)

Research Experience
Graduate Assistant   **University of Nevada, Las Vegas**
   8/2010-present

- Studied the nature of technetium-99 in low activity waste glass with emphasis being placed on temperatures between 600 °C to 1100 °C to observe cold cap effect
- Investigated technetium nitride, technetium phosphide, and volatility of various technetium oxides
- Observation of uranyl nitrate in varying percentages of TBP/dodecane under solvothermal conditions

Research Assistant   **Lawrence Berkeley National Laboratory**
   6/2010-8/2010

- Assisted in production of carbon-11 and fluorine-18 radiotracers. Developed an apparatus to quantify amount of fluorine-18 produced by way of iodine production with a simple spectrophotometer.

Summer Intern   **Lawrence Berkeley National Laboratory**
   6/2009-8/2009

- Developed a method to reduce radiation exposure during production of carbon-11 and fluorine-18 radiotracers.

Student Intern   **University of Tennessee, Knoxville**
   6/2008-8/2008

- Performed research with a University of Tennessee graduate student as well as two nuclear engineering students on simulated control loops for nuclear reactors.

Summer Intern   Oak Ridge National Laboratory
   5/2007-8/2007

- Performed experiments in non-radioactive and radioactive laboratories in order to electroplate a thin platinum wire to probe a cancerous cell.

Teaching Experience

Teaching Assistant   University of Nevada, Las Vegas
   8/2011–present

- Taught general and organic chemistry laboratory to enrolled students
- Prepared lesson plan, conducted laboratory classes and exams, and graded reports and exams

Teaching Assistant   Nuclear Fuel Cycle Summer School   UNLV
   Summer 2011, 2013, 2015

- Taught students during a six week school about nuclear fuel cycle as well as assisted in class recitations
- Conducted fundamental fuel cycle experiments with students as well as performed fuel cycle research with them based on projects currently being conducted in the radiochemistry program at UNLV

Laboratory and Instrumentation Skills
Analytical
Alpha Spectroscopy, UV-Visible Spectroscopy , Infrared Spectroscopy, Gamma Spectroscopy, ICP- Atomic Emissions Spectroscopy, ICP- Mass Spectrometry, High Performance Liquid Chromatography, Neutron Detection, Nuclear Magnetic Resonance, Liquid Scintillation Counting, Scanning Electron Microscopy, Powder X-Ray Diffraction, Single Crystal X-Ray Diffraction. X-ray absorption Spectroscopy
Synthesis
Arc Melter, Tube Furnace, Muffle Furnace, Pressure Vessels (Parr), Vacuum Ga Manifold (Schlenk Line), Non-Destructive Assay Techniques, Chemical Digestions, Radiochemical Separations
Radioactive Isotopes
Technetium-99, Uranium-238, Uranium-235, Uranium-234, Neptunium-237, Plutonium-239, Carbon-11, Flourine-18, Tellurium-125m, Thorium-232, Strontium-90, Americium-241, Gadolinium-148, Thallium-204, Yttrium-90, Cobalt-60, Cobalt-57, Cesium-137, Europium 152, Barium-133, Manganese-54, Bismuth-214, Lead-212, Lead-214, Barium-137m, Plutonium-238

External Collaborators

Alfred P. Sattelberger - Deputy Lab Director for Programs, Argonne National Laboratory
Gordon Jarvinen – Scientist, Los Alamos National Laboratory
Lynn Francesconi – Professor, Hunter College-CUNY

Awards

1. Innovations in Fuel Cycle Research Awards sponsored by the U.S. Department of Energy, Office of Fuel Cycle Technologies. in the Competition for Students Who Attend Universities with Less than $600 Million in 2014 R&D Expenditures. His award-winning research paper, "The Nature of the Volatile Technetium Species Formed During Vitrification of Borosilicate Glass,"

Publications

1. Childs, B.C.; Poineau, F.; Czerwinski, K.R.; Sattelberger, A.P. The nature of the volatile technetium species formed during vitrification of borosilicate glass, *Journal of Radioanalytical and Nuclear Chemistry* **2015** *306* (2), 417-421.
2. Childs, B.C.; et al. Ditechnetium Heptoxide Revisited: Solid-state, Gas Phase and Electronic Structure Studies. *Inorg. Chem.*, **2016**, *55* (20), pp 10445–10452.
3. Lawler, K. V.; Childs, B. C.; Mast, D. S.; Czerwinski, K. R.; Sattelberger, A. P.; Poineau, F.; Forster, P. M. Molecular and Elctronic Structures of M2O7 (M= Mn, Tc, Re). *Inorg. Chem.***2017,** *56* (5), pp 2448–2458.

Oral Presentations (select list)

1. Childs, Bradley C.; Poineau, F.; Czerwinski, K. R.; Sattelberger A.P.; The nature of the volatile technetium species formed during vitrification of borosilicate glass. International Conference on Radioanalystical and Nuclear Chemistry, Budapest, Hungary, April 10-15, 2016.
2. Childs, Bradley C.; Poineau, F.; Czerwinski, K. R.; Sattelberger A.P.; The nature of the volatile technetium species formed during vitrification of borosilicate glass. 8th International Symposium on Technetium and Rhenium, Pornichet, La Baule, France, September 29 – October 3, 2014.
3. Childs, Bradley; Kerlin, William; Czerwinski, Ken. Synthesis of binary technetium phosphide in low temperature conditions. 246th ACS National Meeting & Exposition, Indianapolis, IN, United States, September 8-12, 2013.
4. Bradley C. Childs, F.P. Poineau and K. R. Czerwinski. Technetium retention in low activity waste glass. Methods & Applications of Radioanalytical Chemistry (MARC) IX, Kailua-Kona, Hawaii, USA. March 25 – March 30, 2012.
5. Childs, Bradley; Poineau, Frederic; Czerwinski, Ken. Technetium speciation in glass. 242nd ACS National Meeting & Exposition, Denver, Colorado, United States, August 28 – September 1, 2011.

Poster Presentations (select list)

1. Bradley C. Childs, W. M. Kerlin and K. R. Czerwinski. Binary Technetium Phosphide Synthesis at Low Temperature Conditions. 5th Asia-Pacific Symposium

on Radiochemistry, APSORC' 13. September 22 – September 27, 2013 Kanazawa, Japan.

2. Bradley C. Childs, F.P. Poineau and K. R. Czerwinski. Synthesis and Characterization of Volatile Technetium Species. 5th Asia-Pacific Symposium on Radiochemistry, APSORC' 13. September 22 – September 27, 2013 Kanazawa, Japan.